1-1-2016

Design And Synthesis Of Enzalutamide-Isothiocyanate Hybrid Drug As Anti-Prostate Cancer Agent

Siyu Ou
Wayne State University,

DESIGN AND SYNTHESIS OF ENZALUTAMIDE-ISOTHIOCYANATE HYBRID DRUG AS ANTI-PROSTATE CANCER AGENT

by

SIYU OU

THESIS

Submitted to the Graduate School

of Wayne State University,

Detroit, Michigan

in partial fulfillment of the requirements

for the degree of

MASTER OF SCIENCE

2016

MAJOR: PHARMACEUTICAL SCIENCES

Approved By:

_____

Advisor Date

DEDICATION

To my parents for their unfailing love, support and sacrifices.

ACKNOWLEDGMENTS

First, I would like to express appreciation to my advisor, Dr. Zhihui Qin, for all the guidance, patience and encouragement which he provided throughout the duration of this project.

I would like to thank my committee member, Dr. Aloke K. Dutta and Dr. Yubin Ge, for their encouragement, insightful comments and constructive criticism.

I am also thankful to Ms. Liping Xu for the selfless teaching and help in my biological experiments.

I would also like to acknowledge Dr. Bailing Chen for the help and support as a friend and colleague.

In addition, I would like to thank my lab mate and roommate, Yi Liao for all the support.

Last but not least, I would like to thank all my friends, especially my girlfriend, for their encouragement and support.

TABLE OF CONTENTS

LIST OF TABLES

LIST OF FIGURES

LIST OF SCHEMES

Chapter 1. Introduction

1.1 Prostate Cancer

Prostate cancer (PCa) is the most common male malignancy and the second leading cause of cancer-related death in men in the U.S. The risks of getting PCa are related to ancestry, increasing age as well as the environment and lifestyle, e.g., the incidence of PCa in African Americans is twice higher than White Americans and is 15-20-fold higher than native Asian, and the risk among immigrant Asian is significantly higher than native Asian [1]. Besides, Family history of PCa is the only definite risk factor for prostate cancer. First-degree relatives of men with prostate cancer have about twice higher risk of disease compared to men in the general population [2].

Prostate-specific antigen (PSA), also known as kallikrein-3 (KLK3), is a glycoprotein enzyme encoded in humans by the *KLK3* gene. The blood PSA level in men with prostate cancer is usually increased and the PSA test was approved by the FDA for monitoring the progression of PCa in men who had already been diagnosed with the disease. PSA test, as a method for PCa screening, are able to detect the disease at an early stage. However, the clinical benefits of this screening are uncertain: the elevated PSA level doesn't necessarily mean cancer, benign prostatic hyperplasia (BPH), or an enlarged prostate since prostatitis can also raise PSA levels. Studies indicate that about 70% to 80% of men with an elevated PSA do not have cancer as determined by biopsy, and 40% to 56% will be affected by over-diagnosis leading to invasive treatment, while about 20% of men who have cancer have a normal PSA level [3, 4]. Besides, the value of PSA screening in preventing cancer-related death is also contradictory. Randomized Prostate-Cancer

Screening Trials showed no significant benefit on decreasing death rate in the U.S.[5], but did show a 20% decrease of death rate in PCa patients in Europe [6].

Since the first demonstration in 1941 by Huggins and Hodges that androgen manipulation in patients with advanced PCa has great influence on the progression of the disease [7], androgen deprivation therapy (ADT) has been a standard treatment for men with advanced PCa. ADT can be achieved by either surgical castration which removes testicles or by chemical castration which uses luteinizing hormone-releasing hormone (LHRH) agonists or antagonists to block the production of testicular testosterone via negative feedback or competitive inhibition, respectively [8]. Despite the initial effectiveness of ADT, PCa cells could develop mechanisms of resistance leading to castration-resistant PCa (CRPC) within 2-3 years of ADT [9]. Androgen receptor (AR) signaling is a driving force of PCa at all stage, including CRPC. Mechanisms to re-activate AR signaling under ADT include: 1) AR gene amplification [10, 11] or AR protein overexpression [12] to respond to low levels of androgen; 2) AR mutations (promiscuous pathway) which broaden the specificity of AR so it can be activated by molecules such as corticosteroids or clinically-used AR antagonists other than androgen [13, 14]. For example, T877S/H874Y and W741C/W741L mutations convert flutamide and bicalutamide (**Figure 1**) to AR agonists, respectively [15, 16]; 3) Alternative androgen production by increasing intratumoral androgen levels via de novo androgen synthesis. [17, 18]. FDA-approved abiraterone blocks androgen biosynthesis within testes, adrenal gland and prostate via inhibiting cytochrome P450 17A and shows clinical benefits in CRPC patients [19]; 4) Expression of AR splice variants (AR-Vs) without ligand binding domain (LBD) also contributes to the development of CRPC [20, 21]: AR-

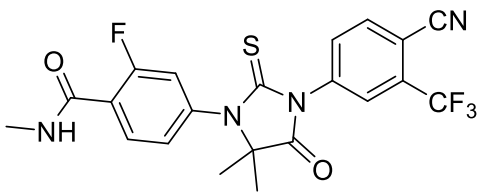

Enzalutamide

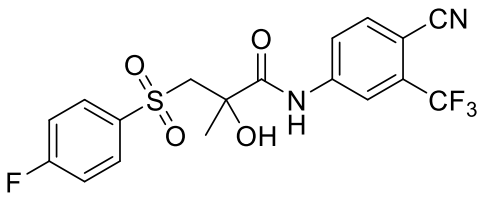

Bicalutamide

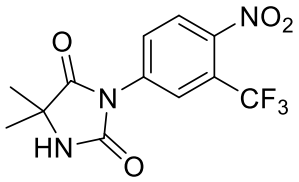

Nilutamide

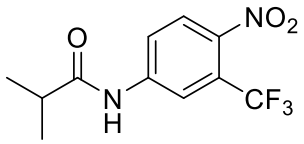

Flutamide

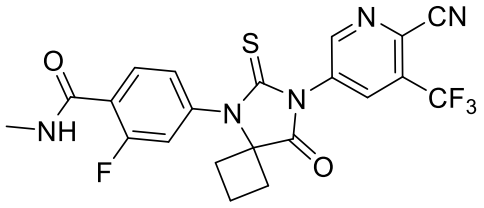

ARN-509

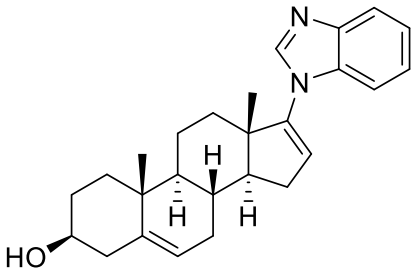

Galeterone

Figure 1. AR antagonists in clinical use or in clinical development.

Vs are constitutively active and their biological functions cannot be inhibited by conventional AR antagonists targeting LBD or by abiraterone targeting androgen biosynthesis; 5) Activation of AR in a ligand-independent manner (outlaw pathway) is also an important mechanism of resistance: examples includes growth-factor-activated outlaw pathways [22], receptor-tyrosine-kinase-activated outlaw pathways [23, 24] and

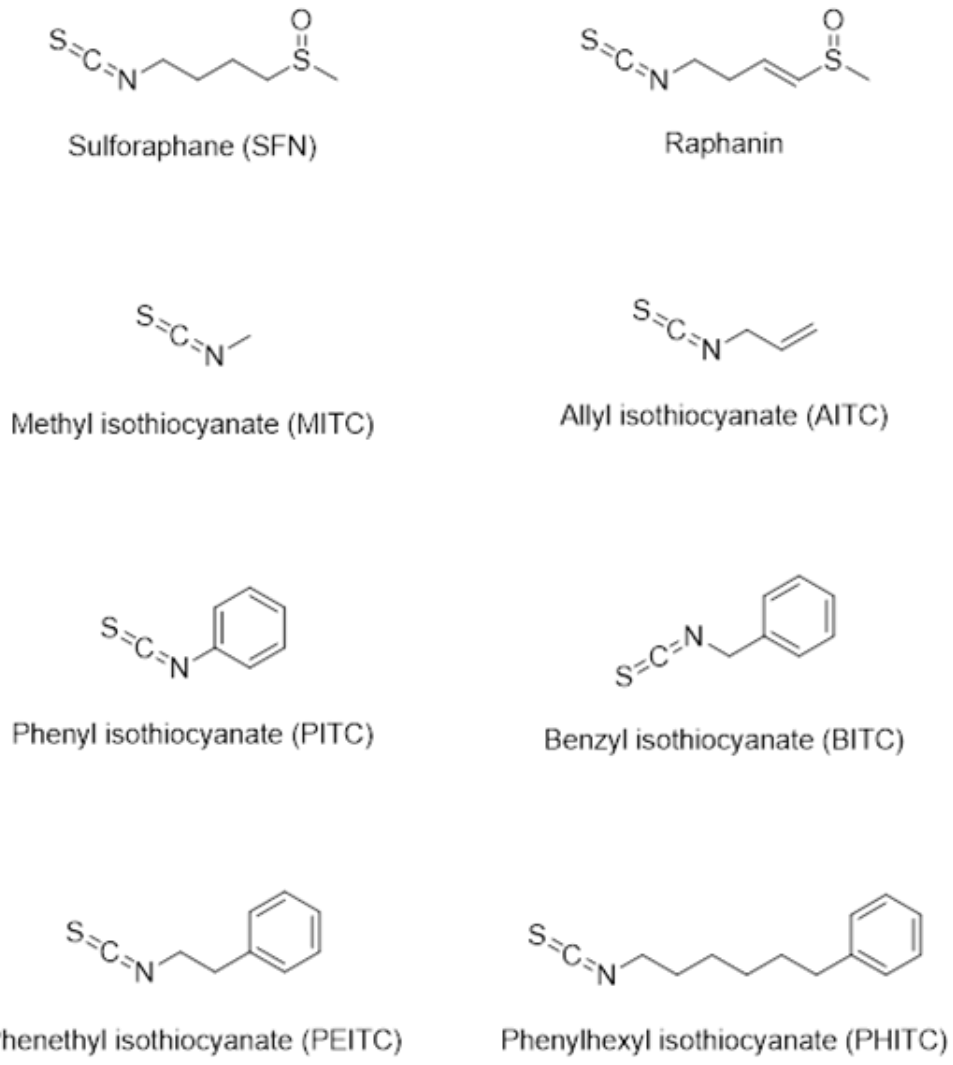

Figure 2. The chemical structures of dietary and synthetic isothiocyanate derivatives.

the activation of Akt pathway [25]; 6) CRPC can also be promoted by activation of compensatory signaling pathways which bypass AR axis, e.g. PI3K/AKT and AR signaling pathways cross-regulate each other by reciprocal feedback which means down-regulation of one pathway will activate the other [26]. Simultaneous inhibition of both pathways synergistically inhibited cancer progression [27] and delayed the emergence of resistance [28]. Because AR is the most therapeutically-relevant drug target in PCa

treatment, new AR antagonists, such as enzalutamide [29] , ARN-509 [30] and galeterone [31] (**Figure 1**) have been developed to block AR signaling pathway in CRPC patients.

1.2 Enzalutamide

Enzalutamide (Enz, **Figure 1**) is a potent AR antagonist and was approved for the treatment of metastatic CRPC. It has higher AR binding affinity (5-8 fold, [32]) compared to last-generation AR antagonists, such as bicalutamide, and doesn't induce AR nuclear translocation. Enz has multiple inhibitory functions on the AR axis: it competes androgen for AR binding, inhibits androgen-stimulated AR nucleus translocation, and inhibits liganded AR binding to DNA on the androgen response elements (ARE). Its approval was based on two successful Phase 3 clinical studies. AFFIRM trial was conducted in patients with metastatic CRPC (mCRPC) who have gone through docetaxel chemotherapy. The results indicated that Enz prolongs the median overall survival for 4.8 months compared with placebo group [33], which led to its approved by FDA in 2012 for the treatment of mCRPC after chemotherapy. Another phase 3 trial known as PREVAIL trial was focused on chemotherapy naïve mCRPC patients. Enz significantly reduced the risk of radiographic progression and significantly improved overall survival [34]. FDA further approved enzalutamide for this patient population [35]. However, acquired resistance to enzalutamide emerges after short period of treatment and patient survival benefit is short-lived. The mechanisms leading to enzalutamide resistance include AR mutations (e.g., F876L mutation converted enzalutamide into an AR agonist [36]), up-regulation of AR splice variants, glucocorticoid receptor overexpression, intracrine synthesis of androgens, crosstalk with

growth factor, neuroendocrine transformation, neuroendocrine transformation, and immune evasion [37].

1.3 Dietary Isothiocyanates

Isothiocyanates (ITCs) (**Figure 2**) are active metabolites of glucosinolates from cruciferous vegetables (e.g. broccoli, cabbage, watercress). Epidemiological studies suggest a correlation between high intake of cruciferous vegetables and low incidence of PCa [38, 39]. ITCs have been demonstrated as one of the major dietary components contributing to this benefit.

Sulforaphane (SFN) is one of the ITCs that has both chemopreventive and therapeutic activities against PCa [40]. It is generated from the myroinase-catalyzed hydrolysis of glucoraphanin [41] (**Figurer 3**). Epithiospecifier protein (ESP), a protein also presented in broccoli, leads to the formation of SFN nitrile which has no anticarcinogenic activity [42]. Gentle heating decreases ESP activity and could increase SFN formation while excessive heating denatures myroinase, thus decreases conversion of glucoraphanin to SFN (**Figure 3**) [43]

After intake into the body, SFN is metabolized through the mercapturic acid pathway. SFN first conjugates with GSH by glutathione S-transferases (GSTs). Then with the help of γ-glutamyl-transpeptidase (GTP) and cysteinyl-glycinease (GCase), glutamic acid and glycine residues of GSH are removed to form SFN-Cys conjugate. Finally, *N*-acetyltransferase (NAT) acetylates cysteine conjugate to form SFN-NAC which is then getting into systemic circulation via active transportation and is excreted in urine (**Figure 4**).

The epidemiological relationship between cruciferous vegetables and PCa triggered extensive studies to illustrate the mechanisms behind the anti-prostate cancer activity of SFN and other ITCs, such as PEITC, BITC, etc. [44]. A phase 2 clinical study testing SFN-rich broccoli sprout extracts in men with recurrent prostate cancer was completed recently [45], although the treatment regimen (200 μmoles/day of SFN-rich extracts, up to 20 weeks) did not lead to ≥50% PSA declines in the majority of patients, the on-treatment PSA doubling time was significantly lengthened (9.6 months vs. 6.1 months) without Grade 3 adverse events, indicating a promising safety profile and a potential for further dose escalation. The biological effects and potential molecular targets of SFN (or other ITCs) in prostate cancer cells are briefly reviewed as follows.

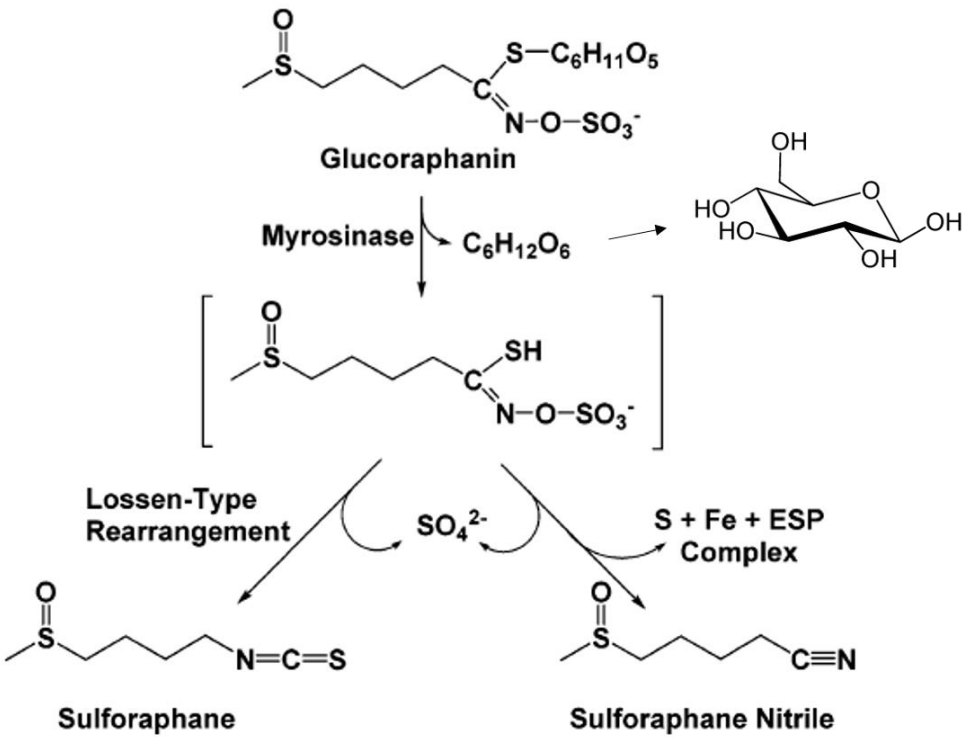

Figure 3. Mechanism for the formation of sulforaphane and sulforaphane nitrile in broccoli florets and sprouts. Myrosinase catalyzes transformation of glucosinolate to SFN.

1.3.1. Observed Anticancer Effects of SFN

Induction of cell cycle arrest

SFN (20 μM) induced S phase arrest due to down-regulation of cyclin D1, cyclin E, Cdk4, and Cdk6 proteins in LNCaP cell [46]. SFN also induced G_2/M arrest by activation of Chk2-mediated phosphorylation of Cdc25C in PC-3 or JNK-mediated signaling in DU145 cells [47, 48].

Induction of apoptosis

SFN-induced apoptosis in PC-3 cell was associated with up-regulation of Bax,

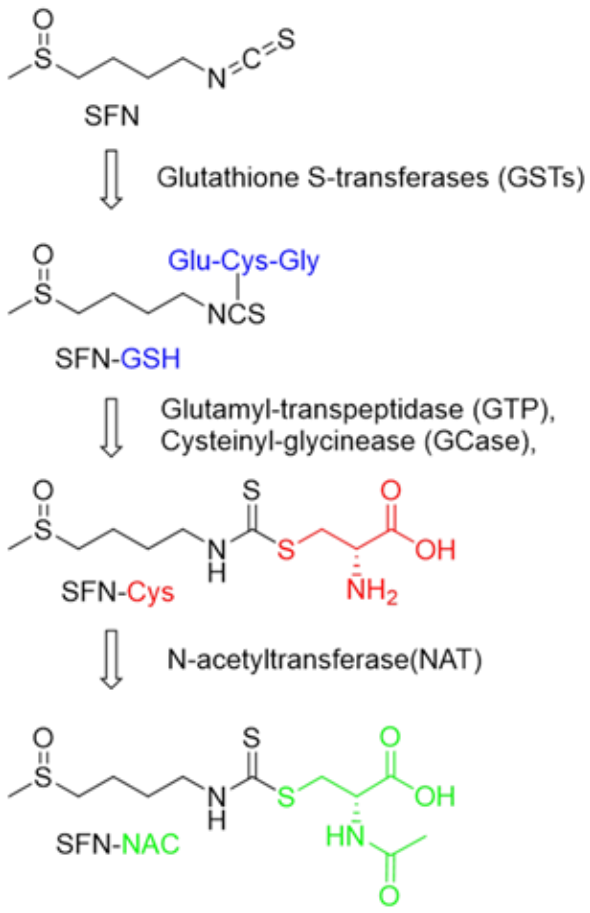

Figure 4. Mecaputuric acid pathway. SFN is metalized by various enzymes to become SFN-NAC conjugate.

down-regulation of Bcl-2 and activation of caspases-3, -9 and -8 [49]. SFN treatment results in decreased protein levels for inhibitor of apoptosis (IAP) family members (cIAP1, cIAP2 and XIAP) and nuclear factor κB (NFκB) in PC-3 cells, and increased protein levels for Apaf-1 in both PC-3 and LNCaP cells [50]. Survivin which is an inhibitor of apoptosis and a mitosis regulator is down-regulated by SFN in PC-3 cells [51].

Inhibition of migration and metastasis

Epithelial-mesenchymal transition (EMT) is a biological process by which epithelial cells are polarized to gain enhanced ability of migration, invasion, resistance to apoptosis and production of microenvironment extracellular matrices (ECMs) components to become mesenchymal cell phenotype [52]. EMT is involved in the cancer progression and is responsible for the metastasis of cancer, including PCa[53]. E-cadherin as a tumor suppressor is critical for the formation and maintenance of adherent junctions between epithelial cells. Loss of E-cadherin expression is an important factor leads to EMT-associated invasion and metastasis [54]. In cancer cells, overexpression of onco-protein ERG causes up-regulation of its downstream target chemokine receptor type 4 gene (CXCR4) which is positively correlated with the cell motility [55]. CXCR4 has recently been identified as a novel target of SFN in PCa cells: treatment of LNCaP, 22Rv1, C4-2 and PC-3 cells with SFN (5 μM, 12 h) resulted in down-regulation of CXCR4 and inhibition of cell migration [56]. Labsch *et al*. demonstrated that SFN, particularly in combination with TNF-related apoptosis-inducing ligand (TRAIL), reduces the levels of proteins required for EMT and cell migration in PC-3 and DU145 cells [57]. A recent study also indicated that SFN inhibits invasion of PCa (DU145 cells)

by activating ERK1/2 to up-regulate E-cadherin and down-regulate CD44v6, which further leads to reduced matrix metalloproteinase-2 (MMP-2) expression and activity [58].

Inhibition of cancer stem cells

Cancer stem cells (CSCs) refers to a subset of tumor cells that possess characteristics of normal stem cells but are responsible for tumor initiation, metastasis, resistance and relapse due to self-renewal, multi-lineage differentiation and resistance to chemotherapy and radiation therapy [59-61]. SFN was reported to inhibit breast CSCs both *in vitro* and *in vivo* [60]. The aldehyde dehydrogenase (ALDH)–positive breast CSCs was decreased by SFN via daily injection (50 mg/kg, 2 weeks) in a mouse model. The inhibition of breast CSCs by SFN is potentially due to down-regulation of the Wnt/β-catenin self-renewal pathway [60]. Kallifatidis *et al.* indicated that SFN increases drug-induced toxicity toward CSCs in both prostate and pancreatic cancer. In vivo, the combination of SFN and gemcitabine completely abolished growth of pancreatic CSC xenografts and tumor-initiating potential without induction of additional toxicity [59]. SFN was reported to inhibit prostate CSC properties, e.g., inhibiting the expression of Nanog, SOX2, CXCR4, Jagged1 and notch 1; it also disrupts TRAIL-caused NF-κB binding; a combination of SFN and TRAIL effectively suppressed tumor engraftment and tumor growth without obvious adverse effects *in vivo* [57].

1.3.2. Cellular Targets of ITCs

The pleiotropic anticancer effects of SFN and other dietary ITCs are derived from their interactions with various cellular targets. The ITC functionality, which is a biological-tolerable electrophile in certain dosage range, is capable of conjugating with cellular glutathione (GSH), protein thiols and other nucleophilic amino acid residues.

These fundamental chemical properties determine the interactions of ITCs with their cellular targets , leading to the aforementioned cellular effects [62]. In the following section, we focus on the influence of SFN on histone deacetylase (HDAC) and heat shock protein 90 (Hsp90). Both HDAC inhibition and Hsp90 disruption are effective ways to antagonize AR functions in PCa cells.

Inhibition of HDACs

HDAC are a class of enzymes that remove the acetyl group from lysine residues of histones or non-histone proteins. HDACs can be classified into four classes: class I (HDAC1, HDAC2, HDAC3, and HDAC8), class II (HDAC4, HDAC5, HDAC7, and HDAC9 in the IIa subclass, and HDAC6 and HDAC10 in the IIb subclass), class III (Sirt1 to Sirt7), and class IV (HDAC11) [63]. Class I, II and IV are zinc dependent enzymes. HDACs are abundantly expressed in prostate cancer [64] and play important roles in the regulation of the AR [65]. HDAC1 is up-regulated in both androgen sensitive and hormone refractory prostate cancer cells, leading to significant enhancement of cell proliferation [66]. It has also been reported that HDAC2, HDAC3 and HDAC8 are overexpressed in cancer tissues compared to normal epithelium [67]. Up-regulated SIRT1 expression was found in androgen-refractory PC-3 and DU145 cells compared to androgen-sensitive LNCaP cells [68]. HDAC inhibitor (HDACi) LAQ824 were found to decrease AR protein levels in PCa cells via inhibition of HDAC6, which causes increased proteasomal degradation of AR [69, 70]. Another HDACi SAHA (**Figure 5**) inhibits AR at the transcriptional level to reduce AR mRNA production [71], Consequently, HDACis have been clinically tested for the treatment of CRPC. Although multiple HDACis have been approved for the treatment of lymphoma and myeloma, e.g. vorinostat (i.e. SAHA)

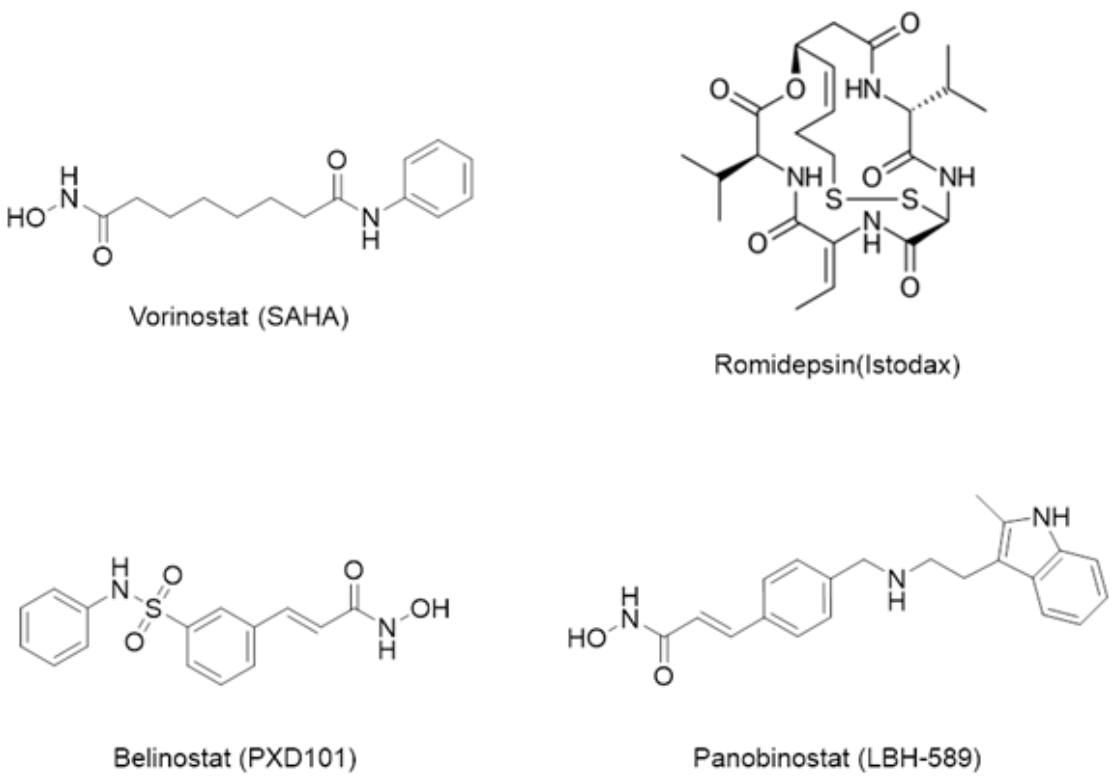

Figure 5. The structures of FDA-approved HDAC inhibitors

and romidepsin for cutaneous T cell lymphoma, belinostat for peripheral T cell lymphoma and panobinostat for multiple myeloma, all the clinical trials of HDACis for solid tumors (including prostate cancer) failed due to lack of efficacy and systemic side effects (*e.g.*, cardiovascular toxicity).

The HDAC inhibition activity of SFN was first reported by Myzak et al.: SFN dose-dependently (3, 9, 15 μM) increased TOPflash activity which is inversely correlated with the HDAC activity. Both global and localized histone acetylation were increased by the treatment of SFN. It was also indicated that the cysteine and *N*-acetylcysteine metabolites of SFN had HDAC inhibition activity while SFN itself and glutathione conjugate didn't [72]. This work proposed a chemistry foundation of ITC-caused HDAC inhibition. The similar effect was found in prostate epithelial cell lines BPH-1, LNCaP

and PC-3, SFN (15 μM) decreased HDAC activity in all the three cell lines by 30-40% with 50-100% increase in acetylated histone [73].

HDACi activity of SFN was also demonstrated *in vivo*. Significant inhibition of HDAC activity and increase in acetylated histones H3 and H4 in the colonic mucosa were observed when mice were treated with a single oral dose of 10 μmol SFN. Long-term dietary treatment increased acetylated histones and $p21^{WAF1}$ in multiple tissues including prostate. Tumor multiplicity in Apc^{min} mice was also suppressed by SFN with increased acetylated histones in the promoter regions of the *P21* and *Bax* genes [74]. Besides, daily consumption of 7.5 μmol per animal of SFN for 21 days suppressed growth of human PC-3 cells in male nude mice as well as HDAC activity in xenografts, prostate and mononuclear blood cells (MBC) [75]. A single dose of 68g broccoli sprouts inhibited HDAC activity in peripheral blood mononuclear cells (PBMC) in human subjects [75]. These works demonstrated bioavailability and tissue accumulation of SFN in experimental animal models and in human subjects.

HDAC6 is a zinc-dependent, class-IIb HDAC enzyme and locates in cytoplasm due to the presence of nuclear export signals (NES) and serine-glutamine-containing tetradecapeptide modules [76]. A portion of HDAC6 physically associates with Hsp90 and functions as an Hsp90 deacetylase [77], and deacetylated Hsp90 can chaperone and stabilize its client proteins [78]. The mechanism of SFN to antagonize AR was proposed by Gibbs et al. Their study found that SFN (10-20 μM) can inhibit HDAC6 enzymatic activity, reduce HDAC6 protein levels and cause hyperacetylation of Hsp90, leading to dissociation of AR from Hsp90. The dissociated AR was subjected for proteasomal degradation [79] (**Figure 6**).

Direct interactions between SFN and Hsp90

In addition to inhibiting HDAC6 and causing Hsp90 hyperacetylation, direct interactions between SFN with Hsp90 were also reported. As electrophilic compounds, ITCs (including SFN) may covalently modify Hsp90 on surface-exposed nucleophilic amino acid residues and disrupt its biological functions. By using nuclear magnetic resonance spectroscopy and LC-MS peptide mapping methods, SFN (around 15 μM) was found to be covalently attached to the *N*-terminal domain of Hsp90 and this modification attenuated the interaction of Hsp90 with a co-chaperone Cdc37, which promoted the proteasomal degradation of Hsp90 client proteins such as Akt and Cdk4, resulting in cell death in a pancreatic cancer model [80]. In another study, an SFN analogue 6-HITC (25μM) was incubated with human recombinant Hsp90β. Proteomics analysis showed that 6-HITC formed covalent adduct with Cys-521 amino acid residual of Hsp90. Interestingly, through a transthiocarbamoylation mechanism, even conjugation with a

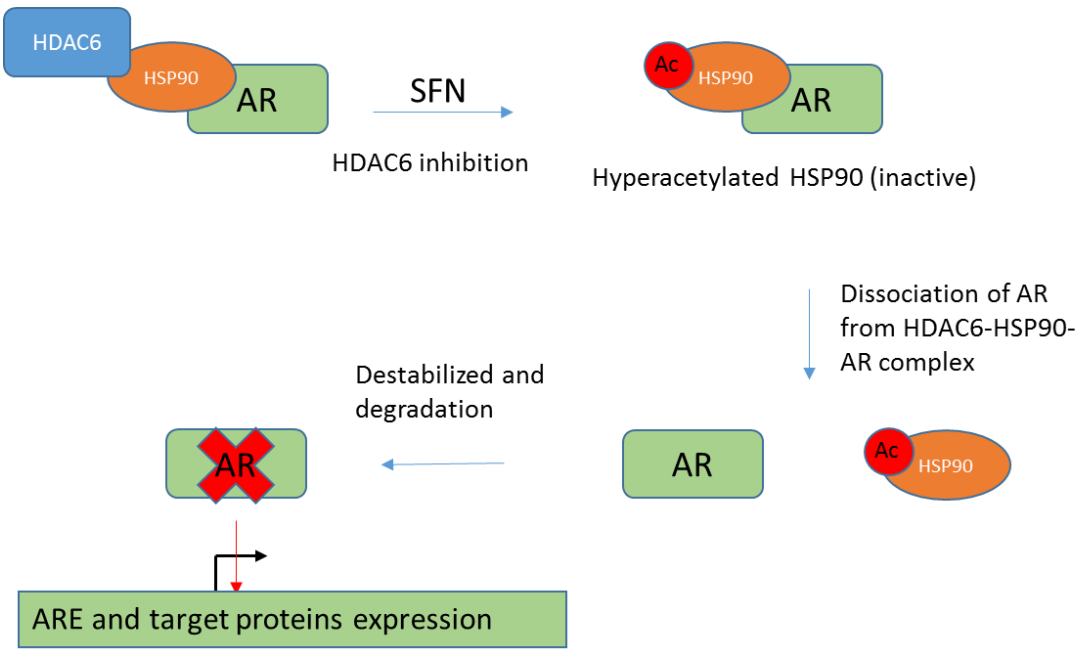

Figure 6. SFN attenuate AR signaling via HDAC6 inhibition.

small molecule thiol cannot abrogate the capability of 6-HITC to modify cysteine residues of cellular proteins [81]. SFN mimetic, sulphoxythiocarbamates, were also found to form cysteine adducts with recombinant Hsp90β, which caused degradation of client proteins in MCF-7 cell (RAF1, HER2, CDK1, CHK1, etc.) and inhibited MDA-MB-231 breast cancer cell proliferation [82]. These results suggest that electrophilic compounds, such as ITC, can be used to target the cysteine residues or other nucleophilic amino acid residues of Hsp90, drug-protein adducts formation would lead to degradation of client proteins and growth inhibition of cancer cell.

Chapter 2. Rationale and Experimental Design

2.1. Rationale

Androgen receptor (AR), especially mutated full length AR and truncated AR-Vs, are major driving forces of CRPC. An agent that can effectively compete androgen binding, meanwhile down-regulating AR/AR-Vs and AR compensatory pathways will certainly advance CRPC treatment. In addition to inducing the degradation of full length AR, recent study also suggested that disrupting Hsp90 could down-regulate AR-Vs: although AR-Vs are not Hsp90 client proteins, the mRNA splicing process could be

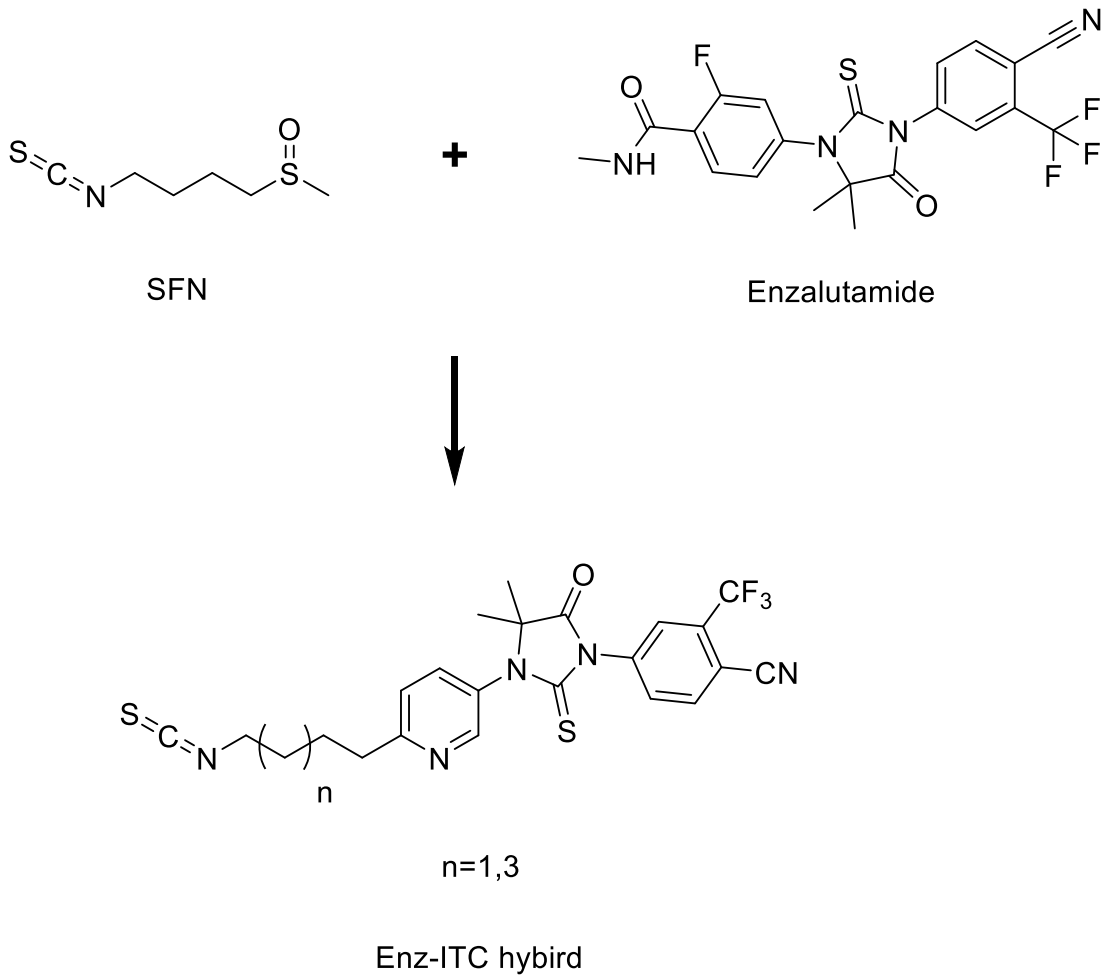

Figure 7. The structures of proposed Enz-ITC hybrids.

negatively influenced by heat shock response, a typical cellular adaption to Hsp90 inhibition [83]. Considering the biological connections of AR and Hsp90 as well as the pharmacological properties of enzalutamide (Enz) and dietary ITCs, we have designed a class of Enz-SFN hybrid compound (**Figure 7**) to target AR-Hsp90-HDAC6 complex as a way to achieve aforementioned therapeutic goals, i.e. antagonizing AR function and simultaneously down-regulating compensatory onco-proteins, such as Akt which are also chaperoned by Hsp90.

We **hypothesized** that an Enz-like, high affinity AR ligand could be used as vehicle to concentrate ITC components to AR-overexpressing CRPC tumors and then intracellularly deliver ITC to AR-Hsp90-HDAC6 complex. The locally concentrated ITC could more efficiently disrupt Hsp90 by either inhibiting a pool of AR-associated HDAC6 or by covalently modifying Hsp90, which further triggers Hsp90 dysfunction and degradation of AR and other oncogenic client proteins, such as HDAC6 and Akt (**Figure 8**). The **goal of this thesis** is to establish an efficient synthetic route toward AR

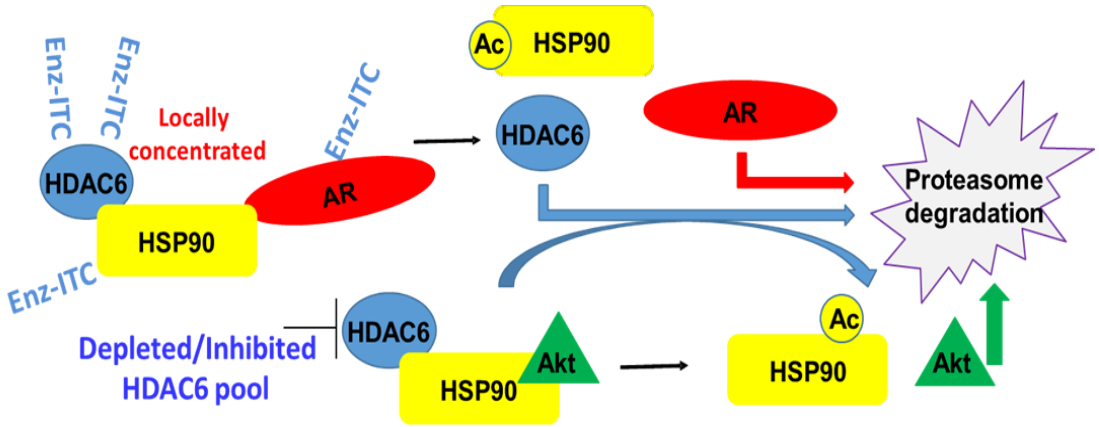

Figure 8. Proposed mechanism of AR-directed HDAC6/Hsp90 inhibition by Enz-ITCs.

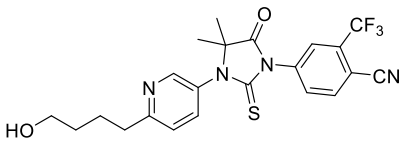

9a (C4-OH)

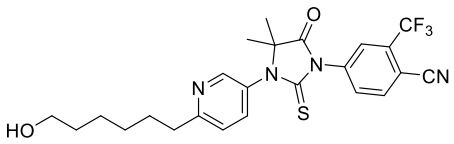

9b (C6-OH)

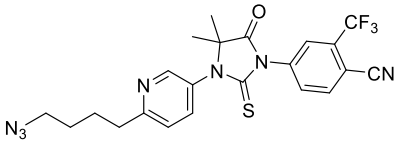

11a (C4-N_3)

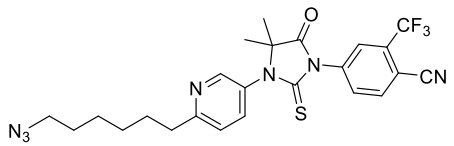

11b (C6-N_3)

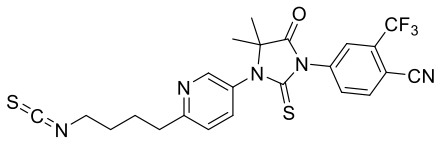

12a (C4-ITC)

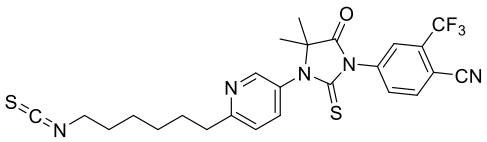

12b (C6-ITC)

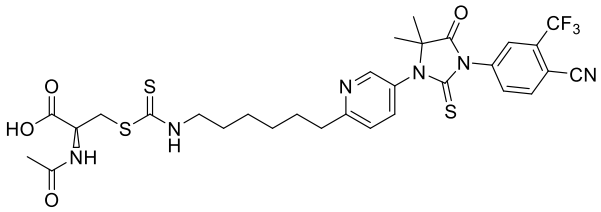

13 (C6-NAC)

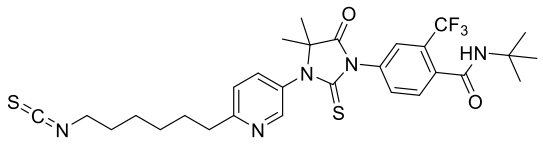

19 (C6-amide-ITC)

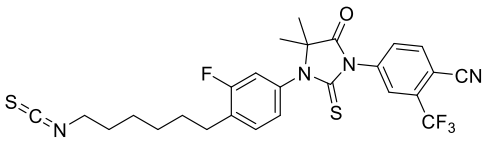

30

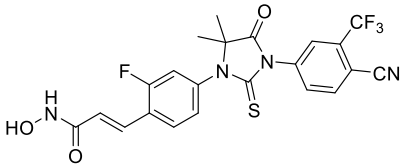

1005

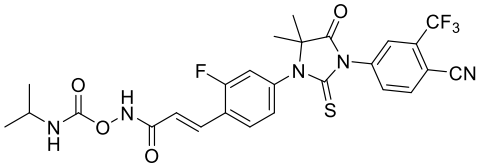

29 (1005pro)

Figure 9. The chemical structures of synthetic targets.

ligand (Enz)-ITC hybrids and preliminarily investigate their effects on the growth and the function of AR, such as transcriptional activity and expression levels in representative prostate cancer cell lines.

2.2. Experimental Design

2.2.1. Chemistry

Previous SAR [84] and our molecular docking of Enz to AR suggested that the trifluoromethyl benzonitrile ring points inside the AR binding cavity in LBD and cyano group is essential for AR binding by forming hydrogen bonds (H-bonds) with Arg752 and Gln711. Thiohydantoin ring of Enz is in its optimized form from an extensive SAR study [29] and was kept intact in our molecular design. This conformationally restricted ring forces the rest of the molecule extend outside the AR pocket and point to a "H11 pocket", a region near the C terminus of helix 11 and the loop connecting helices 11 and 12 [36]. Based on this predicted AR binding mode, we decided to introduce ITC group on fluorobenzene ring which points toward the opening of AR binding pocket where enough space is available to accommodate ITC moiety. We also replaced fluorobenzene ring of Enz with a pyridine ring, supported by the lowered cLogP values (6.29 of compound **12b** vs 7.93 of compound **30**, **Figure** 9), we hypothesized that this modification would improve water solubility of Enz-ITC hybrid drug and would not interfere AR binding.

The chemical reactivity of ITC is a critical factor to influence its biological effects. A general observation is that the chemical reactivity of an arylalkyl ITC is reduced with increasing the length of carbon chain, in another word, an arylalkyl ITC with a relative longer chain (up to six methylene units) is more stable and may achieve better *in vitro*

potency/*in vivo* efficacy for chemoprevention or anticancer effects [85]. To modulate ITC in hybrid drugs, we designed two Enz-ITC hybrids with four-carbon (compound **12a**) and six-carbon chain (compound **12b**), respectively (**Figure** 9). Since we hypothesized that the cellular effects of ITC could be locally directed to Hsp90-AR complex by an AR ligand, compound **19** which is a close structural analogue of **12b** (C6-ITC) was designed to investigate the directing effect of AR. The cyano (CN) group, which forms H-bond with AR, was converted to *t*-Butyl amide to eliminate AR binding property from compound **12b**. It worth to mention that **19** and **12b** have similar LogP values (6.37 and 6.39, respectively), suggesting similar lipophilicity and potentially close intracellular accumulation of these two compounds. If AR affinity plays a role in the cellular effect of **12b** (C6-ITC), **12b** should be more effectively disrupt Hsp90 and causes AR degradation at a lower concentration compared to **19** and SFN. The comparison of **12b** with a synthetic intermediate **11b** (C6-N_3) will also be made using kb2-cell-based ARE luciferase assay. **12b** and **11b** has identical chemical structure except the ITC (N=C=S) moiety in **12b** and chemically inert azide group (N=N=N) in **11b**. We envisioned that **11b** is an ideal **12b** analogue to study the AR antagonist activity of the chemical scaffold shared by **12b** and **11b**. Compound **11b** is expected to display Enz-comparable AR antagonist activity in ARE-luciferase assay.

The *N*-acetyl cysteine (NAC) conjugates are the ultimate metabolites of many dietary ITCs. It should be noted that ITC-NAC conjugates are still biologically active, comparable to parental ITCs [86, 87]. NAC conjugates could be seen as a carrier of ITC in systemic circulation. At least three mechanisms have been proposed to understand the bio-effectiveness of ITC-NAC: 1) ITC-NAC and parental ITC forms equilibrium in

biological matrix [88], the NAC conjugate acts as a pool to release ITC; 2) The NAC conjugate directly acts as a HDAC inhibitor, in contrast to parental compound [72]; and 3) ITC-NAC directly modify protein thiols via transthiocarbamoylation reaction [81]. Based on these reported mechanisms, we also designed and synthesized compound **13**, the NAC conjugate of **12**. In our opinion, there are at least three potential advantages for **13**: 1) increased water solubility; 2) direct HDAC inhibition; and 3) reduced plasma protein binding in circulation which may improve *in vivo* efficacy.

As a moderate electrophile, the interactions between ITC and cancer cells are complicated, multiple cellular targets could be hit. Although this might be a reason for

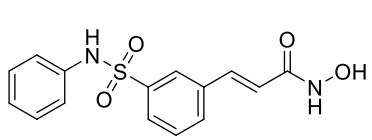

Belinostat

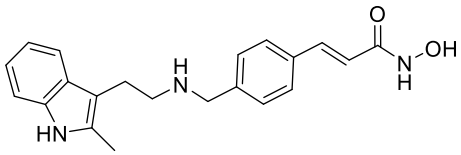

Panobinostat

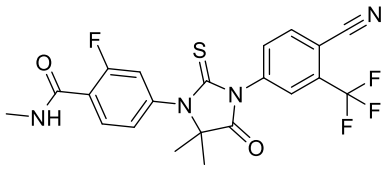

Enzalutamide

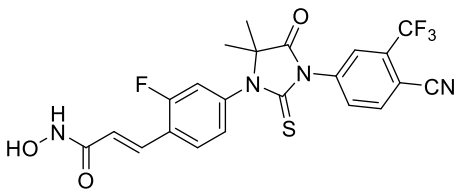

1005

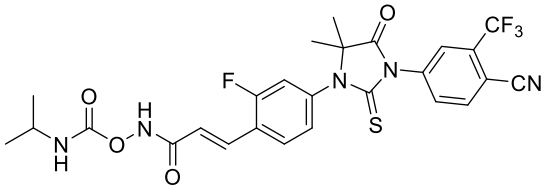

1005pro

Figure 10. The chemical structures of proposed Enz-HDACi hybrid and its prodrug.

ITCs (e.g., SFN) to display broad anticancer effects in various cancer types (including PCa), the lack of specificity of ITC may lead to moderate potency and undesired side effects if used at high dose range. In this thesis, we proposed to use an Enz-derived AR ligand to localize ITC's effects at AR-Hsp90-HDAC6 complex as way to improve the potency and specificity of ITC. From this angle, another relevant but different strategy to target AR-Hsp90-HDAC6 axis is to use a conventional HDACi pharmacophore instead of ITC. The comparisons between the two classes of compounds, Enz-ITC *vs.* Enz-HDACi on AR degradation, Hsp90 disruption and growth inhibition of PCa cells, will enable the mechanistic dissection of the cellular actions of Enz-ITC series. To preliminarily explore Enz-HDACi class, we designed compound **1005** and its carbamate prodrug **1005pro (29) (Figure 10)**. A three-carbon cinnamyl linker was used to link the Enz moiety with hydroxamic acid, a typical and potent zinc binding group for HDAC inhibition. The cinnamyl linker is frequently used in the design of HDACis, as seen in FDA-approved panobinstat and belinostat. Because hydroxamic acid is known to be metabolic labile due to phase 2 conjugation and has poor permeability to penetrate solid tumor [89], we also converted **1005** to a carbamate prodrug according to a published procedure [90] with an intention to avoid these liabilities. The carbamate bond is expected to be hydrolyzed by esterases inside the cell to release **1005**. The interactions of **1005** with AR and HDAC6 are supported by our molecular docking results.

2.2.2. Biological Evaluation

To demonstrate AR directing hypothesis, we need to firstly investigate if the hybrid scaffold keeps the AR affinity as well as AR antagonistic activity. We planned to use dihydrotestosterone (DHT)-stimulated LNCaP cell growth inhibition and MDA-Kb2

cell based ARE luciferase assays for this purpose. The growth of androgen-sensitive PCa cell line, e.g. LNCaP, is stimulated by androgen such as DHT, and AR antagonist (e.g., Enz) would block such growth stimulation. If the Enz-ITC hydroxyl analogue **9** with no ITC activity could reverse the stimulation, then the result would partially supports the AR antagonist property of the hybrid. A more direct ARE-luciferase assay was utilized to characterize the interactions of a small molecule ligand with AR. MDA-kb2 cell line, a breast cancer MDA-MD-453 cell line derivative, expresses high levels of AR and is permanently transfected with an androgen-responsive luciferase reporter plasmid. It responses to androgen and produce luminescence after incubation with a luciferase substrate [91]. By measuring the luciferase activity of drug-treated cells in the presence of DHT, we could clearly know the influence of drug on the transcriptional activity of AR. We intend to use ARE luciferase activity as a readout of the interactions between an AR ligand and the receptor. A high-affinity AR antagonist is expected to more effectively inhibit luciferase activity compared to a low-affinity antagonist.

By comparing with SFN and analogues without AR binding, we also investigated if the proposed Enz-ITC hybrid could more effectively cause degradation of Hsp90 clients, such as AR and Akt in AR+ LNCaP cells. Western blot analysis was performed to determine the change of protein levels for AR and Akt. In addition to Hsp90 clients, because ITCs has been reported to be cellular HDACis [44], acetylated histone 3 (Ac-H3), acetylated histone 4 (Ac-H4) and acetylated tubulin (Ac-Tub) which are markers representing globe HDACi activity in nuclear and cytosol respectively, was examined via western blot analysis and was correlated with the cellular protein levels of AR.

Then overall anticancer effects of Enz-ITC hybrid were tested on both androgen-sensitive (LNCaP) and androgen-insensitive (22Rv1 and PC-3) PCa cell lines using MTT assay and compared with those of SFN and Enz, the parental compounds. Among these cell lines, LNCaP and 22Rv1, both express full length, mutated AR, while 22Rv1 also express AR splice variants (e.g., AR-V7); androgen-insensitive PC-3 doesn't express AR [92].

In addition to PCa, Enz has the potential to be used for breast cancer treatment [93]. As a starting point to test tolerability of Enz-ITCs in noncancerous cells, we chose a noncancerous breast cancer cell line MCF-10A as cell culture model. Comparisons were made between Enz-ITCs and SFN in MCF-10A cells using MTT assay.

2.2.3. Molecular Docking of Enz-ITC with AR

Molecular docking is an important methodology in modern drug discovery to understand the interactions of a ligand with its protein target. We used molecular docking to examine the AR binding of proposed hybrid.

AR belongs to the nuclear receptors superfamily and consists of five domains: N-terminal regulatory domain contains the activation function 1 (AF-1) which functions independent of ligand biding. DNA-binding domain (DBD) binds to specific androgen response elements (ARE) on DNA to transcript target genes upon hormone activation. Ligand binding domain (LBD) is responsible for hormone binding, dimerization process and includes a ligand dependent transcriptional activity (AF-2). Hinge region is a flexible domain that connects the DBD with the LBD which includes a part of the nuclear localization signal [94, 95]. Androgen binding activates AR and results in a conformational change of the receptor which leads to dissociation of AR from cytosolic

heat shock proteins, dimerization and translocation to nucleus. Then DBD interacts with ARE as a homodimer to recruit transcription machinery and transcript AR-regulated target genes [95]. Revealed by X-ray diffraction structures of several nuclear receptors complexed with their antagonists, the receptor antagonism is caused by antagonist-induced displacement of helix 12 from its hormone-bound configuration and distortion of coactivator binding site [84]. It has been suggested that nuclear receptor family shares similar structure, function and mechanism, however, the conformation of antagonistic AR has not been experimentally resolved. Due to the distinct conformational difference between AR agonistic and antagonistic forms, traditional molecular modeling method such as “flexible ligand-rigid protein” and “induced fit docking” are not suitable for the study of the interactions of AR with a given antagonist. Although molecular dynamic (MD) simulation is theoretically competent, dramatic AR conformational transformation between agonistic and antagonistic forms make the simulation extremely time and computational power consuming.

Homology modeling is a method that could achieve a balance between computational power and precise result [96]. Homology modeling technique constructs an atomic-resolution model of target protein with known amino acid sequence based on the three-dimensional structure of homologous protein (template). This method is based on the observation that proteins with similar sequences usually possess similar 3D structures because protein tertiary structure is better conserved than amino acid sequence. Wilkinson’s study [97] suggested that glucocorticoid receptor (GR) and mineralocorticoid receptor (MR) are more suitable 3D templates for AR. However, the structure of MR in antagonist form is not currently available. Combining with the

experience of Pepe's group [96], we decided to use antagonistic GR structure (PDB code: 1NHZ) [98]) as the template for homology modeling. The molecular docking was performed by using Glide software (trial version).

Chapter 3. Result and Discussion

3.1. Chemistry

3.1.1. Synthesis of Enz-ITC (Compound 13)

The synthesis of Enz-ITC hybrid is described in . Four- or six-carbon chain was first introduced to pyridine ring through Sonogashira coupling to generate **3**. To prevent the potential interferences in following steps, the hydroxyl group of **3** was protected with methoxymethyl acetal (MOM) protecting group. Then nitro group and alkyne were reduced through catalytic hydrogenation to afford aromatic amine **5** which was alkylated by **6** in the presence of sodium acetate in ethanol. Because of the low reactivity of the aromatic amine, the alkylation reaction was refluxed for 10 days to achieve a reasonable yield (73%). Several methods were reported for the synthesis of thiohydantoin ring [99-101], here we used **21** which was prepared by mixing **20** with thiophosgene to react with **7** in DMSO at 80 ℃ to generate the cyclization product **8** with good yield (90%). MOM protecting group was removed by using hydrochloric acid, then the free hydroxyl group was activated to form methanesulfonate **10**. Azide moiety was then installed by substitution of the highly active methanesulfonyl group with sodium azide to give **11**. The azide intermediate **11** was converted to ITC via a one-pot two-step procedure [102]: triphenylphosphine (PPh_3) reacted with the azide to generate phosphazide or iminophosphorane intermediates which further reacted with carbon disulfide (in excess) to afford Enz-ITC **12**. Conjugation of **12b** with NAC in the presence of sodium bicarbonate afforded the NAC conjugate **13**.

Scheme 1. Synthesis of Enz-ITC hybrid

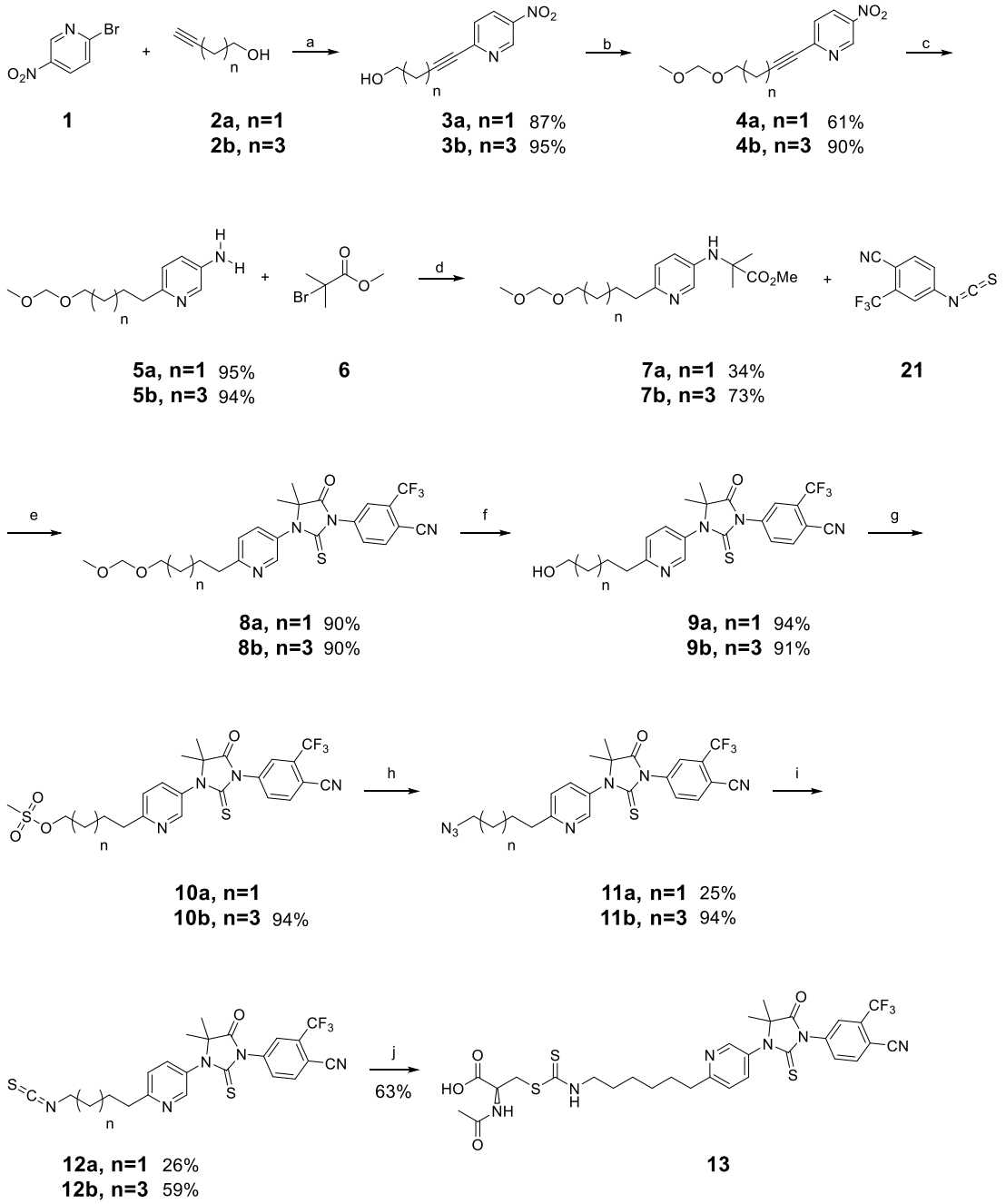

Reagents and conditions: (a) CuI, $Pd(PPh_3)_2Cl_2$, TEA, CH_3CN, rt, 2 h; (b) DIPEA, MOMBr, THF, rt, 6 h; (c) H_2, Pd/C, rt, overnight. (d) NaOAc, EtOH, reflux, 10 d; (e) DMSO, 80°C, overnight; (f) HCl, MeOH, 3 h; (g) TEA, MsCl, DCM, rt, 30 min; (h) NaN_3, DMF, rt, 6 h; (i) 1. PPh_3, THF, reflux, overnight; 2.CS_2, THF, reflux, 5 h; (j) NAC, $NaHCO_3$, 45°C, overnight.

Purification of NAC conjugate **13** was not straightforward. Although the

conjugation reaction was smooth and clean when NAC was used in excess, it was difficult to separate **13** from remained NAC by using either column chromatography or preparative TLC. Rf values of NAC and **13** are extremely close on the TLC plate with about 80% overlaps. We could not get a clean NMR spectrum even after repetitive purifications. Because of their differences in water solubility, we also dissolved crude **13** in ethyl acetate or DCM, tried to wash NAC away with water. The procedure was not successful at the beginning: the water and organic phases couldn't be separated during work up despite using different organic phases and long hours of standing. This inconvenience was a reflection that **13** might function as an emulsifier due to the presence of both lipophilic AR ligand and hydrophilic NAC moieties in the same molecule. To our delight, an unexpected separation was achieved after storage of the washing mixture at -20℃ overnight. The water phase containing NAC was frozen and was removed by pouring organic phase to another flask to evaporate. **13** with desirable purity was finally obtained for subsequent biological studies.

In order to study whether AR affinity plays a role in the biological effects of Enz-ITC, we proposed to prepare compound **19** as a critical control (**Scheme 2**). To synthesize this molecule, cyano group of intermediate **8b** need to be converted to *tert*-Butyl amide analogue **19** by *tert*-Butyl acetate in the presence of sulfuric acid. We expected that the acidic condition would also simultaneously remove the acid-labile MOM protecting group. Indeed, as shown in proton NMR spectrum, single peak of *tert*-Butyl group (δ 1.43, s, 9H, three methyl groups) emerged accompanied by the loss of MOM peaks (δ 4.60, s, 2H; 3.34, s, 3H). However, it came to our attention that an extra acetyl peak (3H) at 2.00ppm was observed in proton NMR, which made us suspect that

Scheme 2. Synthesis of Enz-ITC amide analogue 19

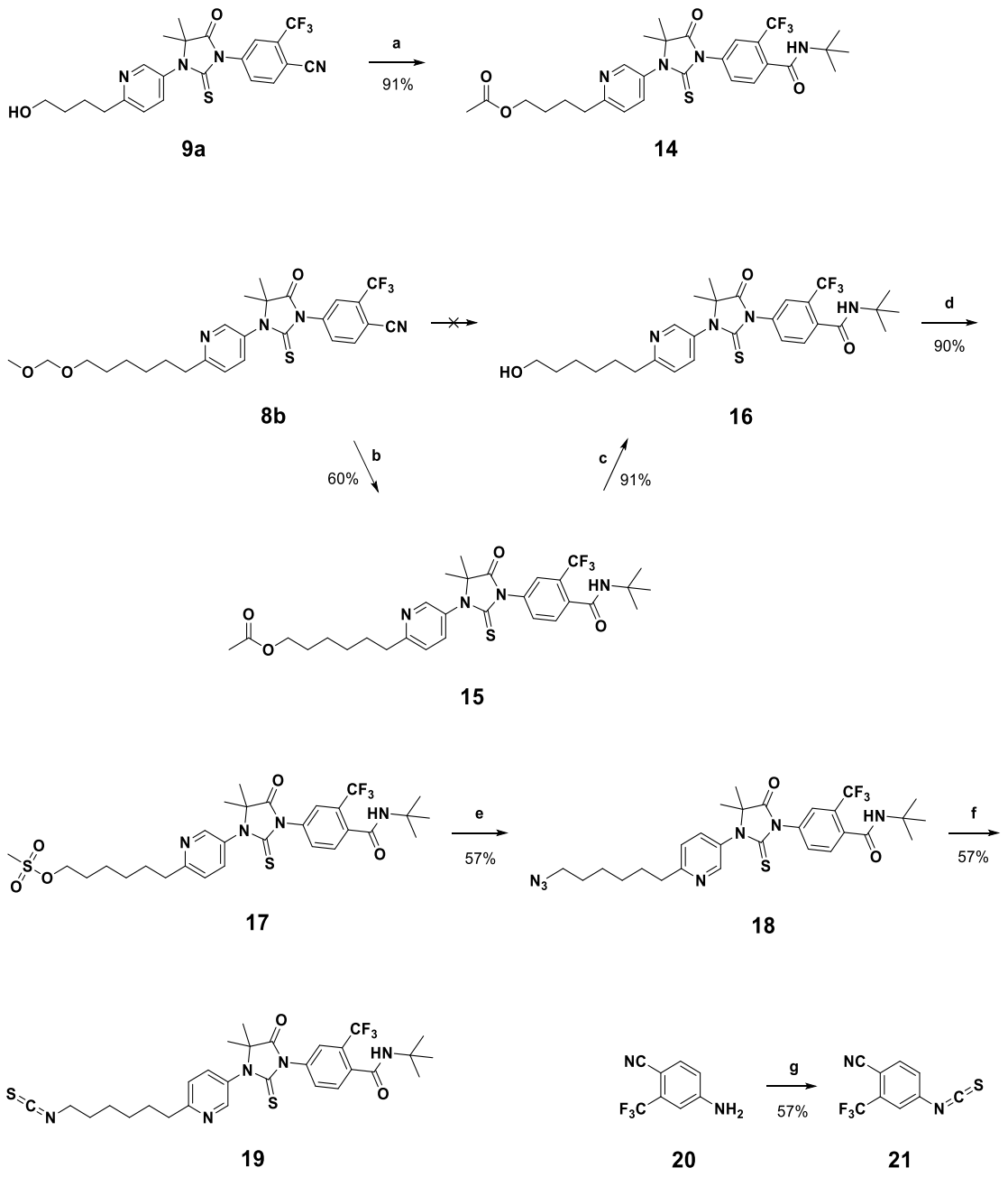

Reagents and conditions: (a) H_2SO_4, TBAc, 42°C, 2 h; (b) H_2SO_4, TBAc, 42°C, 2 h; (c) H_2SO_4, MeOH, 1 h; (d) TEA, MsCl, DCM, rt, 30 min; (e) NaN_3, DMF, 50°C, overnight; (f) 1. PPh_3, THF, reflux, 2 h; 2.CS_2, THF, reflux, 1 h; (g) Thiophosgene, H_2O/THF,rt, 1 h

the primary alcohol of expected **16** was acetylated by *tert*-Butyl acetate in an acidic

reaction mixture. This speculation was further confirmed by ^{13}C and high resolution MS analysis and we designated the reaction product as acetate **15**. Hydrolysis of **15** by sulfuric acid in methanol resulted in the 'true' hydroxyl intermediate **16**. By following the same procedures as described for the synthesis of **13**, **19** was made as a model compound

Scheme 3. Synthesis of Enz-HDACi hybrid

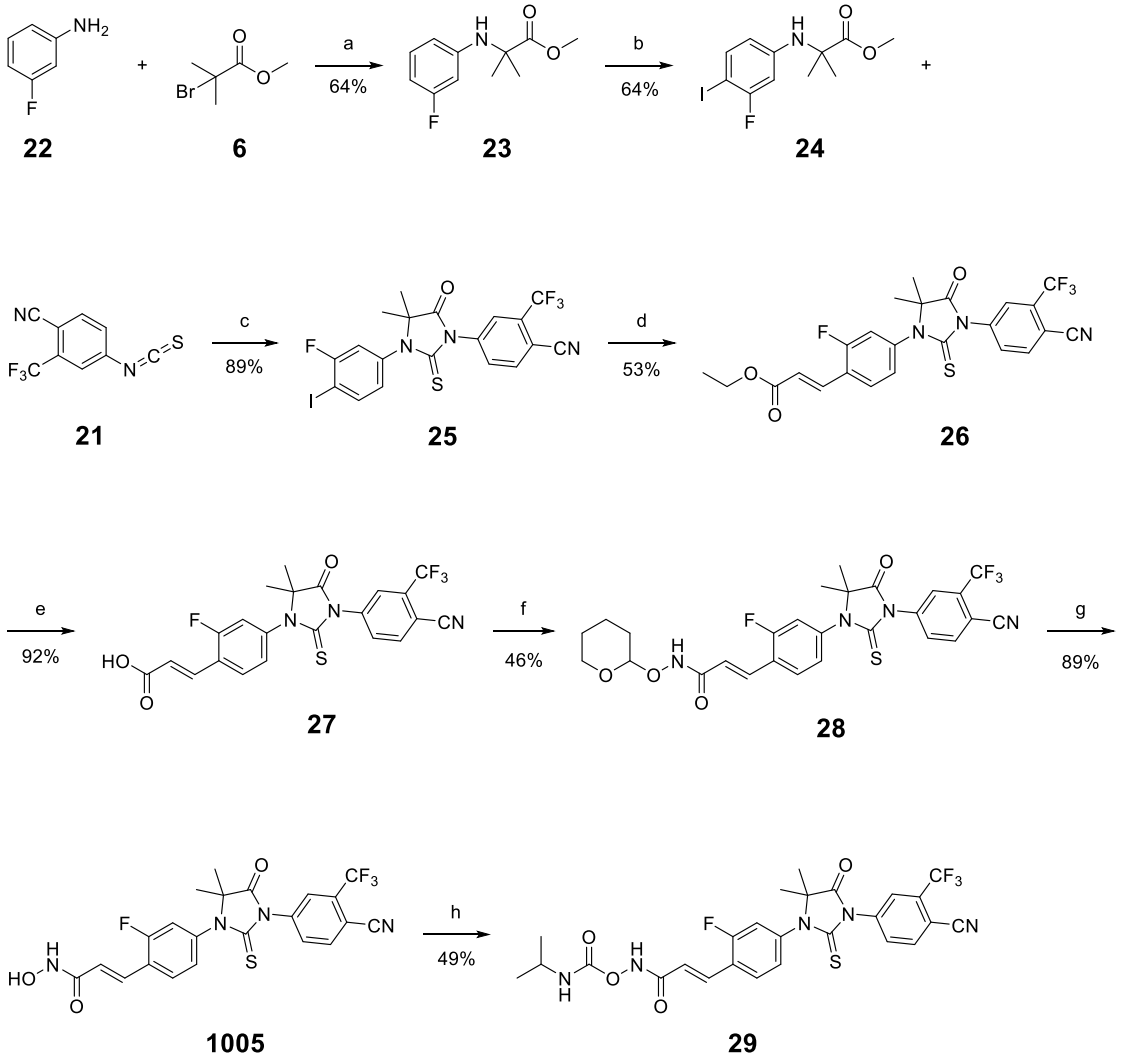

Reagents and conditions: (a) NaOAc, EtOH, reflux, overnight; (b) Iodine, NaHCO3, H2O/Dioxane, rt, 3 h; (c) DMSO, 80°C, overnight; (d) Pd(OAc)2, P(O-tolyl)3, Ethyl acrylate, DMF/DIPEA; (e) HCl, CH3CN, reflux, overnight; (f) NH2OTHP, BOP, DIPEA, DMF, rt, overnight; (g) TFA, MeOH, rt, 6 h; (h) 1. CDI, CH3CN, rt, 2 h; 2. Isopropylamine, rt, 1 h.

with ITC group and reduced AR affinity.

3.1.2. Synthesis of Enz-HDACi

Synthetic strategy for Enz-HDACi hybrid **1005** and its prodrug **1005pro** (**29**) was similar to that of Enz-ITC hybrid as depicted in . We first did the alkylation reaction to generate **23** followed by the iodination at the para site of aniline which enabled the introduction of linker to construct HDACi. The cyclization reaction was performed as described previously to give thiohydantoin intermediate **25**. Then a three-carbon chain was introduced through Heck reaction by reacting compound **25** with ethyl acrylate in the presence of palladium(II) acetate and tri(o-tolyl)phosphine. Acidic hydrolysis of ester **26** using a mixture of aqueous hydrochloric acid (37% v/v) and acetonitrile afforded carboxylic acid **27** which was coupled with tetrahydropyran (THP)-protected hydroxyl amine to generate intermediate **28**. Final compound **1005** was obtained by removing THP using TFA in methanol. Enz-HDACi **1005** was further converted to carbamate prodrug **29** according to a published procedure by reacting **1005** with carbonyldiimidazole (CDI) and isopropylamine [90].

3.2. Enz-ITC chemical scaffold inhibits dihydrotestosterone (DHT)-stimulated LNCaP cell growth

To test our hypothesis, we first need to demonstrate that the synthesized Enz-related chemical scaffolds retain AR binding/AR antagonist activity. One convenient way for this purpose is to test whether a compound can block DHT-stimulated LNCaP cell growth. DHT is a potent endogenous androgen and the growth of AR+ LNCaP cell is sensitive to the stimulation of DHT [103]. Compound **9b** (C6-OH) was chosen as a

representative Enz-ITC scaffold to exclude the potential interference of ITC on the viability of cells. LNCaP cells were seeded in RPMI1640 medium supplemented with 10% steroid-free charcoal-stripped serum. Measured by using MTT assay, DHT (1nM) significantly stimulated cell growth (96h), and this enhanced growth was completely inhibited by the treatment of C6-OH (10 μM or 20 μM) (**Figure 11**). Enz (10 μM) was used as the positive control. When cells were grown in charcoal-stripped media without DHT, compared to DMSO control, Enz (10 μM) or C6-OH (10 μM, 20 μM) neither

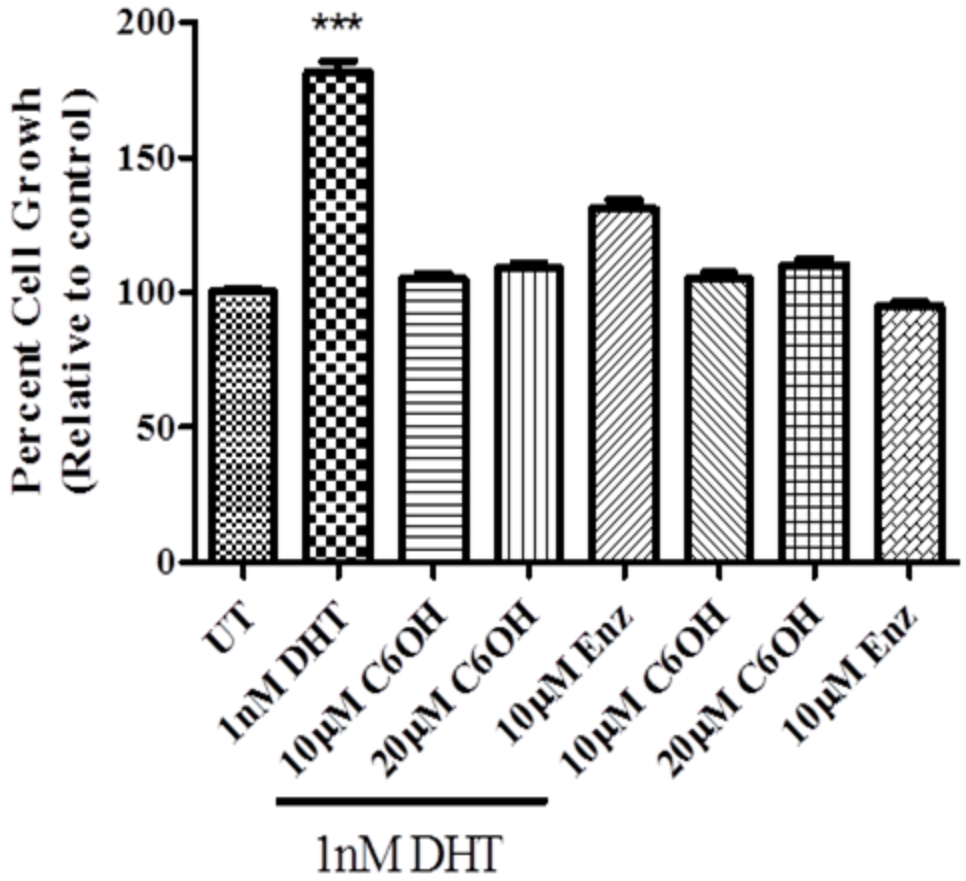

Figure 11. Enz-ITC chemical scaffold inhibied dihydrotestosterone (DHT)-stimulated LNCaP cell growth. *** $P < 0.0001$

stimulated cell growth nor reduced the viability of LNCaP cells. These results suggest that C6-ITC scaffold is not cytotoxic, the drug-caused counteraction to DHT was due to AR antagonist activity of the new chemical scaffold.

3.3. Enz-ITC scaffold inhibits AR transcriptional activity

Results from DHT growth stimulation assay could only indirectly demonstrate AR antagonistic binding of C6-OH. To directly measure the influence of Enz-ITC scaffold on AR transcriptional activity, we performed ARE luciferase assay in MDA-kb2 Cells. MDA-kb2 cell line was derived from the breast cancer cell line MDA-MD-453 which was stably transfected with an androgen-responsive luciferase reporter plasmid driven by the mouse mammary tumor virus (MMTV) promoter. MDA-MD-453 and MDA-kb2 cell lines express high levels of AR and the androgen responsive feature of MMTV promoter has been well characterized [91]. When DHT binds to AR, the liganded AR can further activate the MMTV.neo.luc response element which leads to induction of luciferase expression. Since AR antagonist competes with DHT for AR binding, the activation of AR by DHT would be diminished in the presence of an antagonist, which silences luciferase expression. After adding luciferase substrate, fluorescence is generated and the intensity is proportional to the extent of DHT binding. Within the same series of antagonist, since they have similar interaction mode with AR, luciferase activity can be correlated with the binding affinity of AR: a high-affinity antagonist can more effectively inhibit DHT-induced luciferase activity compared to a low-affinity analogue.

In our experiment, DHT treatment (1nM) significantly increased luciferase activity (**Figure 12A**). Enz, as the positive control, inhibited luciferase activity at all

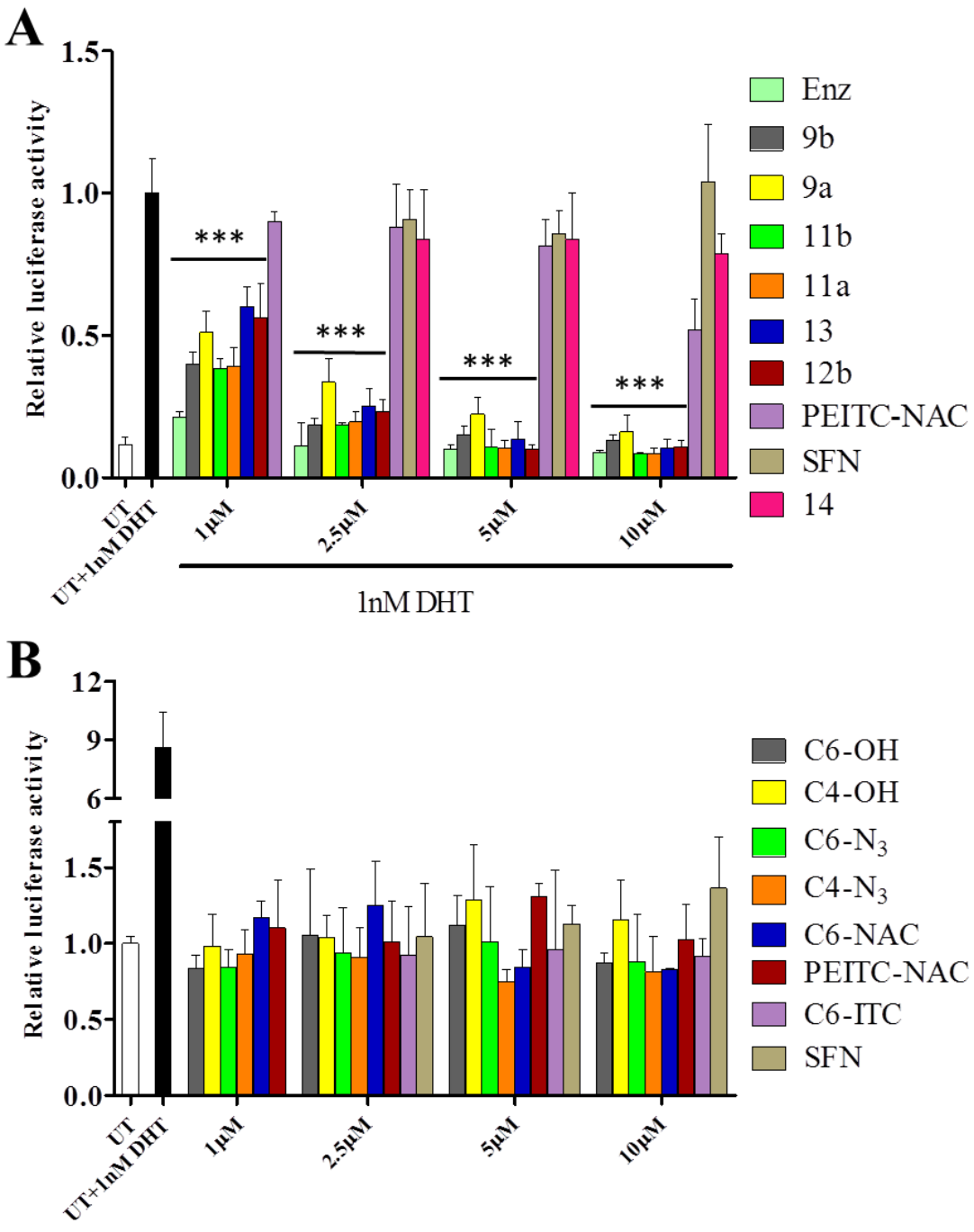

Figure 12. Enz-ITC scaffold antagonistically binds to AR (A). Treatment with compounds alone do not reduce luciferase activity (B). *** $P < 0.0002$

concentrations (1-10 μM). All the compounds with Enz-ITC scaffold decreased luciferase activity in a dose-dependent fashion. **9b** (C6-OH), although was not as good as Enz at

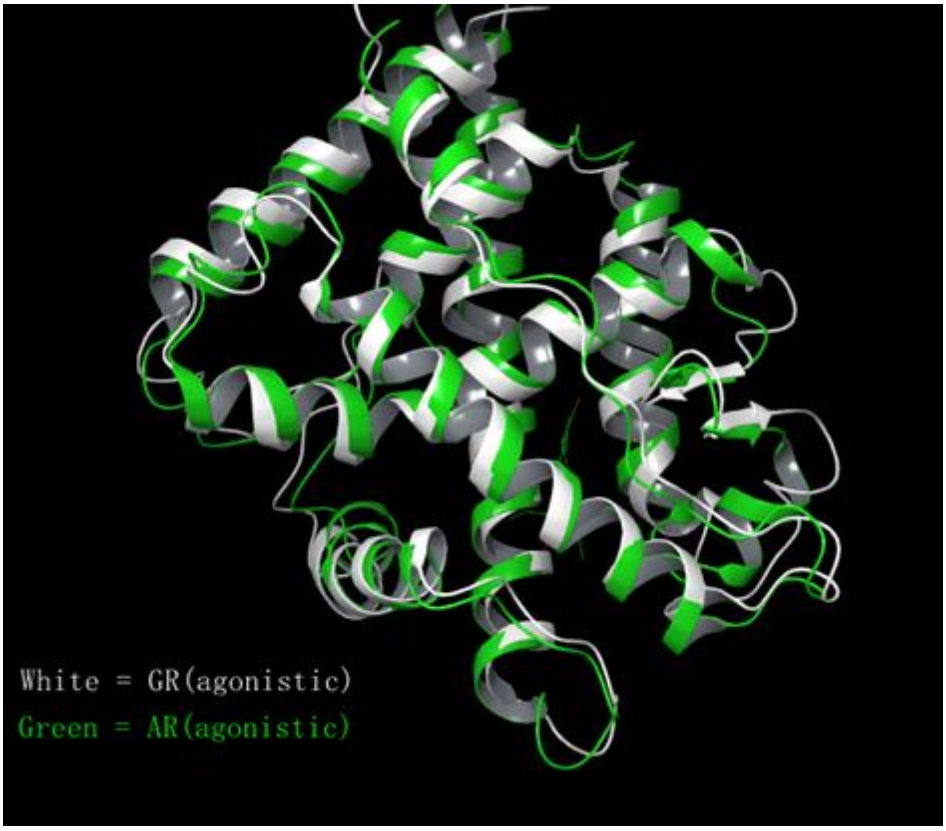

Figure 13. Superposition of AR and GR in agonistic form. Two entities have very similar 3-D structure.

1 μM, it was comparable to Enz at higher concentrations (2.5-10 μM). **9a** (C4-OH) which has a shorter linker was inferior to C6-OH, suggesting that the length of carbon chain influences AR binding. However, two azide analogues C6-N_3 and C4-N_3 had almost identical potency in this assay and were similar to that of C6-OH. C6-ITC (**12b**) and the conjugate C6-ITC-NAC (**13**) has similar pattern as to that of C6-OH, less effective at 1 μM but comparable to Enz at higher concentrations. Isothiocyanate derivatives, SFN and PEITC-NAC which is a NAC conjugate of PEITC, didn't decrease luciferase activity due to lack of AR binding moiety. This also demonstrates that the reduced luciferase activity is only related with Enz moiety at the tested concentration range ((1-10 μM) and

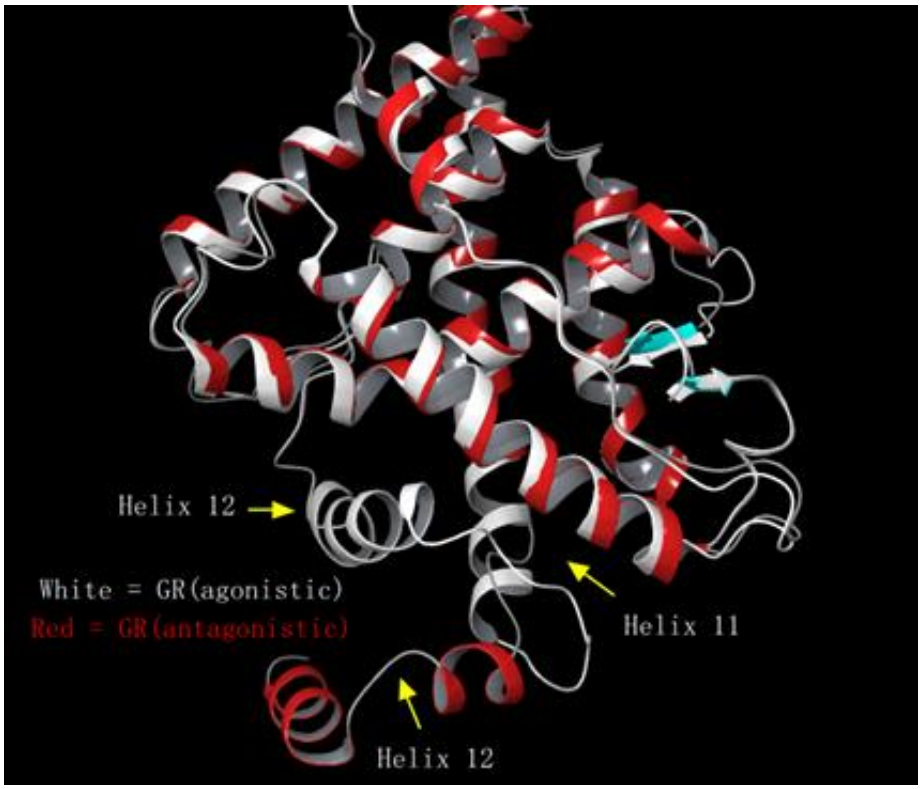

Figure 14. Superposition of GR in agonistic and antagonistic form. Two entities have identical structure except for displaced helix 12 in antagonistic form.

time frame (24h). Amide analogues **14** didn't have AR binding as we expected maybe because of missing important H-bond interaction on cyano group. No luciferase activity was either reduced or induced when treated with compounds alone at full range of concentrations, (**Figure 12B**) indicating reduced luciferase activity came from the inhibition of DHT binding to AR.

3.4. Molecular Docking of Enz-ITC to AR

Molecular docking studies were performed to better understand the interactions of Enz-ITC with AR.

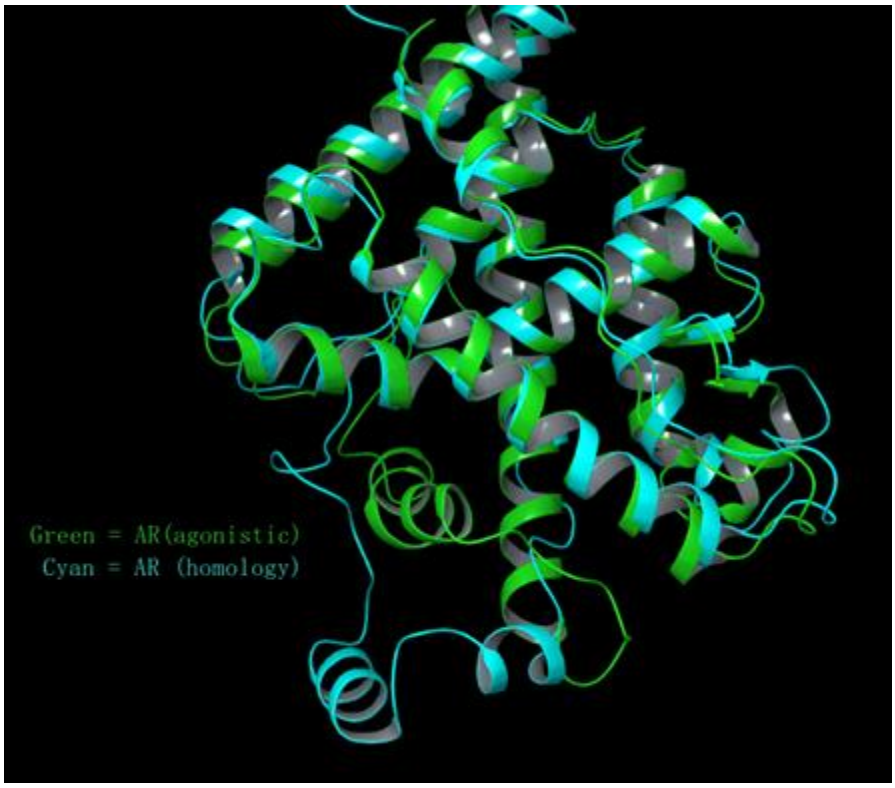

Figure 15. Superposition of agonistic AR and homologous AR. Helix 12 in homologous AR is pushed away from binding pocket to generate antagonistic form of AR.

By examining the structures of AR and GR in antagonistic form, we found that after superposition, the two entities have very similar 3-D structures (**Figure 13**) which supports the use of GR as a suitable homology modeling template for AR. Besides, agonistic and antagonistic form of GR had identical 3D structure except for helix 12 which is pushed away from binding pocket in the antagonist mode (**Figure 14**), this result is consistent with the general antagonistic mechanism of nuclear receptor. When superposing agonistic AR (complexed with DHT) (PDB code: 2AMB) [104] with AR in antagonistic form obtained from homology modeling, two structures overlapped very well and the displaced helix 12 of homologous AR created space to accommodate larger

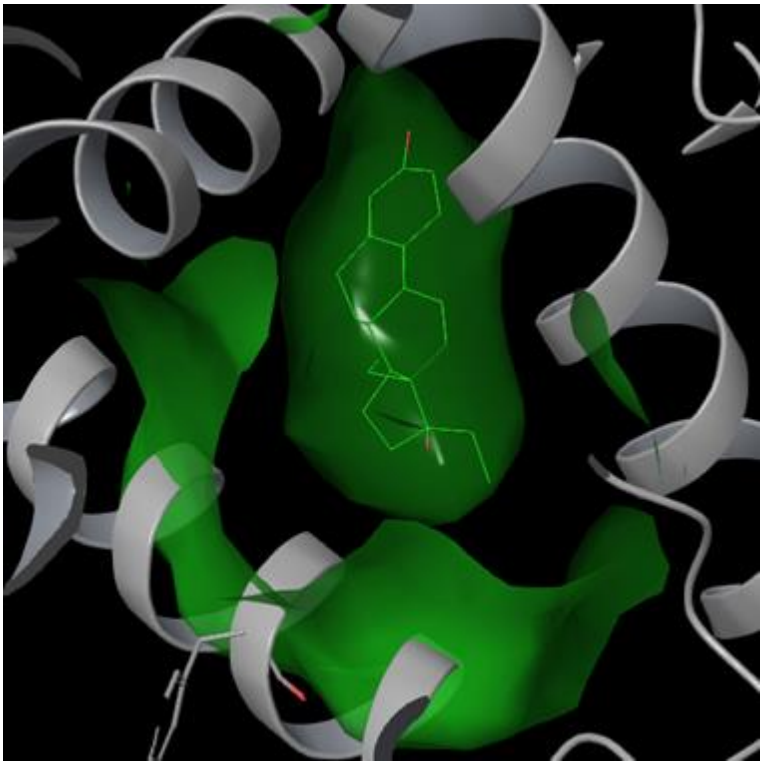

Figure 16. Surface of binding cavity of native ligand (DHT). Space in binding cavity is closed and limited.

antagonist (**Figure 15**). And all these computational models built the foundation for reliable docking studies.

The surface of binding cavity of agonistic AR with naive ligand (DHT) as depicted in (**Figure 16**) indicates a closed and very limited space for ligand binding. Four new pockets were identified in new homologous model (**Figure 17 left**), two opened toward back of helix 11 (not shown in figure), one squeezed into the space between helix 11 and helix 12 and caused relaxation of helix 11 to form the pocket. Another pocket opened toward the space where were originally occupied by helix 12 from agonistic conformation (**Figure 17 right**).

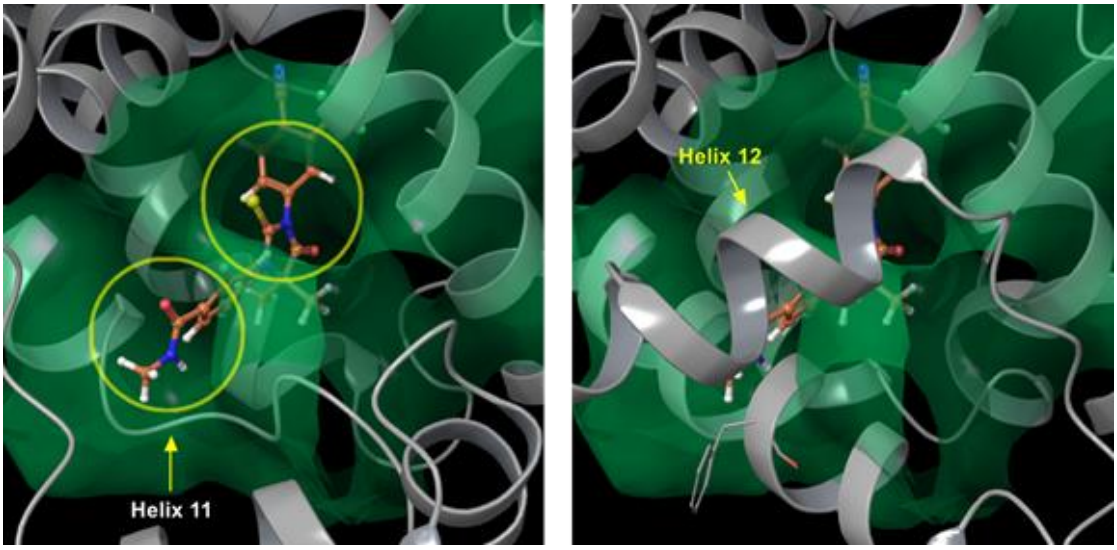

Figure 17. New binding pockets in homologous AR. Two open toward back of helix 11 (not shown in figure), one squeezes into the space between helix 11 and helix 12 (left). Another one opens toward the space (indicated by yellow circle) where were originally occupied by helix 12 from agonistic conformation (right).

Docking results indicate C6-ITC had the similar binding mode and position to that of Enz (**Figure 18**) in which cyano group on both C6-ITC and Enz formed two H-bond with Gln711 and Arg752. This result emphasized the importance of cyano group in AR binding of Enz scaffold and might explain why **14** lost its binding ability to AR. Besides, Pi-Pi interactions were formed between Phe764 and benzonitrile rings on both C6-ITC and Enz. Enz formed an extra H-bond with Phe876 through the hydrogen on amide group. New pocket formed by relaxation of helix 11 provided the space for accommodation of extended part of Enz as depicted in **Figure 17**. In conclusion, Enz-ITC scaffold kept the antagonistic AR binding activity and potentially had the similar binding mode to that of Enz.

3.5. Enz-ITC hybrid inhibits HDAC and causes downregulation of AR

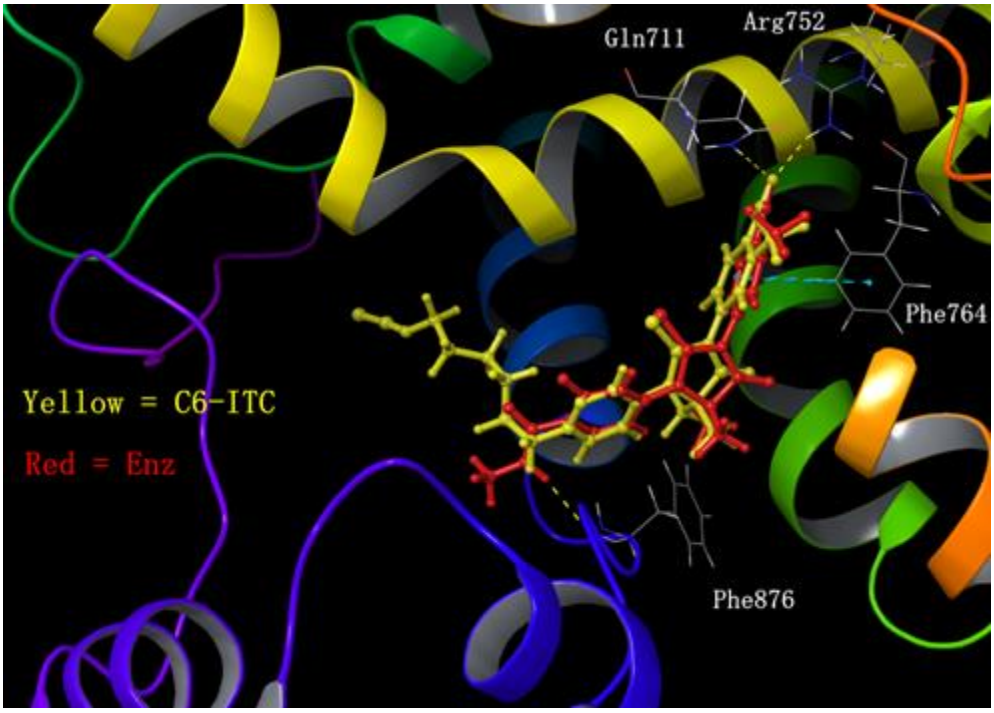

Figure 18. Docking of Enzalutamide and C6-ITC in homologous AR. Two molecules have similar binding mode. Both form two H-bonds with AR (Gln711 and Arg752) via cyano group and Pi-Pi interaction with Phe764. Enzalutamide forms extra H-bond with Phe876.

We performed western blot analysis to investigate if the hybrid keeps the HDAC inhibition and AR degradation activity of ITC. Acetyl-histone H3 (Ac-H3) and acetyl-histone H4 (Ac-H4) are associated with HDAC activity in the nucleus, while acetyl-α-tubulin (Ac-Tub) level is regulated by HDAC6 in the cytosol. Drug-induced HDAC inhibition should cause increased globe acetylation of histones H3 and H4 and tubulin. As shown in **Figure 19.**, SAHA, as the positive control significantly increased acetylated protein levels in a dose-dependent manner. C6-ITC also up-regulated Ac-H3 and Ac-tub levels at 20μM, but had no effect on the level for Ac-H4. The C6-ITC-NAC showed similar effects as C6-ITC but to a much lesser extent in protein acetylation. SFN also increased Ac-tub level at 20μM but its nuclear effect was very weak.

AR level was significantly down-regulated by C6-ITC even at 5μM, in contrast SFN was not effective at this concentration. Although C6-ITC-NAC was inferior compared to C6-ITC, it still outperformed SFN which only decreased AR level at high concentration (20μM). AKT is an Hsp90 client protein and inhibition of Hsp90 leads to degradation of Akt [105]. C6-ITC and C6-ITC-NAC decreased Akt level in a dose-dependent fashion, suggesting that Enz-ITC hybrid disrupted the function of Hsp90. It is worth to mention that PI3K/Akt pathway is up-regulated in CRPC and is involved in many oncogenic processes. Previous study suggested that the AR and PI3K/AKT pathways cross-regulate each other by reciprocal feedback which means inhibition of one activates the other, thus maintaining tumor cell survival [26]. Recently, it was reported that combination treatment with AZD5363 (an AKT inhibitor) and Enz significantly delayed development of Enz resistance via synergistic increases of apoptosis and cell

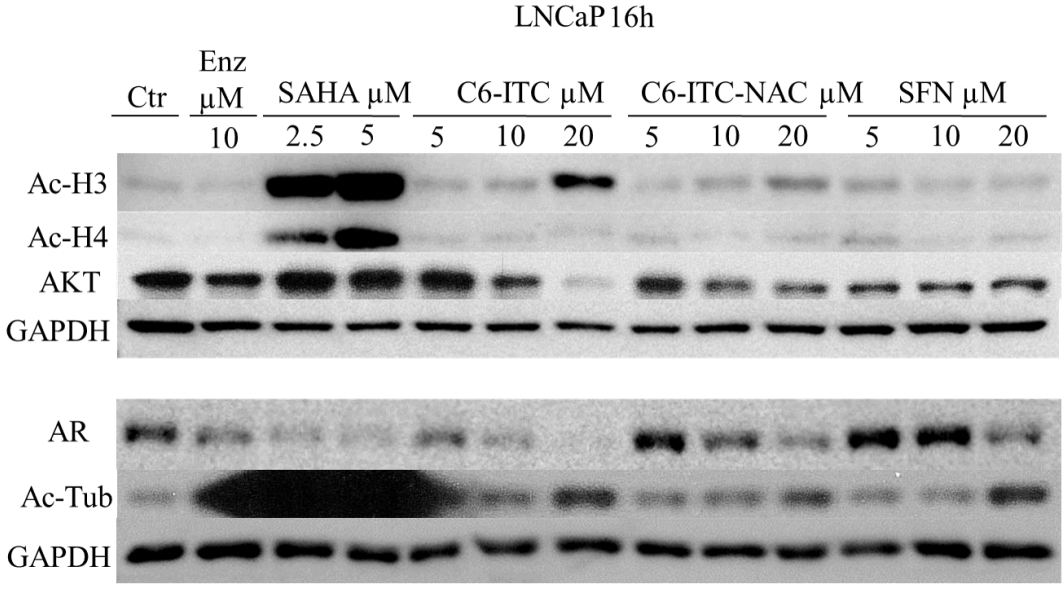

Figure 19. Enz-ITC hybrid inhibits HDAC and causes downregulation of AR.

cycle arrest [28]. Thus, effectively down-regulating both AR and Akt may indicate a potential therapeutic advantage which needs to be further verified in other PCa models. Whether C6-ITC-caused AR degradation is relevant to AR binding will be further studied via the side by side comparison of C6-ITC and its analogue **19** which has just been synthesized. Molecular docking study indicated that cysteine conjugate of C6-ITC has similar binding mode with native ligand SAHA and can form four extra H-bond with homologous HDAC6 (**Figure 20**), suggesting the possibility of HDAC6 inhibition through forming ITC-Cys conjugate.

3.6. Enz-ITC inhibits proliferation in both androgen sensitive and insensitive prostate cancer cell lines

We performed MTT assays to test overall antiproliferation activity of Enz-ITC

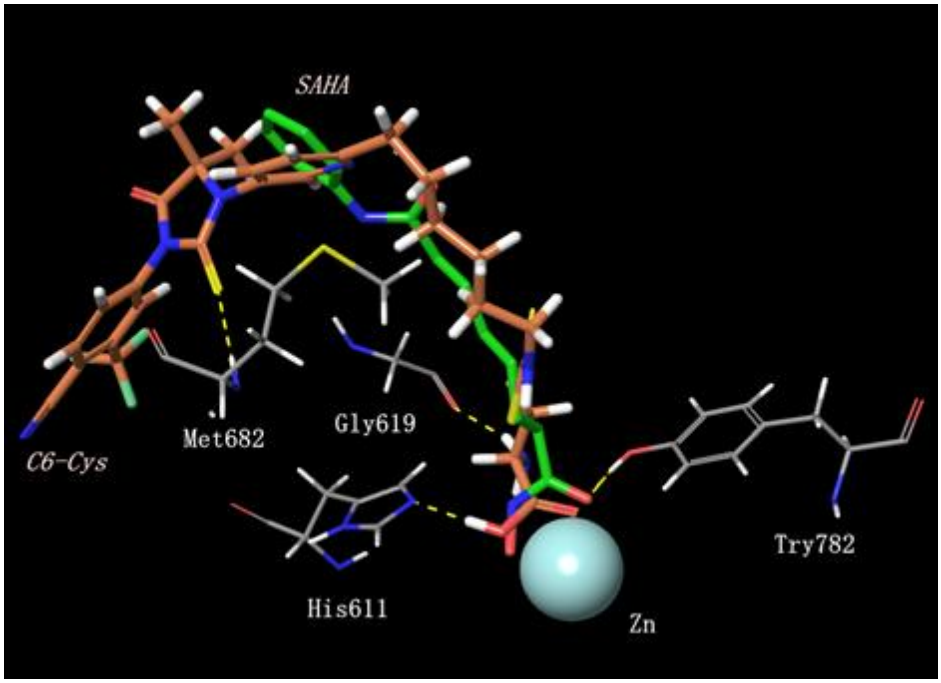

Figure 20. Binding mode of cysteine conjugate of C6-ITC with HDAC6.

Table 1. In Vitro Inhibitory Activity (IC_{50}).

Compd.	IC_{50}(μM)		
	LNCaP	**PC-3**	**22Rv1**
C6-ITC	4.56 ± 0.34	4.38 ± 0.31	4.59 ± 0.15
C4-ITC	8.27 ± 0.78	7.34 ± 0.36	8.18 ± 1.12
C6-NAC	8.82 ± 1.34	7.43 ± 0.52	*b*
SFN	19.69 ± 1.47	17.74 ± 2.21	*b*

[a] Values are the mean of a minimum of three experiments. [b] Not tested

hybrids. As indicated in **Table 1**, all Enz-ITC hybrids were more potent than SFN in all the tested cell lines (LNCaP, 22Rv1 and PC-3) and C6-ITC (**12b**) was more active than C4-ITC (**12a**). Although NAC conjugation reduced its antiproliferation activity, C6-NAC (**13**) was still more effective than SFN. When cells were grown in full medium, as expected, androgen insensitive cell lines PC-3 and 22Rv1 showed no response to Enz. Because full growth media contains various steroid, such as estrogens that can also stimulate LNCaP cells [106], Enz only showed weak growth inhibition effect to LNCaP cell under this condition, e.g., Enz suppressed growth about 20% at 5μM (**Figure 21**). Because no differences were seen between AR positive and AR negative cell lines (**Table 1**), the results from MTT assay seemed to be dominated by the "ITC" group. In order to highlight the action of Enz moiety in hybrid, other AR positive, Enz-sensitive CRPC cell lines, such as VCaP cells, need to be tested in future experiments. Results from

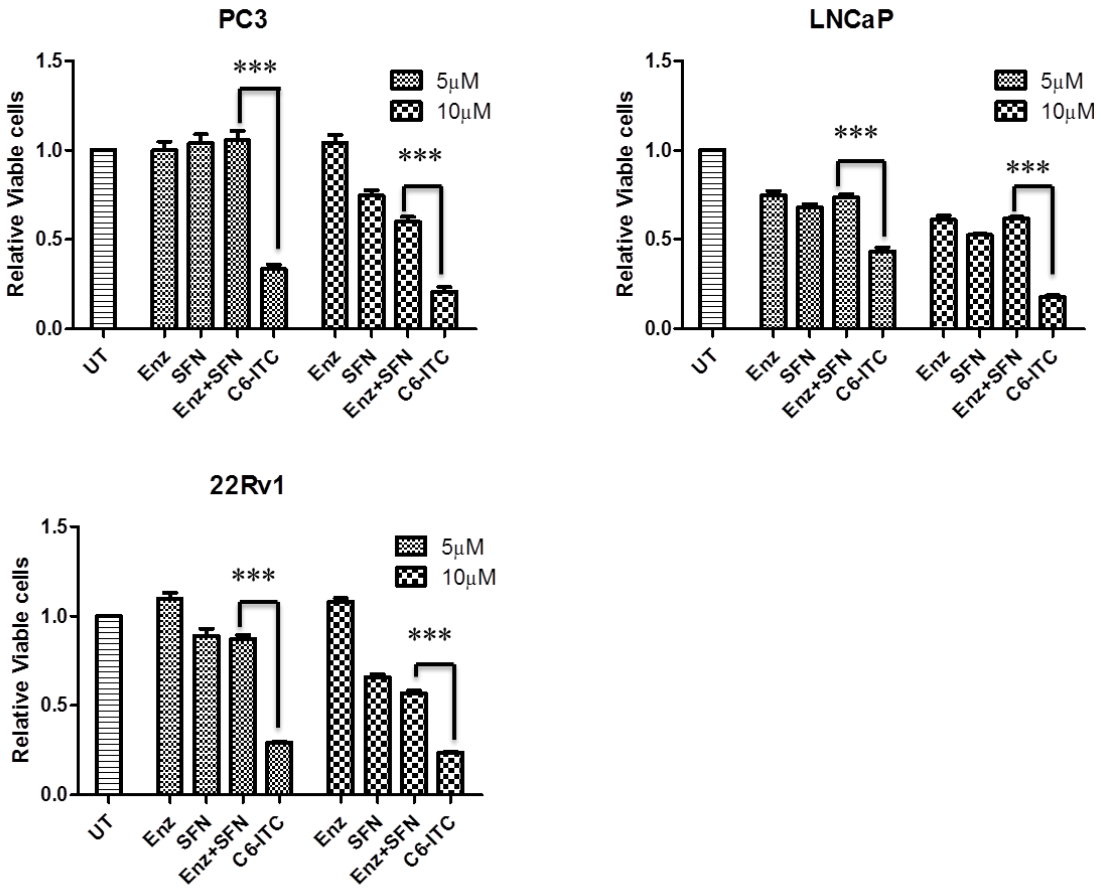

Figure 21. Comparation of combination treatment with Enz and SFN with Enz-ITC hybird in different prostate cancer cell lines. * $P < 0.05$, ** $P < 0.01$, *** $P < 0.005$

combination treatment showed that Enz and ITC had no synergistic effect. Interestingly, 6-ITC treatment was superior than the combination at the same concentration in all the three tested cell lines (**Figure 21**). Increased intracellular concentration might be partially responsible for this "conjugation effects", and whether AR binding also plays a role in AR(+) cells, will be further investigated in VCaP cell through the comparison between compound **13** (C6-ITC) and its analogue **19** which has reduced AR affinity.

3.7. Enz-ITC hybrids are more tolerable in MCF-10A cells than SFN

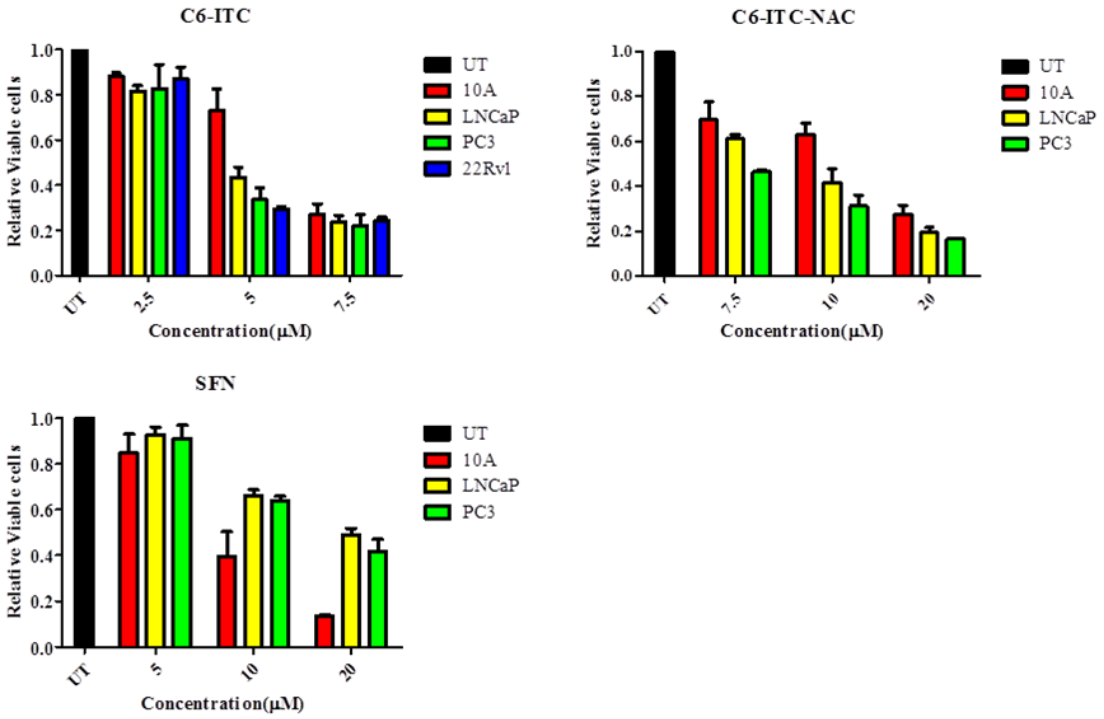

Figure 22. Treatment of normal bresat cell (MCF-10A) and PCa cells (LNCaP, PC-3 and 22Rv1) with Enz-ITC hybrids and SFN.

Our previous experiments have demonstrated the effectiveness of Enz-ITC hybrid in PCa cells. The effects on non-cancerous cells is another very important property of an anti-cancer agent. Normal breast cell line MCF-10A was chosen to be tested considering the promising potential of Enz and its analogues for breast cancer treatment. As shown in **Figure 22**, at concentrations that induce effective AR down-regulation, C6-ITC (12b, 5 μM) and C6-ITC-NAC (13, 10 μM) showed certain selectivity between MCF-10A and PCa cells. C6-ITC-NAC (13) was also more tolerable than SFN in MCF-10A cells.

3.8. Enz-HDACi inhibits proliferation in both androgen sensitive and insensitive cell lines

HDAC is one of the potential cellular targets of ITCs. To dissect the anti-PCa mechanisms of Enz-ITCs, we synthesized Enz-HDACi to further evaluate if AR can direct HDACi to Hsp90 complex. **1005** and its amide prodrug **29** (1005pro) were synthesized and accessed in PCa cells by using MTT assay. The results (**Figure 23**) indicate that **1005** has better inhibition activity than C6-ITC and is more potent in androgen sensitive cell line, potentially due to AR directing effect. Prodrug **29** (1005pro) retains the activity against PCa cells while slightly less effective than the parental drug.

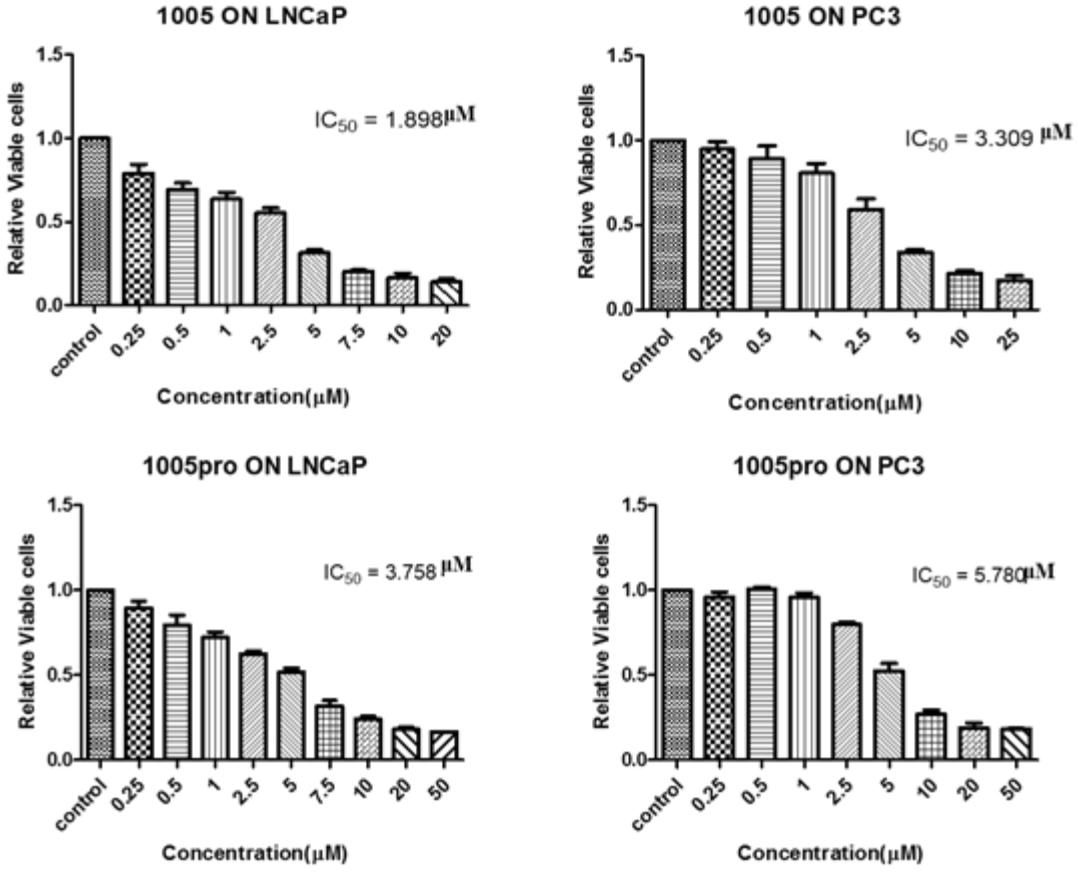

Figure 23. Enz-HDACi inhibits proliferation in both androgen sensitive and insensitive cell lines

3.9. Summary and future direction

In this project, we've successfully synthesized two Enz-ITC hybrids and NAC prodrug as well as a series of relevant analogues to illustrate the mechanism of bioactivity and SAR. MTT and ARE-luciferase assays indicate that the chemical scaffold of Enz-ITC retains AR antagonist activity. Enz-ITC hybrid induces AR down-regulation more effectively than SFN potentially due to HDAC inhibition and/or Hsp90 disruption. In addition, the hybrids inhibit proliferation of both androgen sensitive (LNCaP) and insensitive cell lines (22Rv1, PC-3). No synergistic antitumor effect is observed in the combination of Enz and SFN which is less effective than the hybrids determine by MTT assays in the tested cell lines. Enz-ITC-NAC conjugate were more tolerable in MCF-10A cells than SFN. We've also synthesized Enz-HDACi hybrid and its prodrug to make comparison with Enz-ITC hybrids and our MTT results suggest that both compounds have anti-proliferation activity against androgen sensitive and insensitive prostate cancer cell lines.

To investigate if AR binding plays a role in hybrid drug-induced AR down-regulation and growth suppression, Enz-ITC and Enz-HDACi will be compared with their counterparts with reduced AR affinity, respectively. In addition, to understand chemical reactivity of ITC hybrids, analysis of ITC conjugation with GSH and ITC-NAC decomposition to release ITC will be performed by using HPLC. Since inhibition of both prostate and breast cancer stem cells by SFN has been reported [60, 107], it is interesting to test whether Enz-ITCs has similar effects against prostate and/or breast cancer stem cells.

Chapter 4. Experimental

4.1. Chemistry

All reagents and solvents were purchased from commercial suppliers and used without further purification unless otherwise stated. All of the reported yields are for isolated products and are not optimized. The reactions were monitored by thin layer chromatography (TLC) on precoated silica gel UV254 plates (SORBTECH) and visualized under UV light or after staining by dip into a solution of phosphomolybdic acid or Potassium permanganate and then heating on a hot plate. All NMR spectra were obtained using Varian INOVA 600 MHz NMR spectrometer. Chemical shifts are expressed in ppm as a δ value, and singlet (s), doublet (d), triplet (t), quartet (q), multiplet (m) and broad singlet (br s) are used as abbreviations.

4-(5-Nitropyridin-2-yl)but-3-yn-1-ol (3a). In argon atmosphere, to a mixure of 2-bromo-5-nitropyridine (10.0g, 50mmol) and 3-butyn-1-ol (4.55g, 65mmol) in acetonitrile were added copper iodine (190mg, 1mmol), bis(triphenylphosphine) palladium(II) chloride (175mg, 0.25mmol) and TEA(34mL, 250mmol) slowly. The reaction was stirred at room temperature overnight. Solvent was removed under reduced pressure. The crude product was purified by flash chromatography (Hex/EA: 1:1) to afforded brown oil (8.34g, 87%). ^{1}H NMR (600 MHz, $CDCl_3$) δ 9.33 (d, *J* = 3.0 Hz, 1H), 8.42 (dd, *J* = 8.4 and 2.4 Hz, 1H), 7.55 (d, *J* = 8.4 Hz, 1H), 3.88 (m, 2H), 2.76 (t, *J* = 6 Hz, 2H).

6-(5-Nitropyridin-2-yl)hex-5-yn-1-ol (3b). In argon atmosphere, to a mixture of 2-bromo-5-nitropyridine (13.2g, 65mmol) and 5-hexyn-1-ol (4.9g, 50mmol) in acetonitrile (70mL) were added copper(I) iodide (190mg, 1mmol),

bis(triphenylphosphine) palladium(II) chloride (175mg, 0.25mmol) and TEA (34mL, 250mmol) slowly at 0 ℃. The reaction was stirred at room temperature for 3hrs. Solvent was removed under reduced pressure, mixture was diluted with EtOAc, the organic phase was washed with water and brine, dried over anhydrous sodium sulfate and concentrated. The crude product was purified by flash chromatography (Hex:EA=2:1) to afford brown oil (10.5g, 95%). ^{1}H NMR (600 MHz, $CDCl_3$) δ 9.34 (d, *J* = 2.4 Hz, 1H), 8.40 (dd, *J* = 8.4 and 3 Hz, 1H), 7.51 (d, *J* = 8.4 Hz, 1H), 3.70 (t, *J* = 12 Hz, 2H), 2.54 (t, *J* = 12 Hz, 2H), 1.77-1.72 (m, 4H). ^{13}C NMR (150 MHz, $CDCl_3$) δ 149.10, 145.27, 142.41, 131.26, 126.74, 97.12, 62.19, 31.79, 24.38, 19.36.

2-(4-(Methoxymethoxy)but-1-yn-1-yl)-5-nitropyridine (4a). In argon atmosphere, to a solution of **3a** (8.34g, 43.4mmol) in THF(80mL) were added DIPEA (18mL, 108.6mmol), then bromo(methoxy)methane (7.2mL, 90%, 78mmol) was added slowly. Reaction was stirred at room temperature overnight. Precipitate was filtered, the solvent was evaporated away under reduced pressure, mixture was diluted with EtOAc, the organic phase wash by water and brine. The crude product was purified by flash chromatography (Hex/EA: 6:1→4:1) to afford orange solid (6.3g, 61%). ^{1}H NMR (600 MHz, $CDCl_3$) δ 9.73 (s, 1H), 8.81 (s, 1H), 7.94 (s, 1H), 5.06 (s, 2H), 4.17 (d, *J* = 5.4Hz, 2H), 3.77 (s, 3H), 3.19 (d, *J* = 5.4 Hz, 2H).

2-(6-(Methoxymethoxy)hex-1-yn-1-yl)-5-nitropyridine (4b). In argon atmosphere, to a mixture of **3b** (10.5g, 47.7mmol) in THF (80mL) were added DIPEA (12.5mL, 75.7mmol), then bromo(methoxy)methane (10.5g, 90%, 78mmol) was added dropwise at 0 ℃. Reaction was stirred at room temperature for 6hrs. Solvent was removed under reduced pressure, mixture was diluted with EtOAc, the organic phase was washed

with water and brine, dried over anhydrous sodium sulfate and concentrated. The crude product was purified by flash chromatography (Hex:EA=4:1) to afford brown oil (10.69g, 85%). ^{1}H NMR (600 Mhz, $CDCl_3$) δ 9.34 (d, *J* = 2.4 Hz, 1H), 8.40 (dd, *J* = 8.4 and 2.4Hz, 1H), 7.51 (d, J = 8.4 Hz, 1H), 3.70 (t, J = 12 Hz, 2H), 2.54 (t, J = 12 Hz, 2H), 1.77-1.72 (m, 4H). ^{13}C NMR (150 MHz, $CDCl_3$) δ 149.10, 145.27, 142.41, 131.26, 126.74, 97.18, 80.04, 62.19, 31.79, 24.38, 19.36.

6-(4-(Methoxymethoxy)butyl)pyridin-3-amine (5a). To a solution of **4a** (8.40g) in methanol, palladium on carbon (200mg) was added. Reaction was stirred at pressurized hydrogen atmosphere (60 psi) overnight. during that time reaction was filled with Hydrogen several times. After the mixture was filtered, solvent was evaporated away under reduced pressure to afforded brown oil (7.81g, 95%). ^{1}H NMR (600 MHz, $CDCl_3$) δ 8.00 (s, 1H), 6.90 (m, 2H), 4.59 (s, 2H), 3.56 (br s, 2H), 3.52 (t, *J* = 6.6 Hz, 2H), 3.32 (s, 3H), 2.68 (t, J = 7.2 Hz, 2H), 1.70-1.76 (m, 2H), 1.59-1.64 (m, 2H). ^{13}C NMR (150 MHz, $CDCl_3$) δ 152.04, 140.11, 136.83, 122.61, 122.49, 96.35, 67.62, 55.09, 37.01, 29.34, 26.69.

6-(6-(Methoxymethoxy)hexyl)pyridin-3-amine (5b). To a solution of **4b** (10.68g, 40.4mmol) in methanol was added palladium on carbon (250mg). Reaction was stirred under hydrogen atmosphere (60 psi) overnight. After the mixture was filtered, solvent was removed under reduced pressure to afford brown oil (9.05g, 94%). ^{1}H NMR (600 MHz, $CDCl_3$) δ 8.00 (m, 1H), 6.90 (m, 2H), 4.59 (s, 2H), 3.54 (br s, 2H), 3.48 (t, *J* = 6.6 Hz, 2H), 3.33 (s, 3H), 2.65 (t, J = 15.6 Hz, 2H), 1.68-1.63 (m, 2H), 1.59-1.55 (m, 2H), 1.40-1.32 (m, 4H). ^{13}C NMR (150 MHz, $CDCl_3$) δ 152.46, 140.00, 136.77, 122.57, 122.54, 96.35, 67.79, 55.07, 37.26, 30.10. 29.64, 29.09, 26.07.

Methyl 2-((6-(4-(methoxymethoxy)butyl)pyridin-3-yl)amino)-2-methylpropanoate (7a). To a solution of **5a** (7.81g, 37.2mmol) and **6** (33.7g, 186mmol) in ethanol was added sodium acetate (30.5g, 372mmol). Reaction was refluxed for 5 days. Reaction was filtered, the solvent was evaporated away under reduced pressure. Mixture was diluted with EtOAc, the organic phase washed by water and brine. Product was purified by flash chromatography (Hex/EA: 1:2→EA) to afforded red oil (3.78g, 34.3%). ^{1}H NMR (600 MHz, $CDCl_3$) δ 7.94 (d, *J* = 3 Hz, 1H), 6.91 (d, *J* = 8.4 Hz, 1H), 6.81 (dd, *J* = 8.4 and 3 Hz, 1H), 4.59 (s, 2H), 3.97 (br s, 1H), 3.70 (s, 3H), 3.52 (t, *J* = 6.6 Hz, 2H), 3.33 (s, 3H), 2.68 (t, *J* = 7.8 Hz, 2H), 1.70-1.78 (m, 2H), 1.59-1.66 (m, 2H), 1.53 (s, 6H). ^{13}C NMR (150 MHz, $CDCl_3$) δ 176.16, 152.20, 139.31, 138.32, 123.06, 122.34, 96.36, 67.62, 57.70, 55.01, 52.56, 36.98, 29.38, 26.58, 26.12 (2C).

3-((4-(6-(Methoxymethoxy)hexyl)phenyl)amino)-3-methylbutan-2-one (7b). To a solution of **5b** (3g, 12.6mmol) and **6** (22.8, 126mmol) in ethanol was added sodium acetate (15g, 189mmol). Reaction was refluxed for 13 days. After the mixture was filtered, solvent was evaporated away under reduced pressure. Mixture was diluted with EtOAc, the organic phase was washed with water and brine, dried over anhydrous sodium sulfate and concentrated. The crude product was purified by flash chromatography (Hex:EA=1:2) to afford yellow oil (3.1g, 73%). ^{1}H NMR (600 MHz, $CDCl_3$) δ 7.90 (d, *J* = 3 Hz, 1H), 6.88 (d, *J* = 8.4 Hz, 1H), 6.78 (dd, *J* = 8.4 and 3 Hz, 1H), 4.56 (s, 2H), 4.00 (br s, 1H), 3.67 (s, 3H), 3.60 (t, *J* = 6.6 Hz, 2H), 3.48 (t, *J* = 6.6 Hz, 2H), 3.30 (s, 3H), 2.62 (t, *J* = 8.1 Hz, 2H), 1.66-1.60 (m, 2H), 1.58-1.52 (m, 2H), 1.50 (s, 6H), 1.38-1.29 (m, 4H). ^{13}C NMR (150 MHz, $CDCl_3$) δ 176.17, 152.53, 139.25, 138.21,

123.09, 122.27, 96.31, 67.76, 57.67, 55.03, 52.51, 37.18, 29.96. 29.61, 29.11, 26.09 (2C), 26.04.

4-(3-(6-(4-(Methoxymethoxy)butyl)pyridin-3-yl)-4,4-dimethyl-5-oxo-2-thioxoimidazolidin-1-yl)-2-(trifluoromethyl)benzonitrile (8a). In argon atmosphere, to a solution of **7a** (3.78g, 12.8mmol) in DMSO (25mL), **21** (8.78g, 38.5mmol) was added. Reaction was stirred at 80℃ overnight. The mixture was diluted with EtOAc, the organic phase washed by water and brine, dried over anhydrous sodium sulfate and concentrated. The crude product was purified by flash chromatography (Hex:EA=2:1→1:1) to afforded brown oil (5.8g, 90%). ^{1}H NMR (600 Mhz, $CDCl_3$) δ 8.45 (d, *J* = 2.4 Hz, 1H), 7.96 (d, *J* = 8.4 Hz, 1H), 7.94 (s, 1H), 7.82 (d, *J* = 7.8, 1H), 7.54 (dd, *J* = 8.4 and 2.4 Hz, 1H), 7.33 (d, *J* = 8.4 Hz, 1H), 4.60 (s, 2H), 3.56 (t, *J* = 6.0Hz, 2H), 3.34 (s, 3H), 2.90 (t, *J* = 8.4Hz, 2H), 1.84-1.90 (m, 2H), 1.66-1.72 (m, 2H), 1.58 (s, 6H). ^{13}C NMR (150 MHz, $CDCl_3$) δ 180.32, 174.67, 163.64, 149.58, 137.44, 136.95, 135.26, 133.56 (q, *J* = 33.2 Hz), 132.16, 129.60, 127.04 (q, *J* = 4.7 Hz), 123.42, 121.82 (q, *J* = 273 Hz), 114.76, 110.24, 96.43, 67.43, 66.35, 55.16, 37.82, 29.44, 26.12, 23.71 (2C).

4-(3-(6-(6-(Methoxymethoxy)hexyl)pyridin-3-yl)-4,4-dimethyl-5-oxo-2-thioxoimidazolidin-1-yl)-2-(trifluoromethyl)benzonitrile (8b). In argon atmosphere, to a solution of **7b** (3g, 8.86mmol) in DMSO (15mL) was added **21** (6g, 26.3mmol). Reaction was stirred at 80℃ overnight. The mixture was diluted with EtOAc, the organic phase was washed with water and brine, dried over anhydrous sodium sulfate and concentrated. The crude product was purified by flash chromatography (Hex:EA=1:1→1:2) to afford yellow oil (4.2g, 90%). ^{1}H NMR (600 Mhz, $CDCl_3$) δ 8.46 (d, *J* = 2.4 Hz, 1H), 7.97 (d, *J* = 8.4 Hz, 1H), 7.95 (d, *J* = 1.8 Hz, 1H), 7.83 (dd, *J* = 8.4

and 1.8Hz, 1H), 7.54 (dd, *J* = 8.4 and 2.4 Hz, 1H), 7.32 (d, *J* = 8.4 Hz, 1H), 4.60 (s, 2H), 3.51 (t, *J* = 6.3Hz, 2H), 3.34 (s, 3H), 2.87 (t, *J* = 8.1Hz, 2H), 1.83-1.73 (m, 2H), 1.65-1.56 (m, 2H), 1.59 (s, 6H), 1.46-1.40 (m, 4H). ^{13}C NMR (150 MHz, $CDCl_3$) δ 180.33, 174.69, 164.01, 149.52, 137.42, 136.93, 135.25, 133.61 (q, *J* = 33.2 Hz), 132.14, 129.50, 127.04 (q, *J* = 4.7 Hz), 123.38, 121.82 (q, *J* = 273 Hz), 114.74, 110.30, 96.39, 67.71, 66.35, 55.10, 38.10, 29.60, 29.47, 29.22, 26.05, 23.73 (2C).

4-(3-(6-(4-Hydroxybutyl)pyridin-3-yl)-4,4-dimethyl-5-oxo-2-thioxoimidazolidin-1-yl)-2-(trifluoromethyl)benzonitrile (9a). To the solution of **8a** (5.8g, 11.4mmol) in methanol, Hydrogen Chloride (4N, in 1,4-dioxane) (15mL, 60mmol) was added dropwise. Reaction was stirred at room temperature overnight. Mixture was neutralized by saturated sodium bicarbonate, extracted with EA and washed by water and brine, dried over anhydrous sodium sulfate and concentrated. The crude product was purified by flash chromatography (Hex:EA=1:2 → 1:4 → EA) to afforded brown oil (4.95g, 94%). ^{1}H NMR (600 MHz, $CDCl_3$) δ 8.40 (d, *J* = 2.4 Hz, 1H), 7.93 (d, *J* = 8.4 Hz, 1H), 7.92 (s, 1H), 7.80 (d, *J* = 8.4, 1H), 7.53 (dd, *J* = 8.4 and 2.4 Hz, 1H), 7.31 (d, *J* = 8.4 Hz, 1H), 3.63 (t, *J* = 6.6 Hz, 2H), 2.99 (br s, 1H), 2.86 (t, *J* = 7.8 Hz, 2H), 1.78-1.86 (m, 2H), 1.58-1.66 (m, 2H), 1.54 (s, 6H); 13C NMR (150 MHz, $CDCl_3$) δ 180.34, 174.67, 163.58, 149.43, 137.65, 137.02, 135.31, 133.37 (q, *J* = 33.2 Hz), 132.27, 129.70, 127.06 (q, *J* = 4.7 Hz), 123.62, 121.85 (q, *J* = 273 Hz), 114.81, 110.07, 66.39, 62.02, 37.45, 32.16, 25.66, 23.62 (2C).

4-(3-(6-(6-Hydroxyhexyl)pyridin-3-yl)-4,4-dimethyl-5-oxo-2-thioxoimidazolidin-1-yl)-2-(trifluoromethyl)benzonitrile (9b). To a solution of **8b** (1.68g, 3.14mmol) in methanol (15mL) was added hydrogen chloride (4N, in 1,4-dioxane)

(4mL) dropwise. Reaction was stirred at room temperature for 3hrs. Mixture was neutralized by saturated sodium bicarbonate, extracted with EtOAc and washed by water and brine, dried over anhydrous sodium sulfate and concentrated. The crude product was purified by flash chromatography (Hex:EA=1:1→1:2) to afford yellow foam (1.4g, 91%). ^{1}H NMR (600 MHz, $CDCl_3$) δ 8.42 (d, *J* = 2.4 Hz, 1H), 7.95 (d, *J* = 8.4 Hz, 1H), 7.93 (d, *J* = 1.2 Hz, 1H), 7.81 (dd, *J* = 8.4 and 1.2Hz, 1H), 7.53 (dd, *J* = 8.4 and 2.4 Hz, 1H), 7.31 (d, *J* = 8.4 Hz, 1H), 3.58 (t, *J* = 6.6 Hz, 2H), 2.84 (t, *J* = 7.8 Hz, 2H), 2.16 (br s, 1H), 1.80-1.72 (m, 2H), 1.56 (s, 6H), 1.58-1.50 (m, 2H), 1.44-1.36 (m, 4H); ^{13}C NMR (150 MHz, $CDCl_3$) δ 180.35, 174.71, 163.92, 149.40, 137.62, 136.96, 135.29, 133.53 (q, *J* = 33.2 Hz), 132.19, 129.60, 127.052 (q, *J* = 4.7 Hz), 123.52, 121.81 (q, *J* = 273 Hz), 114.75, 110.18, 66.38, 62.50, 37.88, 32.43, 29.44, 29.00, 25.42, 23.66 (2C). HR-ESI-MS *m/z* Calcd for $C_{24}H_{25}F_3N_4O_2S$ $[M+H]^+$ 491.1729, found 491.1724.

6-(5-(3-(4-Cyano-3-(trifluoromethyl)phenyl)-5,5-dimethyl-4-oxo-2-thioxoimidazolidin-1-yl)pyridin-2-yl)hexyl methanesulfonate (10b). In argon atmosphere, to a stirred solution of 7 (1.35g, 2.75mmol) and triethylamine (1.15mL, 8.25mmol) in dichloromethane (15mL) was added methanesulfonyl chloride (0,42mL, 5.47mmol) at 0 ℃ dropwise. Reaction was stirred at room temperature for 30min. Solvent was removed under reduced pressure. The crude product was purified by flash chromatography (Hex:EA=1:1→1:2) to afford white foam (1.47g, 94%).

4-(3-(6-(4-Azidobutyl)pyridin-3-yl)-4,4-dimethyl-5-oxo-2-thioxoimidazolidin-1-yl)-2-(trifluoromethyl)benzonitrile (11a). In argon atmosphere, to a stirred solution of **9a** (820mg, 1.77mmol) in DCM and triethylamine (1.23mL, 8.87mmol) was added Methanesulfonyl Chloride (0.55mL, 7.1mmol) dropwise at 0 ℃. Reaction was stirred at

0 ℃ for 30min and warm to room temperature for 1h. Mixture was washed by water and brine, the solvent was evaporated away under reduced pressure. Mixture was redissolved in DMF(15mL), sodium azide (345mg, 5.3mmol) was added. Reaction was stirred at room temperature overnight. Mixture was diluted with EA, washed by water and brine. The crude product was purified by flash chromatography (Hex:EA=1:2) to afforded transparent oil (194mg, 25%). ^{1}H NMR (600 Mhz, $CDCl_3$) δ 8.48 (d, *J* = 1.8 Hz, 1H), 7.98 (d, *J* = 8.4 Hz, 1H), 7.95 (s, 1H), 7.83 (d, *J* = 7.8Hz, 1H), 7.57 (dd, *J* = 8.4 and 2.4 Hz, 1H), 7.34 (d, *J* = 8.4 Hz, 1H), 3.44 (t, *J* = 7.2 Hz, 2H), 2.91 (t, *J* = 7.8 Hz, 2H), 1.86-1.92 (m, 2H), 1.68-1.74 (m, 2H), 1.59 (s, 6H); ^{13}C NMR (150 MHz, $CDCl_3$) δ 180.35, 174.65, 163.10, 149.67, 137.60, 136.89, 135.26, 133.65 (q, *J* = 33.3 Hz), 132.12, 129.78, 127.03 (q, *J* = 4.7 Hz), 123.47, 121.81 (q, *J* = 273 Hz), 114.72, 110.34, 66.35, 51.19, 37.43, 28.52, 26.47, 23.75 (2C). HR-ESI-MS *m/z* Calcd for $C_{22}H_{20}F_3N_7OS$ $[M+H]^+$ 488.1491, found 488.1497

4-(3-(6-(6-Azidohexyl)pyridin-3-yl)-4,4-dimethyl-5-oxo-2-thioxoimidazolidin-1-yl)-2-(trifluoromethyl)benzonitrile (11b). To a solution of 7 (1.47g, 2.59mmol) in dimethylformamide (12mL) was added sodium azide (506mg, 7.8mmol). Reaction was stirred at room temperature for 6hrs. Mixture was diluted with EtOAc, the organic phase was washed with water and brine, dried over anhydrous sodium sulfate and concentrated to afford yellow oil (1.5g). ^{1}H NMR (600 Mhz, $CDCl_3$) δ 8.45 (d, *J* = 2.4 Hz, 1H), 7.95 (d, *J* = 11.4 Hz, 1H), 7.95 (s, 1H), 7.82 (dd, *J* = 8.4 and 1.8Hz, 1H), 7.54 (dd, *J* = 8.4 and 2.4 Hz, 1H), 7.31 (d, *J* = 8.4 Hz, 1H), 3.24 (t, *J* = 7.2 Hz, 2H), 2.85 (t, *J* = 7.8 Hz, 2H), 1.81-1.73 (m, 2H), 1.62-1.55 (m, 2H), 1.57 (s, 6H), 1.45-1.38 (m, 4H); ^{13}C NMR (150 MHz, $CDCl_3$) δ 180.33, 174.67, 163.77, 149.55, 137.46, 136.99, 135.26, 133.50 (q, *J* =

33.3 Hz), 132.19, 129.57, 127.05 (q, *J* = 4.7 Hz), 123.41, 121.84 (q, *J* = 273 Hz), 114.77, 110.20, 66.36, 51.35, 37.97, 29.28, 28.87, 28.67, 26.49, 23.68 (2C). HR-ESI-MS *m/z* Calcd for $C_{24}H_{24}F_3N_7OS$ $[M+H]^+$ 516.1785, found 516.1807

4-(3-(6-(4-Isothiocyanatobutyl)pyridin-3-yl)-4,4-dimethyl-5-oxo-2-thioxoimidazolidin-1-yl)-2-(trifluoromethyl)benzonitrile (12a). To a solution of **11a** (194mg, 0.40mmol) in THF (5mL) was added triphenylphosphine (225mg, 0.86mmol). Reaction was refluxed overnight. Then 3mL carbon disulfide was added, refluxed overnight. Solvent was removed under reduced pressure. Mixture was washed by water and brine. The crude product was purified by flash chromatography (Hex/EA: 1:1), afforded transparent oil (53mg, 26%).^{1}H NMR (600 MHz, $CDCl_3$) δ 8.47 (d, *J* = 1.8 Hz, 1H), 7.97 (d, *J* = 8.4 Hz, 1H), 7.95 (s, 1H), 7.83 (d, *J* = 8.4 Hz, 1H), 7.57 (dd, *J* = 8.4 and 1.8 Hz, 1H), 7.34 (d, *J* = 8.4 Hz, 1H), 3.57 (t, *J* = 6.6 Hz, 2H), 2.90 (t, *J* = 7.8 Hz, 2H), 1.86-1.98 (m, 2H), 1.72-1.86 (m, 2H), 1.59 (s, 6H); ^{13}C NMR (150 MHz, $CDCl_3$) δ 180.35, 174.64, 163.67, 149.73, 137.66, 136.94, 135.28, 133.56 (q, *J* = 33.2 Hz), 132.18, 129.88, 127.05 (q, *J* = 4.5 Hz), 123.52, 121.83 (q, *J* = 273 Hz), 114.77, 110.26, 66.38, 44.87, 37.03, 29.73, 29.52, 26.24, 23.74 (2C).

4-(3-(6-(6-Isothiocyanatohexyl)pyridin-3-yl)-4,4-dimethyl-5-oxo-2-thioxoimidazolidin-1-yl)-2-(trifluoromethyl)benzonitrile (12b). To a solution of 8 (1.5g 2.9mmol) in THF (10mL) was added triphenylphosphine (1.52g, 5.8mmol). Reaction was refluxed overnight. Then carbon disulfide (9mL) was added, mixture was refluxed for another 5hrs. Solvent was removed under reduced pressure. The crude product was purified by flash chromatography (Hex:EA=1:1) to afford yellow foam(905mg, 59%). ^{1}H NMR (600 MHz, $CDCl_3$) δ 8.45 (d, *J* = 2.4 Hz, 1H), 7.96 (d, *J* =

9.0 Hz, 1H), 7.95 (s, 1H), 7.83 (dd, *J* = 8.4 and 1.8Hz, 1H), 7.55 (dd, *J* = 8.4 and 2.4 Hz, 1H), 7.32 (d, *J* = 8.4 Hz, 1H), 3.48 (t, *J* = 6.6 Hz, 2H), 2.86 (t, *J* = 7.8 Hz, 2H), 1.82-1.76 (m, 2H), 1.72-1.65 (m, 2H), 1.57 (s, 6H), 1.49-1.38 (m, 4H); ^{13}C NMR (150 MHz, $CDCl_3$) δ 180.33, 174.67, 163.62, 149.57, 137.52, 136.99, 135.27, 133.49 (q, *J* = 33.2 Hz), 132.22, 129.62, 127.06 (q, *J* = 4.5 Hz), 123.47, 121.84 (q, *J* = 273 Hz), 114.77, 110.20, 66.37, 44.97, 37.87, 29.74, 29.16, 28.49, 26.33, 23.70 (2C). HR-ESI-MS *m/z* Calcd for $C_{25}H_{24}F_3N_5OS_2$ $[M+H]^+$ 532.1453, found 532.1478.

N-acetyl-S-((6-(5-(3-(4-cyano-3-(trifluoromethyl)phenyl)-5,5-dimethyl-4-oxo-2-thioxoimidazolidin-1-yl)pyridin-2-yl)hexyl)carbamothioyl)-D-cysteine (13). To a solution of 9 (300mg, 0.56mmol) in acetonitrile (3mL) was added N-acetyl-cysteine (60mg, 0.37mmol) and Sodium bicarbonate (240mg, 2.86mmol). Reaction was stirred at room temperature overnight. Then heated to 45 ℃ overnight. Solvent was removed under reduced pressure. The crude product was purified by flash chromatography (Hex:EA = 2:1 → 1:1 → DCM:MeOH:AcOH = 10:1:1%) . Purified product was washed by water to get rid of remaining NAC and afford white foam (162.2mg, 63%). ^{1}H NMR (600 MHz, $CDCl_3$) δ 8.64 (s, 1H), 8.54 (d, *J* = 1.8 Hz, 1H), 7.97 (d, *J* = 8.4 Hz, 1H), 7.94 (d, *J* = 1.2 Hz, 1H), 7.83 (dd, *J* = 8.4 and 1.8Hz, 1H), 7.67 (dd, *J* = 8.4 and 2.4 Hz, 1H), 7.40 (d, *J* = 8.4 Hz, 1H), 4.70 (q, *J* = 5.4 Hz, 1H), 3.78 (dd, *J* = 14.4 and 6.0 Hz, 2H), 3.70 (t, *J* = 6.6 Hz, 2H), 2.86 (t, *J* = 7.8, 2H), 1.99 (d, *J* = 7.8Hz, 3H), 1.82-1.71 (m, 2H), 1.71-1.63 (m, 2H), 1.59 (s, 6H), 1.50-1.36 (m, 4H); ^{13}C NMR (150 MHz, $CDCl_3$) δ 196.52, 180.46, 174.58, 172.53, 171.71, 163.15, 148.45, 139.13, 136.94, 135.36, 133.53 (q, *J* = 33.2 Hz), 132.29, 130.35, 127.09 (q, *J* = 4.5 Hz), 124.31, 121.83 (q, *J* = 273 Hz), 114.77, 110.28,

66.50, 53.71, 47.69, 36.83, 35.68, 29.36, 28.54, 27.67, 26.21, 23.75 (2C), 22.96. HR-ESI-MS *m/z* Calcd for $C_{30}H_{33}F_3N_6O_4S_3$ $[M+H]^+$ 695.1756, found 695.1743

4-(5-(3-(4-(Tert-butylcarbamoyl)-3-(trifluoromethyl)phenyl)-5,5-dimethyl-4-oxo-2-thioxoimidazolidin-1-yl)pyridin-2-yl)butyl acetate (14). To a solution of **9a** (108mg, 0.23mmol) in tert-butyl acetate (3mL) was added sulfuric acid (0.2mL) at 0 ℃. Reaction was stirred at 42 ℃ for 2hrs. Mixture was neutralized by saturated sodium bicarbonate at 0 ℃, extracted with EtOAc and washed by water and brine, dried over anhydrous sodium sulfate and concentrated. The crude product was purified by flash chromatography (Hex:EA=1:1) to afford transparent oil (121mg, 91%). ^{1}H NMR (600 MHz, $CDCl_3$) δ 8.45 (s, 1H), 7.71 (s, 1H), 7.60 (m, 2H), 7.55 (dd, *J* = 8.4 and 2.4 Hz, 1H), 7.30 (d, *J* = 8.4 Hz, 1H), 5.77 (s, 1H), 4.07 (t, *J* = 6.6 Hz, 2H), 2.87 (t, *J* = 7.8 Hz, 2H), 2.00 (s, 3H), 1.87-1.80 (m, 2H), 1.75-1.68 (m, 2H), 1.54 (s, 6H), 1.41 (s, 9H); ^{13}C NMR (150 MHz, $CDCl_3$) δ 181.29, 175.01, 171.15, 165.94, 163.00, 149.65, 137.68, 137.45, 133.88, 132.02, 129.99, 129.49, 127.93 (q, *J* = 32.6 Hz), 126.64(q, *J* = 5.3 Hz), 123.41, 123.06 (q, *J* = 273 Hz), 66.22, 64.12, 52.41, 37.53, 28.44 (3C), 28.35, 25.81, 23.66 (2C), 20.96.

6-(5-(3-(4-(Tert-butylcarbamoyl)-3-(trifluoromethyl)phenyl)-5,5-dimethyl-4-oxo-2-thioxoimidazolidin-1-yl)pyridin-2-yl)hexyl acetate (15). To a solution of **8b** (1.2g, 2.24mmol) in tert-butyl acetate (20mL) was added sulfuric acid (2mL) at 0 ℃. Reaction was stirred at 42 ℃ for 2hrs. Mixture was neutralized by saturated sodium bicarbonate at 0 ℃, extracted with EtOAc and washed by water and brine, dried over anhydrous sodium sulfate and concentrated. The crude product was purified by flash chromatography (Hex:EA=2:1 → 1:1) to afford light yellow foam (810mg, 60%). ^{1}H

NMR (600 MHz, $CDCl_3$) δ 8.45 (d, *J* = 1.8 Hz, 1H), 7.72 (s, 1H), 7.62 (m, 2H), 7.54 (dd, *J* = 8.4 and 2.4 Hz, 1H), 7.30 (d, *J* = 7.8 Hz, 1H), 5.70 (s, 1H), 4.03 (t, *J* = 6.6 Hz, 2H), 2.84 (t, *J* = 7.8 Hz, 2H), 2.01 (s, 3H), 1.80-1.74 (m, 2H), 1.65-1.59 (m, 2H), 1.55 (s, 6H), 1.43 (s, 9H), 1.45-1.34 (m, 4H); ^{13}C NMR (150 MHz, $CDCl_3$) δ 181.30, 175.03, 171.21, 165.92, 163.63, 149.62, 137.54, 137.45, 133.90, 132.03, 129.79, 129.51, 127.97 (q, *J* = 32.7 Hz), 126.65 (q, *J* = 4.5 Hz), 123.31, 123.06 (q, *J* = 273 Hz), 66.22, 64.44, 52.43, 38.02, 29.35, 29.00, 28.46 (3C), 28.43, 25.71, 23.69 (2C), 20.99. HR-ESI-MS *m/z* Calcd for $C_{30}H_{37}F_3N_4O_4S$ $[M+H]^+$ 607.2566, found 607.2263.

N-(tert-butyl)-4-(3-(6-(6-hydroxyhexyl)pyridin-3-yl)-4,4-dimethyl-5-oxo-2-thioxoimidazolidin-1-yl)-2-(trifluoromethyl)benzamide (16). To a solution of **15** (415mg, 0.68mmol) in methanol (10mL) was added sulfuric acid (1mL). Reactio n was stirred at 50℃ for 1h. Mixture was neutralized by saturated sodium bicarbonate, diluted with EtOAc and washed by water and brine, dried over anhydrous sodium sulfate and concentrated to afford transparent oil (351mg, 91%). ^{1}H NMR (600 MHz, $CDCl_3$) δ 8.46 (d, *J* = 2.4 Hz, 1H), 7.73 (s, 1H), 7.64 (m, 2H), 7.55 (dd, *J* = 8.4 and 2.4 Hz, 1H), 7.31 (d, *J* = 8.4 Hz, 1H), 5.67 (s, 1H), 3.62 (t, *J* = 6.6 Hz, 2H), 2.86 (t, *J* = 7.8 Hz, 2H), 1.82-1.75 (m, 2H), 1.62-1.53 (m, 2H), 1.57 (s, 6H), 1.44 (s, 9H), 1.47-1.37 (m, 4H); ^{13}C NMR (150 MHz, $CDCl_3$) δ 181.32, 175.07, 165.97, 163.73, 149.56, 137.59, 137.45, 133.92, 132.07, 129.77, 129.50, 127.95 (q, *J* = 32.6 Hz), 126.68 (q, *J* = 5.3 Hz), 123.38, 123.07 (q, *J* = 273 Hz), 66.25, 62.71, 37.97, 36.56, 32.52, 29.44, 29.05, 28.46 (3C), 25.45, 23.68 (2C). HR-ESI-MS *m/z* Calcd for $C_{28}H_{35}F_3N_4O_3S$ $[M+H]^+$ 565.2460, found 565.2466

6-(5-(3-(4-(Tert-butylcarbamoyl)-3-(trifluoromethyl)phenyl)-5,5-dimethyl-4-oxo-2-thioxoimidazolidin-1-yl)pyridin-2-yl)hexyl methanesulfonate (17). To a stirred

solution of **16** (351mg, 0.62mmol) in dichloromethane (5mL) was added triethylamine (0.7mL, 8.25mmol) and methanesulfonyl chloride (0.3mL, 5.47mmol). Reaction was stirred at room temperature for 30min. Solvent was removed under reduced pressure. The crude product was purified by flash chromatography (Hex:EA=1:1→1:2) to afford white foam (360mg, 90%).

4-(3-(6-(6-Azidohexyl)pyridin-3-yl)-4,4-dimethyl-5-oxo-2-thioxoimidazolidin-1-yl)-N-(tert-butyl)-2-(trifluoromethyl)benzamide (18). To a solution of **17** (360mg, 56mmol) in dimethylformamide (5mL) was added sodium azide (182mg, 2.8mmol). Reaction was stirred at 50℃ overnight. Mixture was diluted with EtOAc, the organic phase was washed with water and brine, dried over anhydrous sodium sulfate and concentrated to afford yellow oil (359mg). ^{1}H NMR (600 MHz, $CDCl_3$) δ 8.46 (d, *J* = 2.4 Hz, 1H), 7.73 (s, 1H), 7.63 (m, 2H), 7.55 (dd, *J* = 8.4 and 2.4 Hz, 1H), 7.31 (d, *J* = 8.4 Hz, 1H), 5.67 (s, 1H), 3.24 (t, *J* = 6.6 Hz, 2H), 2.85 (t, *J* = 7.8 Hz, 2H), 1.83-1.75 (m, 2H), 1.63-1.58 (m, 2H), 1.56 (s, 6H), 1.44 (s, 9H), 1.46-1.39 (m, 4H); ^{13}C NMR (150 MHz, $CDCl_3$) δ 181.31, 175.04, 165.93, 163.58, 149.63, 137.56, 137.46, 133.90, 132.05, 129.81, 129.53, 127.98 (q, *J* = 32.1 Hz), 126.66 (q, *J* = 5.3 Hz), 123.34, 123.06 (q, *J* = 273 Hz), 66.23, 52.45, 51.36, 37.99, 29.30, 28.90, 28.68, 28.47 (3C), 26.51, 23.70 (2C). HR-ESI-MS *m/z* Calcd for $C_{28}H_{34}F_3N_7O_2S$ $[M+H]^+$ 590.2525, found 590.2520.

N-(tert-butyl)-4-(3-(6-(6-isothiocyanatohexyl)pyridin-3-yl)-4,4-dimethyl-5-oxo-2-thioxoimidazolidin-1-yl)-2-(trifluoromethyl)benzamide (19). To a solution of **18** (180mg, 0.31mmol) in THF (5mL) was added triphenylphosphine (400mg, 1.55mmol). Reaction was refluxed for 1h. Then Carbon disulfide (1.7mL) was added, mixture was refluxed for another 1h. Solvent was removed under reduced pressure. The crude product

was purified by flash chromatography (Hex:EA=2:1→1:1) to afford transparent oil(107mg, 57%). ^{1}H NMR (600 MHz, $CDCl_3$) δ 8.44 (d, *J* = 2.4 Hz, 1H), 7.71 (s, 1H), 7.61 (s, 2H), 7.54 (dd, *J* = 8.4 and 2.4 Hz, 1H), 7.30 (d, *J* = 8.4 Hz, 1H), 5.66 (s, 1H), 3.47 (t, *J* = 6.6 Hz, 2H), 2.84 (t, *J* = 7.8 Hz, 2H), 1.74-1.81 (m, 2H), 1.64-1.71 (m, 2H), 1.55 (s, 6H), 1.41 (s, 9H), 1.37-1.48 (m, 4H); ^{13}C NMR (150 MHz, $CDCl_3$) δ 181.28, 175.03, 165.93, 163.41, 149.64, 149.64, 137.59, 137.42, 133.90, 132.05, 129.84, 129.48, 127.93 (q, *J* = 32.1 Hz), 126.66 (q, *J* = 5.3 Hz), 123.38, 123.06 (q, *J* = 272 Hz), 66.22, 52.42, 44.96, 37.87, 29.74, 29.16, 28.50, 28.46 (3C), 26.33, 23.69 (2C). HR-ESI-MS *m/z* Calcd for $C_{29}H_{34}F_3N_5O_2S_2$ $[M+H]^+$ 606.2184, found 606.2183.

Methyl 2-((3-fluorophenyl)amino)-2-methylpropanoate (23). To a mixture of 3-flouroaniline (22)(10g, 90mmol) and methyl α-bromoisobutyrate (6)(27g, 14.9mmol) in ethanol (70mL) was added sodium acetate (14.8g, 180mmol). Reaction was refluxed overnight. Mixture was filtered, solvent was evaporated under reduced pressure. Mixture was diluted with EtOAc, the organic phase was washed by water and brine, dried over anhydrous sodium sulfate and concentrated. The crude product was purified by flash chromatography (Hex:EA=15:1→10:1) to afford red oil (12.1g, 64%). ^{1}H NMR (600 MHz, $CDCl_3$) δ 7.03-7.09 (m, 1H), 6.39-6.43 (m, 1H), 6.22-6.31 (m, 2H), 4.21 (br s, 1H), 3.71 (s, 3H), 1.56 (s, 6H).

Methyl 2-((3-fluoro-4-iodophenyl)amino)-2-methylpropanoate (24). To a mixture of **23** (4g, 19.0mmol) in H_2O/dioxane (30mL/2mL) was added sodium bicarbonate (6.37g, 75.8mmol) and iodine (5.8g, 22.7mmol). Reaction was stirred at room temperature for 3h. Mixture was quenched by saturated sodium thiosulfate, and extracted with EtOAc, washed by water and brine, dried over anhydrous sodium sulfate

and concentrated. The crude product was purified by flash chromatography (Hex:EA=10:1) to afford yellow solid (5.73g, 89%). ^{1}H NMR (600 MHz, $CDCl_3$) δ 7.30 (t, *J* = 8.4 Hz, 1H), 6.21(dd, *J* = 10.8 and 2.4 Hz, 1H), 6.06 (dd, *J* = 8.4 and 2.4Hz, 1H), 4.45 (br s, 1H), 3.63 (s, 3H), 1.47 (s, 6H); ^{13}C NMR (150 MHz, $CDCl_3$) δ 175.95, 162.08 (d, *J* = 240.3 Hz), 147.76 (d, *J*=9.6Hz), 138.75 (d, *J*=2.3Hz), 112.66, 101.76 (d, *J*=27.5Hz), 64.85 (d, *J*=25.8Hz), 57.22, 52.71, 25.93.

Ethyl (E)-3-(4-(3-(4-cyano-3-(trifluoromethyl)phenyl)-5,5-dimethyl-4-oxo-2-thioxoimidazolidin-1-yl)-2-fluorophenyl)acrylate (26). In argon atmosphere, to a mixture of **25** (4g, 7.9mmol), palladium(II) acetate (420mg, 1.88mmol) and tri(o-tolyl)phosphine (1.25g, 4.11mmol) in DMF/DIPEA (20mL/7mL) was added ethyl acrylate (1.04mL, 9.76mmol). Reaction was stirred at 80℃ overnight. Mixture was diluted with EtOAc, the organic phase was washed by water and brine, dried over anhydrous sodium sulfate and concentrated. The crude product was purified by flash chromatography (Hex:EA=10:1) to afford brown solid (1.51g, 53%). ^{1}H NMR (600MHz, CDCl3): δ 7.96-7.99 (m, 2H), 7.79-7.85(m, 2H), 7.70(t, *J*=8.2Hz, 1H), 7.11-7.17 (m, 2H), 6.61(d, *J*=16.4Hz, 1H), 4.29(q, *J*=7.2Hz, 2H), 1.62(s, 6H), 1.36(t, *J*=7.2Hz, 3H). ^{13}C NMR (150MHz, $CDCl_3$): δ179.74, 174.48, 166.28, 161.14 (d, *J*=255.5Hz), 137.36(d, *J*=10.2Hz), 136.86, 135.51(d, *J*=1.0Hz), 135.24, 133.59(q, *J*=33.3Hz), 132.12, 129.98(d, *J*=4.0Hz), 127.03(q, *J*=4.7Hz), 125.86(d, *J*=3.7Hz), 123.16, 122.85(d, *J*=6.5 Hz), 120.44, 117.91(d, *J*=23.6Hz), 114.68, 110.31(d, *J*=2.0Hz), 66.57, 60.88, 23.76, 14.21.

(E)-3-(4-(3-(4-cyano-3-(trifluoromethyl)phenyl)-5,5-dimethyl-4-oxo-2-thioxoimidazolidin-1-yl)-2-fluorophenyl)acrylic acid (27). To a solution of **26** (1.51g, 2.99 mmol) in acetonitrile (35mL) was added HCl (37%, 25mL). Reaction was refluxed

overnight. Mixture was diluted with EtOAc, the organic phase was washed by water and brine, dried over anhydrous sodium sulfate and concentrated. The crude product was purified by flash chromatography (Hex:EA:AcOH=2:1:0.5%) to afford orange solid (1.31g, 92%). ^{1}H NMR (600MHz, Acetone-d_6) δ 8.28 (d, *J* = 8.0Hz,1H), 8.20 (d, *J* = 1.6Hz,1H), 8.08 (dd, *J* = 8.4Hz, 2.0Hz,1H), 8.01 (t, *J* = 8.4Hz, 1H), 7.83(d, *J* = 16Hz, 1H,), 7.37-7.42 (m, 2H), 6.71 (d, *J* = 16Hz, 1H), 1.68 (s, 6H). ^{13}C NMR (150MHz, Acetone-d_6) δ 181.38, 175.66, 167.21, 161.77 (d, *J* = 251.8Hz), 139.59 (d, *J* = 10.6Hz), 139.03, 136.66, 136.29 (d, *J* = 3.1Hz), 134.28, 132.89 (q, *J* = 32.7Hz), 130.69 (d, *J* = 3.9Hz), 128.50 (q, *J* = 4.9Hz), 127.52 (d, *J* = 3.5Hz), 124.66, 124.23 (d, *J* = 11.6Hz), 123.34 (d, *J* = 5.8Hz), 118.96 (d, *J* = 23.6Hz), 115.62, 110.29, 67.63, 23.65 (2C).

(E)-3-(4-(3-(4-cyano-3-(trifluoromethyl)phenyl)-5,5-dimethyl-4-oxo-2-thioxoimidazolidin-1-yl)-2-fluorophenyl)-N-((tetrahydro-2H-pyran-2-yl)oxy)acrylamide (28). In argon atmosphere, to a mixture of **27** (1.31mg, 2.75mmol), NH2OTHP (0.35g, 3.1mmol) and BOP (1.34g, 3.1mmol) in DMF (15mL) was added DIPEA (0.96mL, 5.50mmol). Reaction was stirred at room temperature overnight. Mixture was diluted with EtOAc, the organic phase was washed by water and brine, dried over anhydrous sodium sulfate and concentrated. The crude product was purified by flash chromatography (DCM:EA=4:1) to afford white solid (730mg, 46%). ^{1}H NMR (600MHz, DMSO-d_6): 11.42 (s, 1H), 8.37 (d, *J*=7.8Hz, 1H), 8.27(s, 1H), 8.05(d, *J* = 8.4Hz, 1H), 7.84(t, *J* = 7.8Hz, 1H), 7.56(d, *J* = 16Hz, 1H), 7.40 (d, *J* = 11Hz, 1H), 7.30 (d, *J* = 8.4Hz, 1H), 6.68 (d, *J* = 16Hz, 1H), 4.91 (s,1H), 3.94 (t, *J* = 8.4Hz, 1H), 3.52 (m, 1H), 1.65 (br s, 3H), 1.52 (br s, 9H).

(E)-3-(4-(3-(4-cyano-3-(trifluoromethyl)phenyl)-5,5-dimethyl-4-oxo-2-thioxoimidazolidin-1-yl)-2-fluorophenyl)-N-hydroxyacrylamide (1005). To the solution of **28** (672mg, 1.30mmol) in methanol (15mL) was added TFA (1.74mL, 22.7mmol). Reaction was stirred at 0℃ for 6hrs. Mixture was diluted with EtOAc, the organic phase was washed by water and brine, dried over anhydrous sodium sulfate and concentrated. The crude product was purified by flash chromatography (Hex:EA=1:2) to afford white solid (510mg, 89%). ^{1}H NMR (600MHz, Methanol-d_4) δ 8.15 (s, 1H), 8.13 (d, *J* = 8.4Hz, 1H), 7.97 (dd, *J*=8.4 and 1.2Hz, 1H), 7.74 (t, *J*=8.4Hz, 1H), 7.71 (d, *J*=16.2Hz, 1H), 7.30 (dd, *J* = 10.8 and 1.8Hz, 1H), 7.26 (dd, *J* = 8.4 and 1.8Hz, 1H), 6.67 (d, *J*=16.2Hz, 1H), 1.57 (s, 6H). ^{13}C NMR (150MHz, Methanol-d_4) δ 180.29, 175.08, 164.11, 160.90 (d, *J*=257.0Hz), 137.86, 135.95, 134.86, 133.89 (q, *J*=37.3Hz), 132.91, 130.90, 128.86 (q, *J*=4.8Hz), 127.70 (d, *J*=3.7Hz), 125.22 (d, *J*=11.7Hz), 125.01, 122.83, 122.30, 119.34 (d, *J*=23.8Hz), 114.55, 109.39, 66.62, 22.30 (2C). HR-ESI-MS *m/z* Calcd for $C_{22}H_{17}F_4N_4O_3S$ $[M+H]^+$ 493.0958, found 493.0960.

(E)-3-(4-(3-(4-cyano-3-(trifluoromethyl)phenyl)-5,5-dimethyl-4-oxo-2-thioxoimidazolidin-1-yl)-2-fluorophenyl)-N-((isopropylcarbamoyl)oxy)acrylamide (29). To a solution of **1005** (58mg, 0.12mmol) in acetonitrile (5mL) was added 1,1′-Carbonyldiimidazole (29mg, 0.18mmol) at 0℃. Reaction was stirred at room temperature for 2h. Then isopropylamine (21mg, 0.36mmol) was added and stirred for another hour. Solvent was evaporated under reduced pressure. The crude product was purified by Flash chromatography (Hex:EA=1:2→DCM:MeOH=20:1) to afford yellow solid (32.7mg, 49%).^{1}H NMR (600MHz, Methanol-d_4) δ 8.16 (s, 1H), 8.15 (d, *J* = 8.4Hz, 1H), 7.98 (dd, *J*=8.4 and 1.8Hz, 1H), 7.82 (t, *J* = 8.4Hz, 1H), 7.79 (d, *J*=18.6Hz, 1H),

7.33 (dd, *J* = 10.8 and 1.8Hz, 1H), 7.29 (dd, *J* = 7.8 and 1.8Hz, 1H), 6.75 (d, *J*=16.2Hz, 1H), 3.30 (m, 1H), 1.58 (s, 6H), 1.19 (d, *J* = 6.6Hz, 6H). ^{13}C NMR (150MHz, Methanol-d_4) δ 180.30, 175.08, 164.34, 161.03 (d, *J*=257.0Hz), 154.58, 137.92, 135.97, 134.86, 133.58 (q, *J*=37.3Hz), 132.91, 130.56, 128.45 (q, *J*=4.8Hz), 127.65 (d, *J*=3.7Hz), 125.10 (d, *J*=11.7Hz), 125.01, 122.83, 122.30, 119.34 (d, *J*=23.8Hz), 114.53, 109.42, 66.62, 43.60, 22.30 (2C), 21.27 (2C). HR-ESI-MS *m/z* Calcd for $C_{26}H_{23}F_4N_5O_4S$ $[M+H]^+$ 600.1305, found 600.1307.

4.2. Cell Cultures

LNCaP, PC-3, 22Rv1 cell lines were maintained in RPMI1640 supplemented with 10% FBS and 1% anti-biotic and grown at 37 ℃ in a humidified air with 5% CO_2. MCF-10A cell line were maintained in DMEM/F12 supplemented with 5% horse serum, 20ng/mL EGF, 0.5mg/mL hydrocortisone, 100ng/mL cholera toxin, 10μg/mL insulin, 1% anti-biotic at 37 ℃ in a humidified air with 5% CO_2.

4.3. MTT Assay

LNCaP, PC-3, and 22Rv1 cells (6×10^3 cells/well) were seeded into 96-well plate overnight in RPMI 1640 containing 10% FBS and 1% anti-biotic (10A in DMEM/F12 supplemented with 5% horse serum, 20ng/mL EGF, 0.5mg/mL hydrocortisone, 100ng/mL cholera toxin, 10μg/mL insulin, 1% anti-biotic) and then incubated with indicated concentrations of compounds for 72h or 96h. Then 20μl 5mg/mL MTT were added to each well and incubated for 3.5h at 37 ℃. Following the incubation, 100μl DMSO was added and incubated for 30min at 37 ℃. After that, Microplate reader (BioTek) was used to measure absorbance of each well at 570 nm.

For DHT growth stimulation assay, LNCaP cells (6×10^3 cells/well) were seeded into 96-well plate overnight in RPMI supplemented with 10% charcoal stripped FBS and 1% anti-biotic and then incubated with indicated concentration of compounds with or without 1nM DHT for 96h. The rest follow the procedure as described previously.

4.4. Luciferase Assay

MDA-kb2 cells were incubated in Leibovitz's L-15 supplemented with 10% charcoal stripped FBS and 1% anti-biotic for 24h. Then MDA-kb2 (1×10^4 cells/well) were seeded into opaque 96-well plate for 24h and incubated with indicated concentration of compounds with or without 1nM DHT for 24h. For all procedure, cells were incubated at CO_2 free condition. After that, 125μl medium was removed and 75μl Steady-Glo® reagent (Promega) was added. Plate was shacked for 10min and microplate reader (BioTek) was used to measure fluorescence.

4.5. Western Blotting

LNCaP cells (4×10^5 cells/well) were seeded into 6-well plate overnight in RPMI 1640 containing 10% FBS and 1% anti-biotic and then incubated with indicated concentrations of compounds for 16h. The cells were detached and collected by centrifugation at 14000rpm for 10min, then pellets were lysed with RIPA buffer containing protease inhibitors and incubated on ice for 30 minutes. Protein concentrations were determined by the Lowry assay. Protein were heated at 95℃ for 5 minutes and resolved by electrophoresis on SDS-PAGE and transferred to PVDF membrane. The membrane was blocked by 5% milk for 1h, followed by incubation with primary antibody

overnight at 4 ℃. Then membrane was incubated with secondary antibody for 2h at room temperature. Then membrane was visualized by ImageQuant™ LAS 4000 Imager (GE).

4.6. Homology Modeling and Molecular Docking

4.6.1 Androgen Receptor

Homology model for AR was constructed by using the antagonistic form of GR structure (PDB code 1NHZ) as template [96]. The amino acid sequence of AR (PDB code 2AMB) was aligned with that of 1NHZ. Homology model was built by using Prime of Schrödinger followed by loop refinement, sidechain prediction, and minimization of non-conserved residues. Molecular docking was performed by using Glide, during which cyano group was set as constraint, all results were generated by XP model and flexible docking, while the rest of setting were kept default. Docking poses were viewed and displayed by Schrödinger Maestro.

4.6.2 HDAC6

Homology model for HDAC6 was constructed by using 1ZZ1 as template [108]. Amino acid sequence of human HDAC6 was aligned with that of 1ZZ1. Homology model was built by using Prime of Schrödinger followed by loop refinement, sidechain prediction, and minimization of non-conserved residues. Molecular docking was performed by using Glide, during which zinc ion was set as constraint, all results were generated by XP model and flexible docking, while the rest of setting were kept default. Docking poses were viewed and displayed by Schrödinger Maestro.

APPENDIX

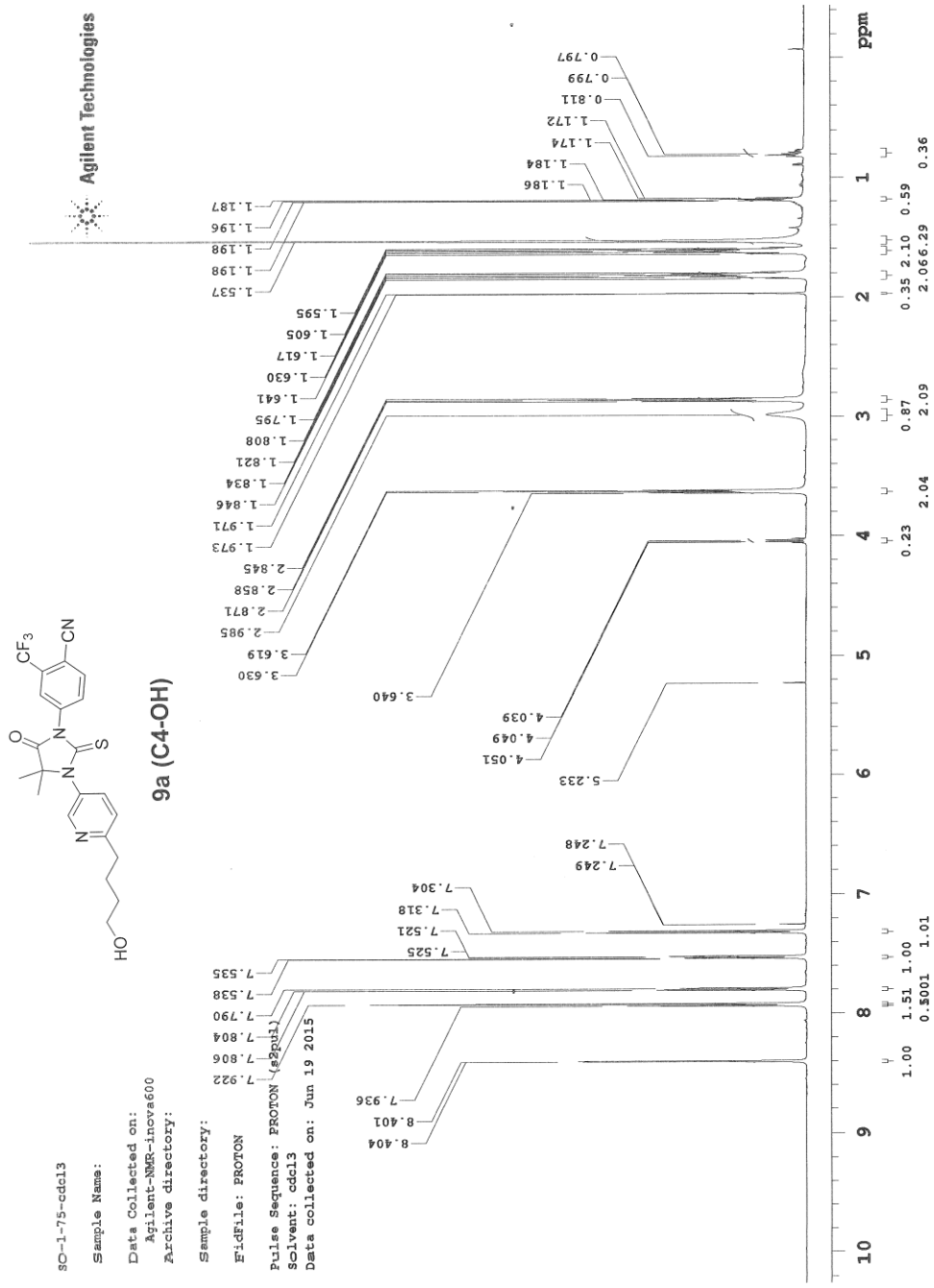
Agilent Technologies
SO-1-75-cdcl3
Sample Name:
Data Collected on:
Agilent-NMR-inova600
Archive directory:
Sample directory:
FidFile: PROTON
Pulse Sequence: PROTON (s2pul)
Solvent: cdcl3
Data collected on: Jun 19 2015
9a (C4-OH)
CF3
CN
O
N
S
HO
ppm

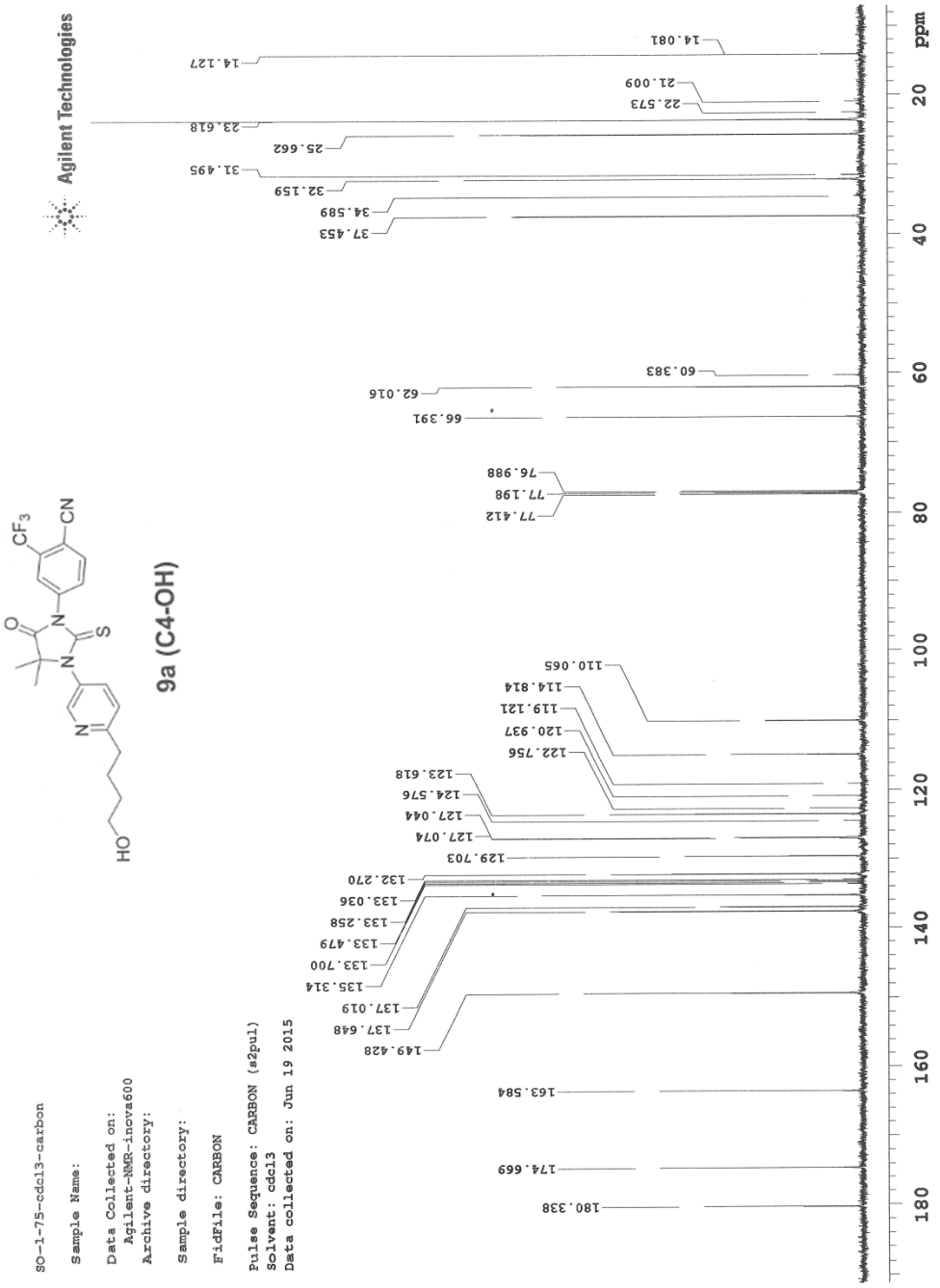
Agilent Technologies
SO-1-75-cdcl3-carbon
Sample Name:
Data Collected on:
Agilent-NMR-incva600
Archive directory:
Sample directory:
FidFile: CARBON
Pulse Sequence: CARBON (s2pul)
Solvent: cdcl3
Data collected on: Jun 19 2015
9a (C4-OH)
CF3
CN
O
N
S
N
N
HO
14.081
14.127
21.009
22.573
23.618
25.662
31.495
32.159
34.589
37.453
60.383
62.016
66.391
76.988
77.198
77.412
110.065
114.814
119.121
120.937
122.756
123.618
124.576
127.044
127.074
129.703
132.270
133.036
133.258
133.479
133.700
135.314
137.019
137.648
149.428
163.584
174.669
180.338
ppm
20
40
60
80
100
120
140
160
180

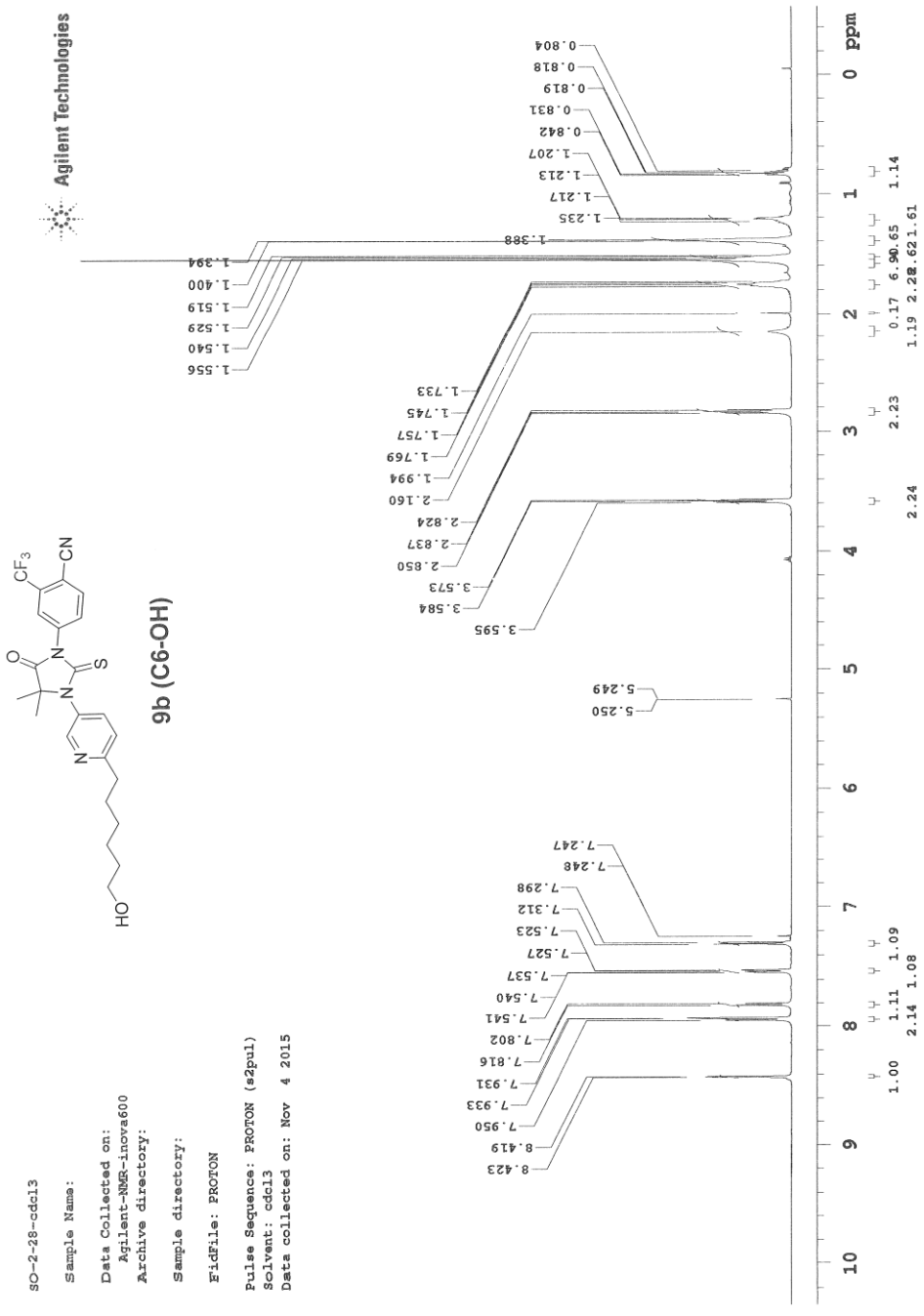
Agilent Technologies
SO-2-28-cdcl3
Sample Name:
Data Collected on:
Agilent-NMR-inova600
Archive directory:
Sample directory:
FidFile: PROTON
Pulse Sequence: PROTON (s2pul)
Solvent: cdcl3
Data collected on: Nov 4 2015
9b (C6-OH)
CF3
CN
O
N
S
N
N
HO
ppm
0 1 2 3 4 5 6 7 8 9 10
0.804
0.818
0.819
0.831
0.842
1.207
1.213
1.217
1.235
1.388
1.394
1.400
1.519
1.529
1.540
1.556
1.733
1.745
1.757
1.769
1.994
2.160
2.824
2.837
2.850
3.573
3.584
3.595
5.249
5.250
7.247
7.248
7.298
7.312
7.523
7.527
7.537
7.540
7.541
7.802
7.816
7.931
7.933
7.950
8.419
8.423
1.00 1.11 1.09
2.14 1.08
2.23
2.24
0.17 6.90 0.65 1.14
1.19 2.28 2.62 1.61

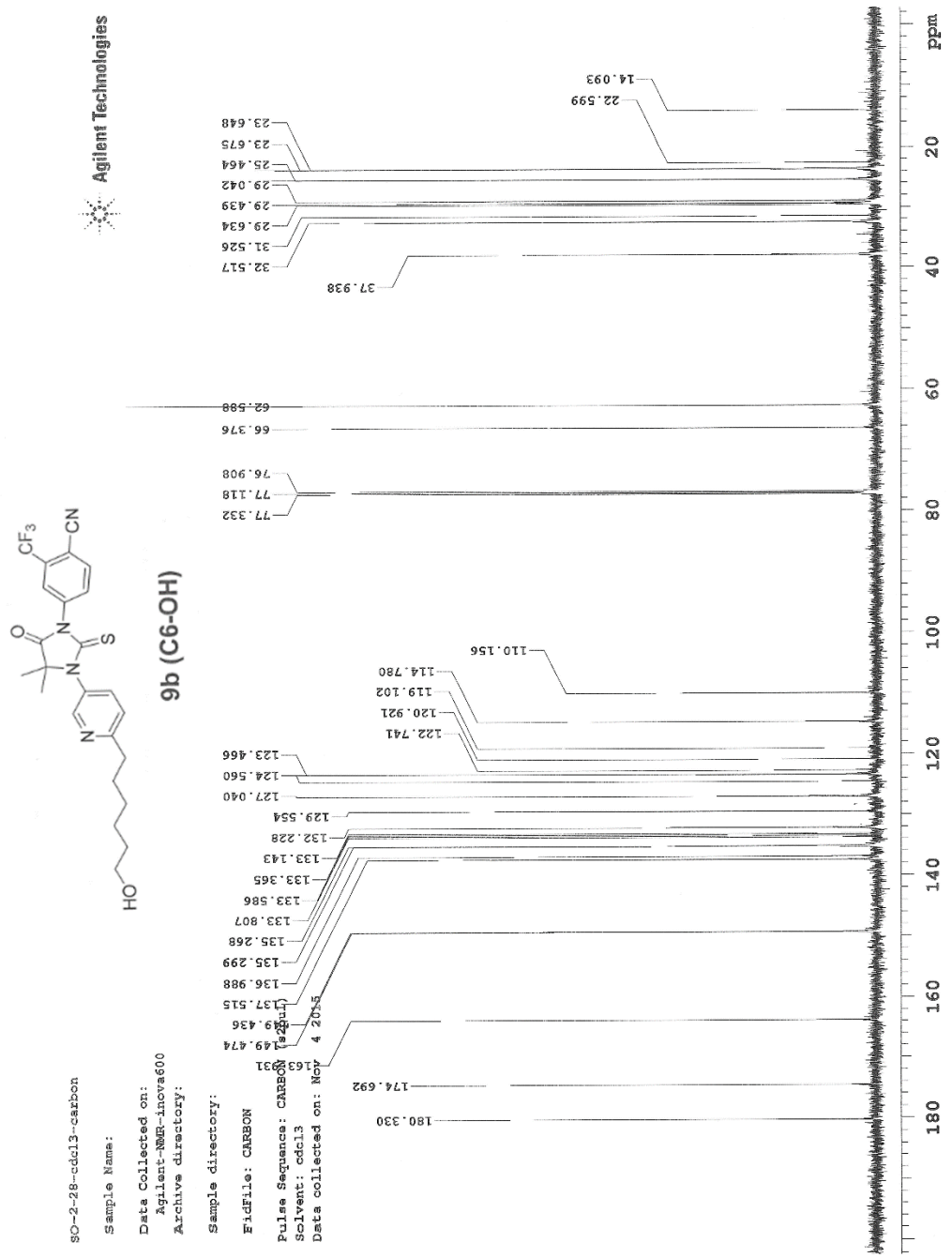
Agilent Technologies
SO-2-28-cdcl3-carbon
Sample Name:
Data Collected on:
Agilent-NMR-inova600
Archive directory:
Sample directory:
FidFile: CARBON
Pulse Sequence: CARBON
Solvent: cdcl3
Data collected on: Nov 4 2015
9b (C6-OH)
CF3
CN
O
N
S
HO
ppm
14.093
22.599
23.648
23.675
25.464
29.042
29.439
29.634
31.526
32.517
37.938
62.588
66.376
76.908
77.118
77.332
110.156
114.780
119.102
120.921
122.741
123.466
124.560
127.040
129.554
132.228
133.143
133.365
133.586
133.807
135.268
135.299
136.988
137.515
139.436
149.474
163.031
174.692
180.330

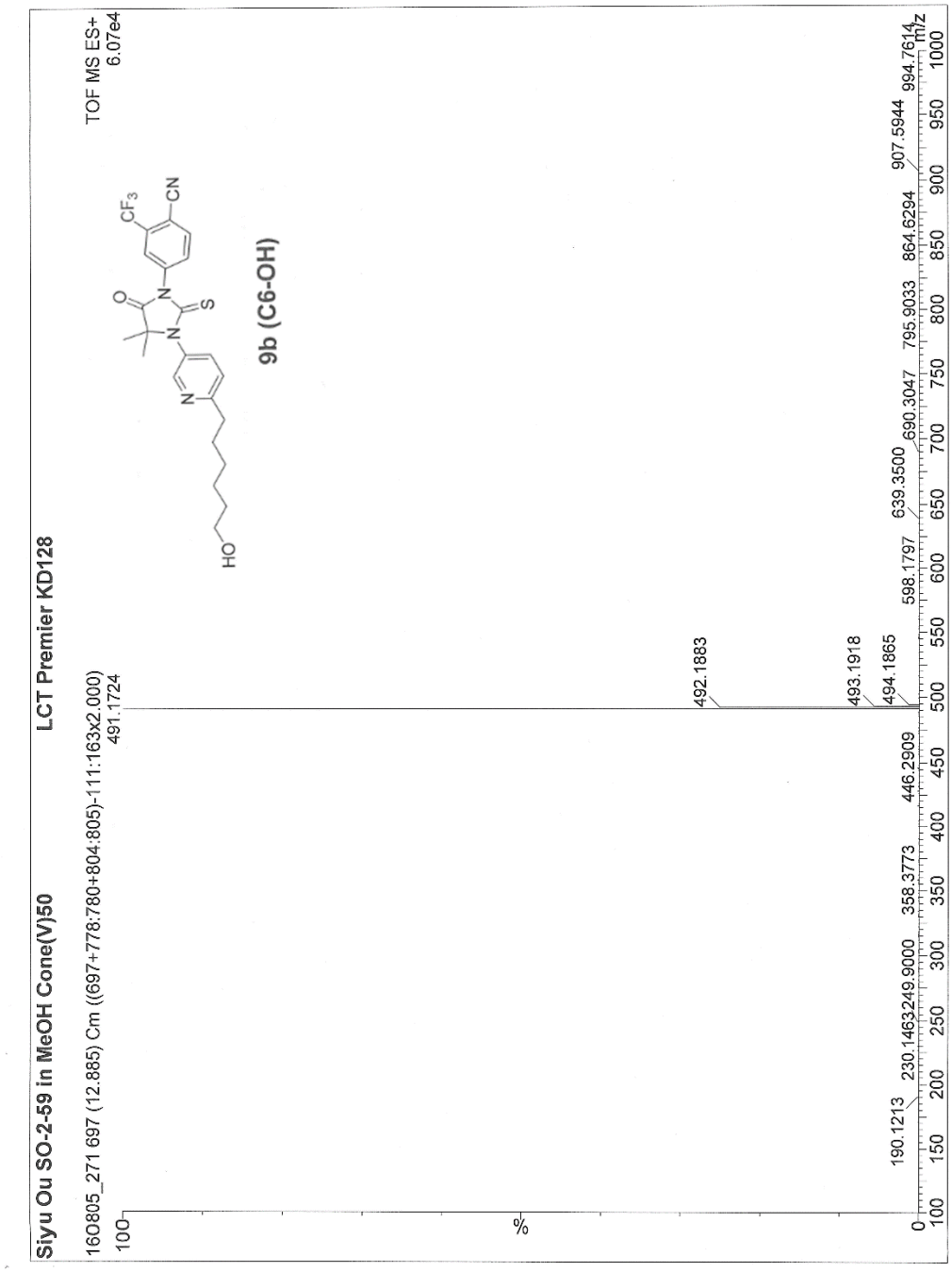
Siyu Ou SO-2-59 in MeOH Cone(V)50
LCT Premier KD128
160805_271 697 (12.885) Cm ((697+778:780+804:805)-111:163x2.000)
TOF MS ES+
6.07e4
100
%
0
9b (C6-OH)
CF3
CN
O
N
S
HO
190.1213
230.1463
249.9000
358.3773
446.2909
491.1724
492.1883
493.1918
494.1865
598.1797
639.3500
690.3047
795.9033
864.6294
907.5944
994.7614
100
150
200
250
300
350
400
450
500
550
600
650
700
750
800
850
900
950
1000
m/z

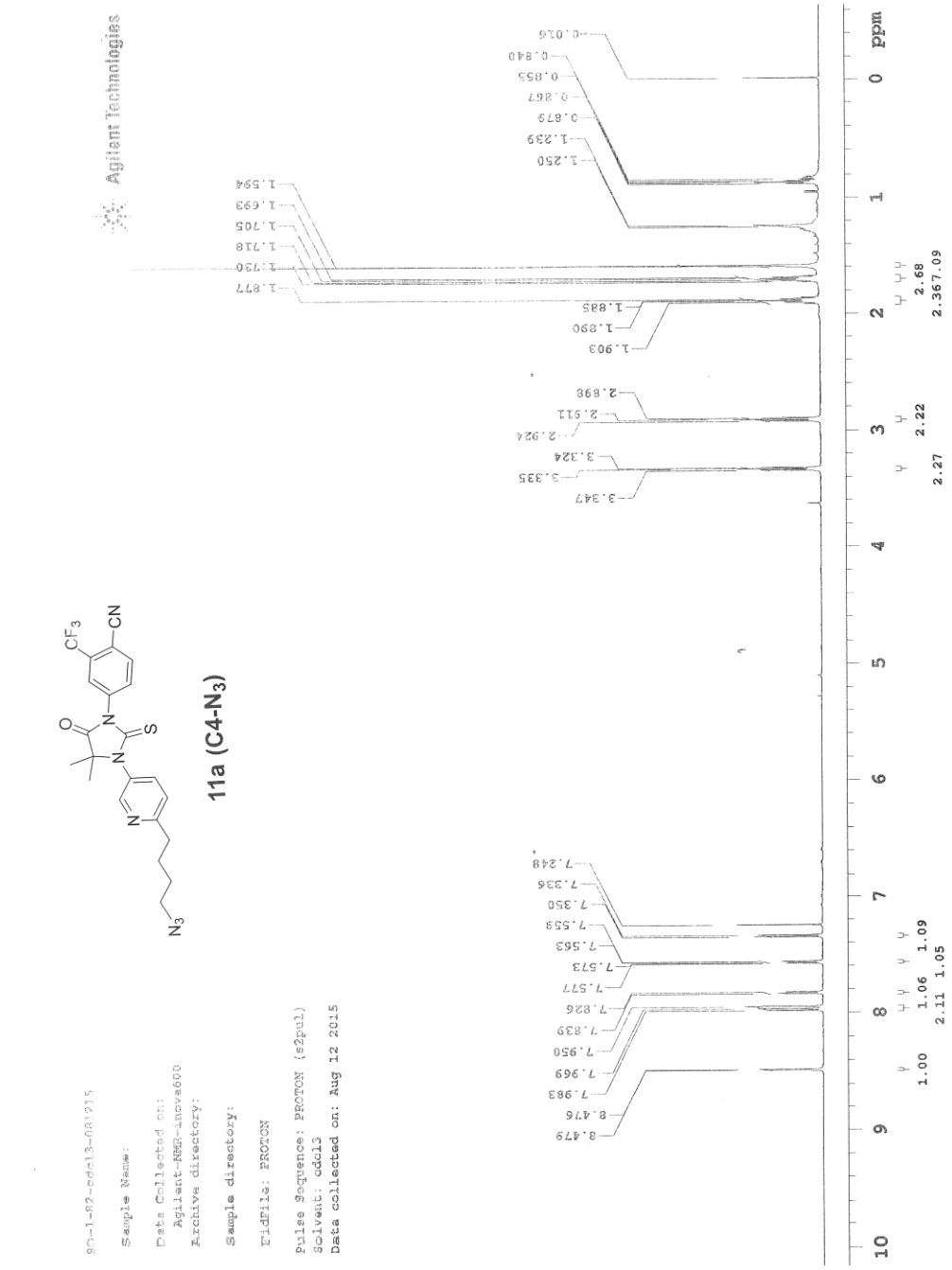
Agilent Technologies
11a (C4-N3)
8.479
8.476
7.983
7.969
7.950
7.839
7.826
7.577
7.573
7.563
7.559
7.350
7.336
7.248
3.347
3.335
3.324
2.924
2.911
2.898
1.903
1.890
1.885
1.877
1.730
1.718
1.705
1.693
1.594
1.250
1.239
0.879
0.867
0.855
0.840
0.016
ppm

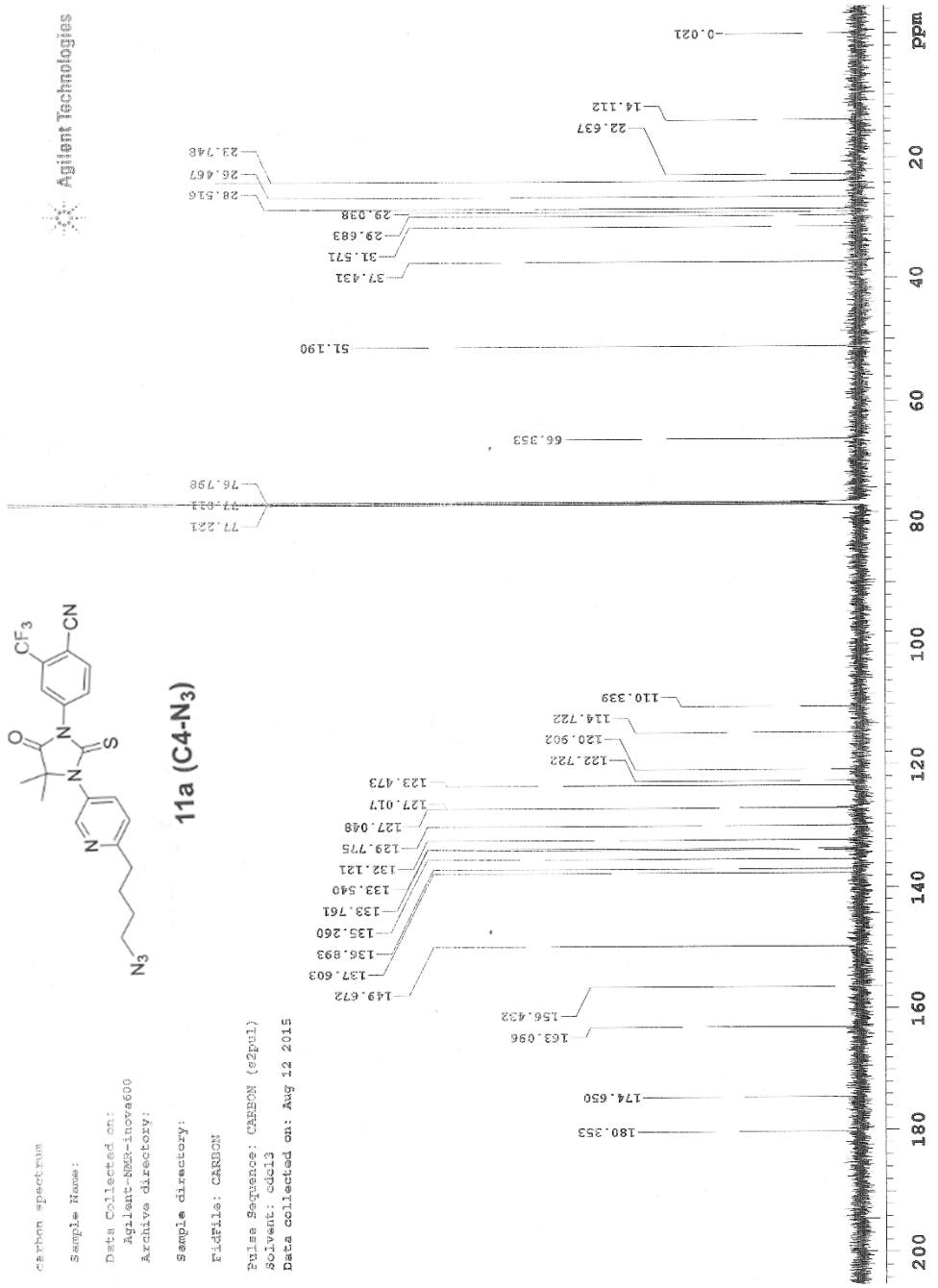
carbon spectrum
Sample Name:
Data Collected on:
Agilent-NMR-inova600
Archive directory:
Sample directory:
FidFile: CARBON
Pulse Sequence: CARBON (s2pul)
Solvent: cdcl3
Data collected on: Aug 12 2015
11a (C4-N3)
Agilent Technologies
ppm

SO-2-11-cdcl3

Sample Name:

Data Collected on:
Agilent-NMR-inova600
Archive directory:

Sample directory:

FidFile: PROTON

Pulse Sequence: PROTON (s2pul)
Solvent: cdcl3
Data collected on: Sep 26 2015

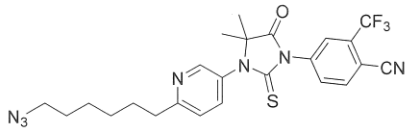

11b (C6-N_3)

Agilent Technologies

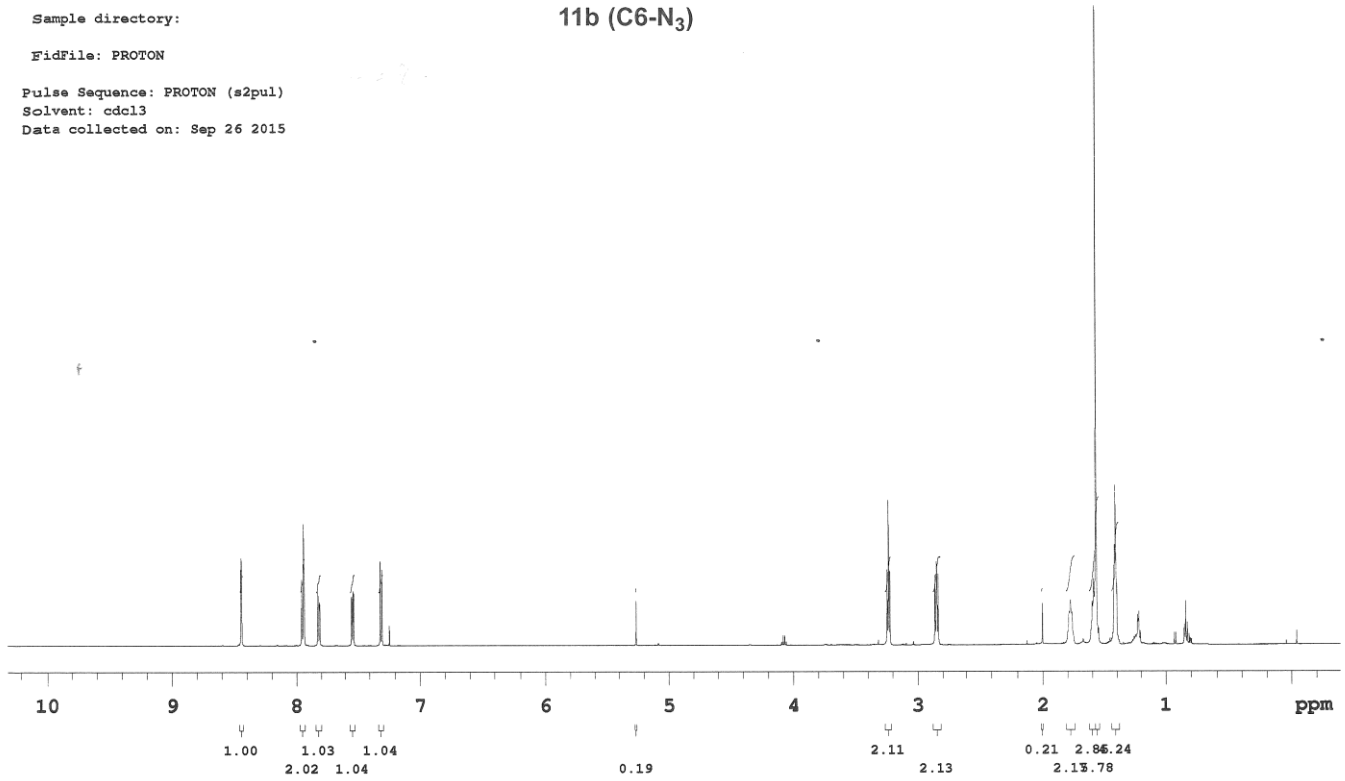

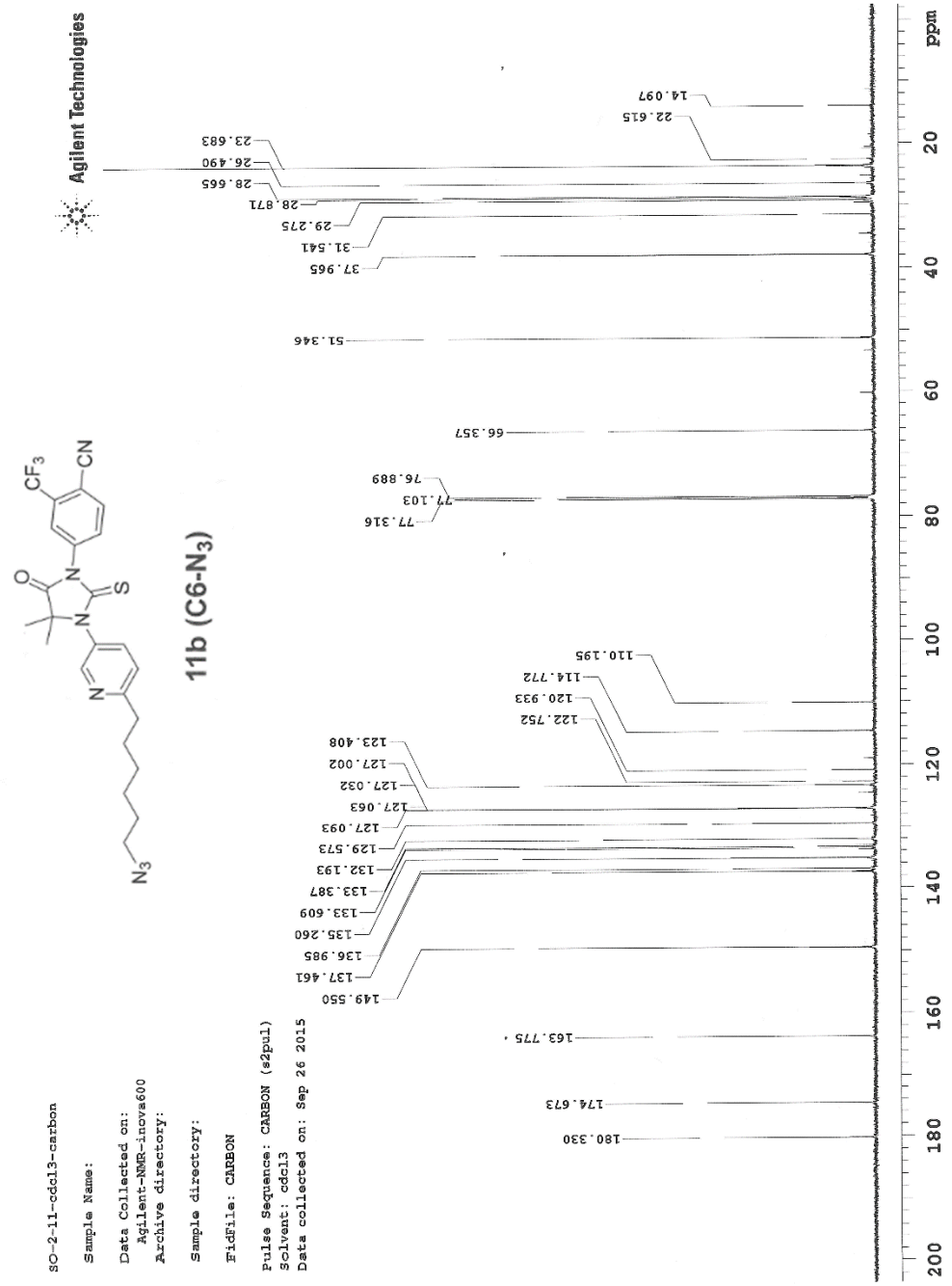
Agilent Technologies
SO-2-11-cdcl3-carbon
Sample Name:
Data Collected on:
Agilent-NMR-inova600
Archive directory:
Sample directory:
FidFile: CARBON
Pulse Sequence: CARBON (s2pul)
Solvent: cdcl3
Data collected on: Sep 26 2015
11b (C6-N3)
CF3
CN
O
S
N
N3
14.097
22.615
23.683
26.490
28.665
28.871
29.275
31.541
37.965
51.346
66.357
76.889
77.103
77.316
110.195
114.772
120.933
122.752
123.408
127.002
127.032
127.063
127.093
129.573
132.193
133.387
133.609
135.260
136.985
137.461
149.550
163.775
174.673
180.330
ppm
200
180
160
140
120
100
80
60
40
20

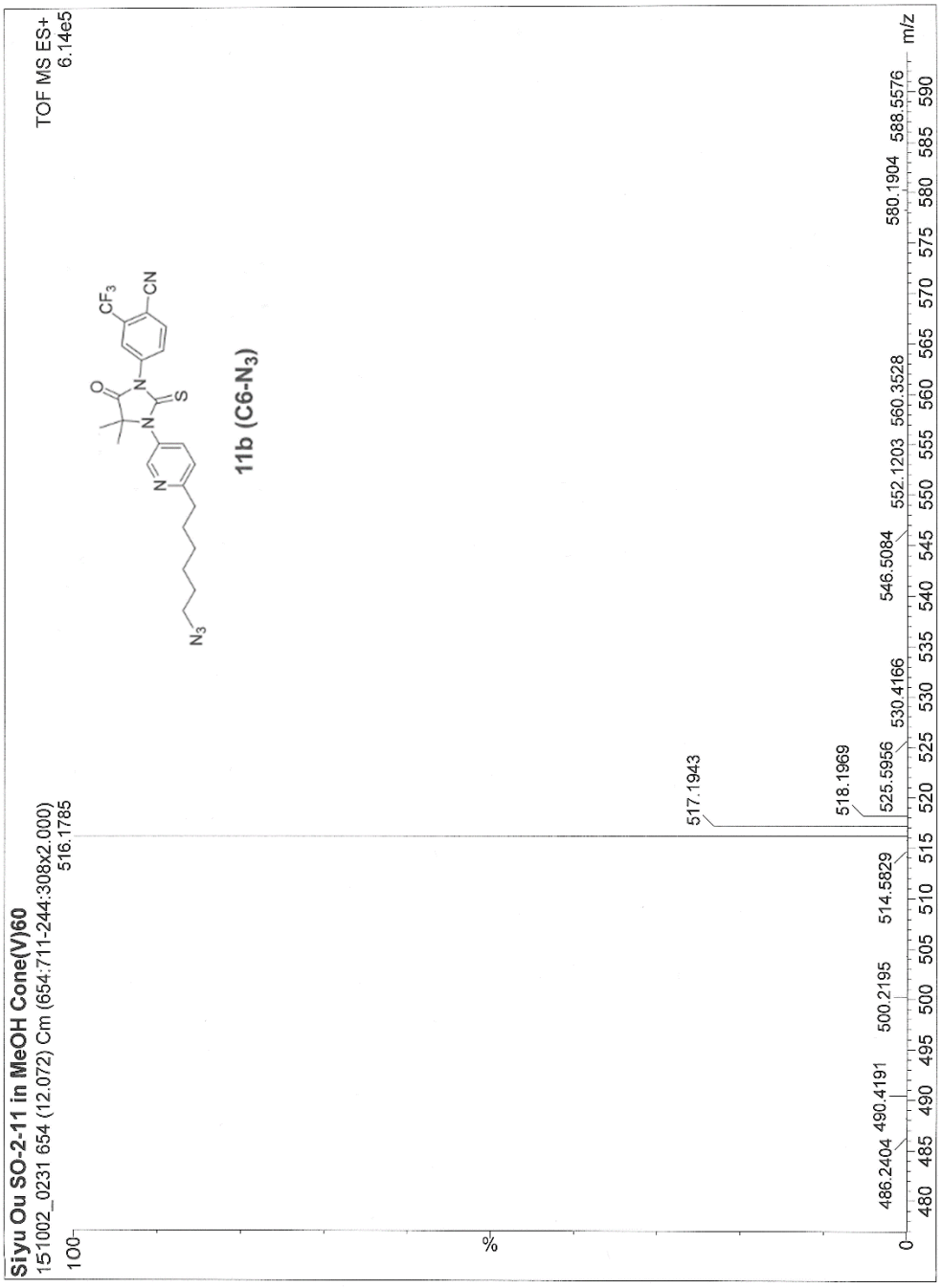
Siyu Ou SO-2-11 in MeOH Cone(V)60
151002_0231 654 (12.072) Cm (654:711-244:308x2.000)
TOF MS ES+
6.14e5
516.1785
100
%
0
11b (C6-N3)
CF3
CN
O
S
N
N3
517.1943
518.1969
525.5956
530.4166
546.5084
552.1203
560.3528
580.1904
588.5576
486.2404
490.4191
500.2195
514.5829
480 485 490 495 500 505 510 515 520 525 530 535 540 545 550 555 560 565 570 575 580 585 590
m/z

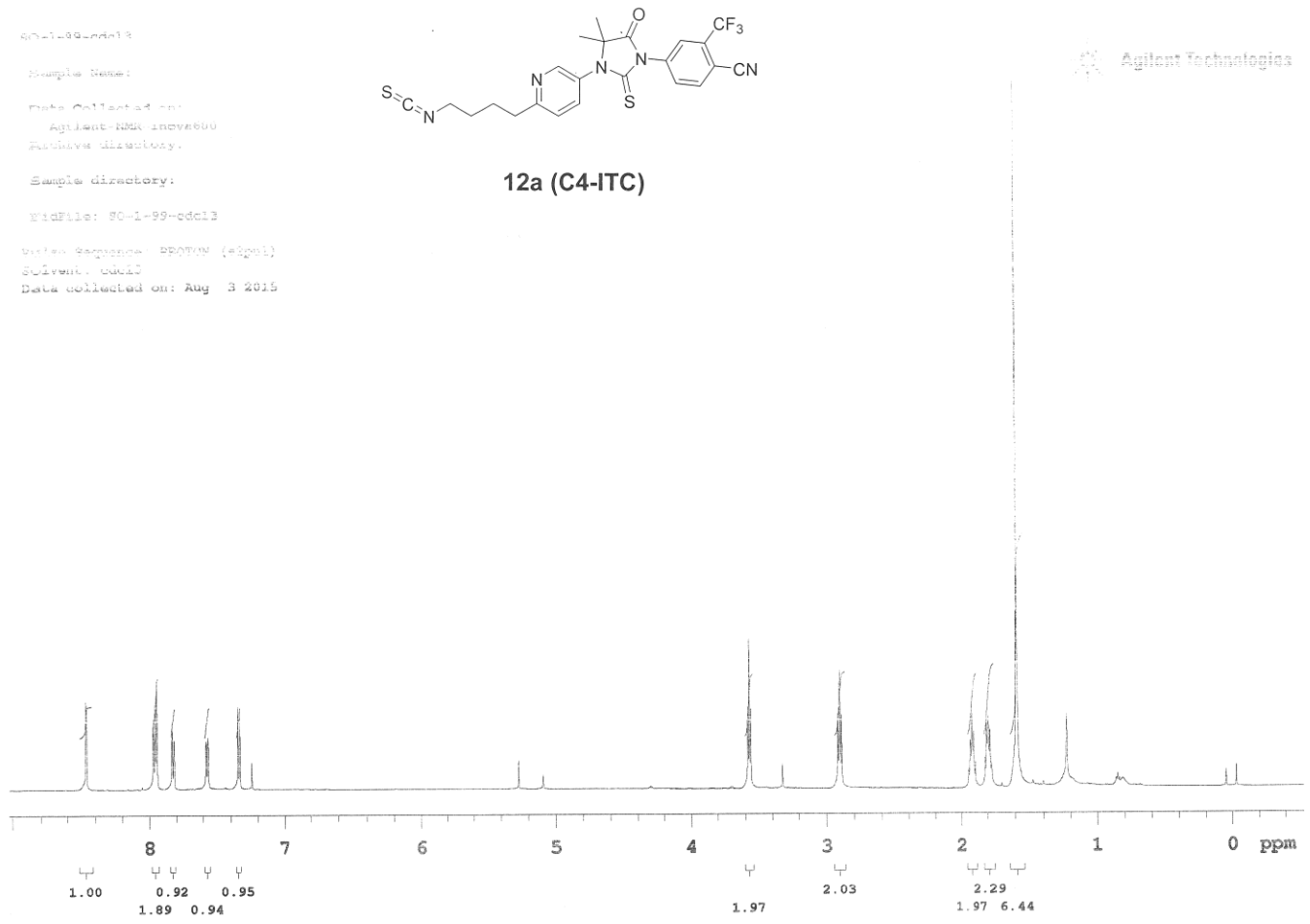
Sample Name:
Sample directory:
Solvent: cdcl3
Data collected on: Aug 3 2015
12a (C4-ITC)
8
7
6
5
4
3
2
1
0 ppm
1.00
0.92
0.95
1.89
0.94
1.97
2.03
2.29
1.97
6.44

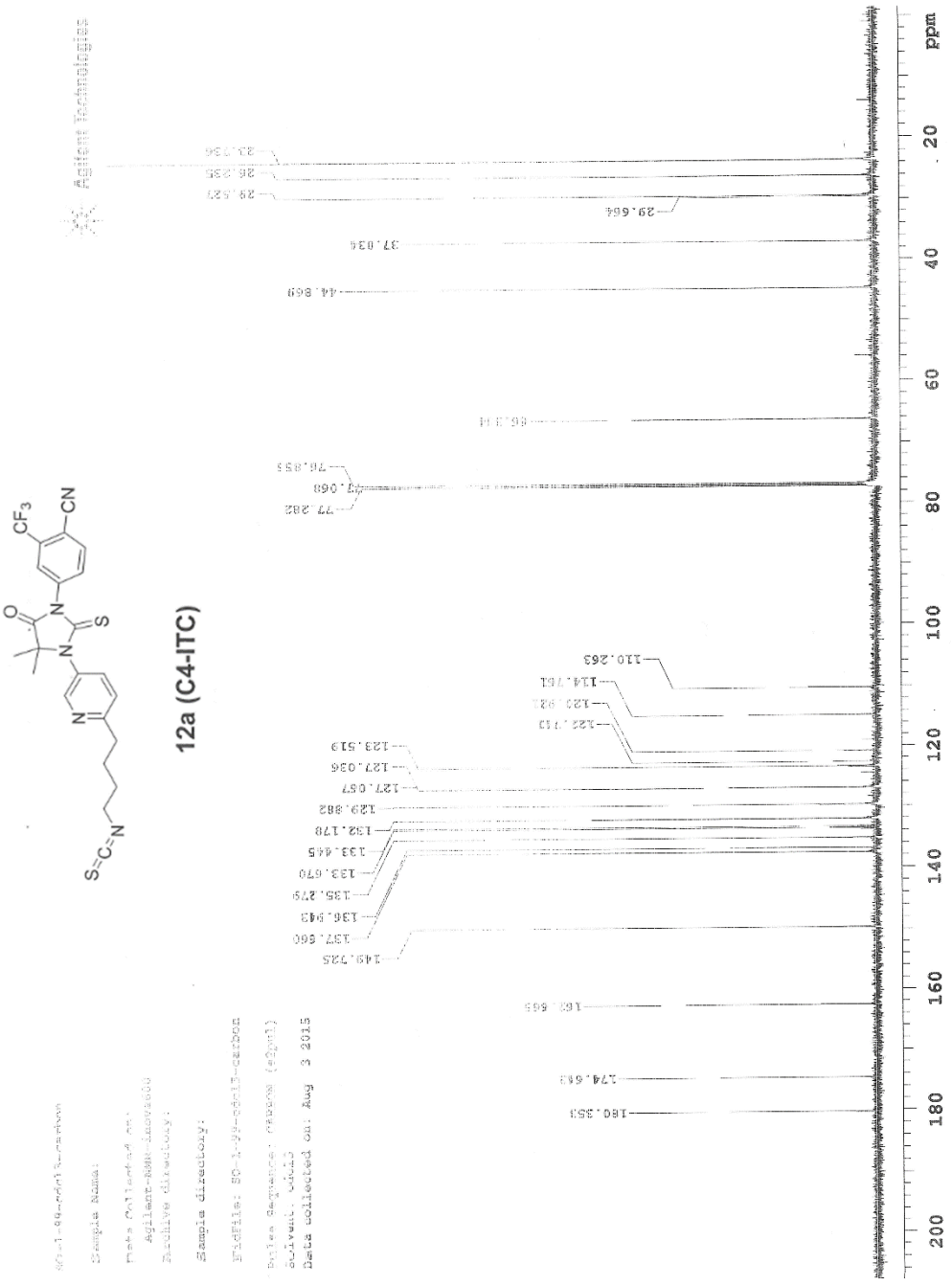
12a (C4-ITC)
CF3
CN
O
N
S
S=C=N
ppm
20
40
60
80
100
120
140
160
180
200
29.621
29.664
37.034
44.869
70.855
77.282
123.519
127.036
127.057
129.882
132.178
133.445
133.670
135.279
136.943
137.660
149.735
160.665
174.613
180.353

SO-2-13-cdcl3

Sample Name:

Data Collected on:
Agilent-NMR-inova600
Archive directory:

Sample directory:

FidFile: PROTON

Pulse Sequence: PROTON (s2pul)
Solvent: cdcl3
Data collected on: Sep 29 2015

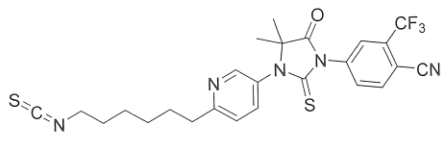

12b (C6-ITC)

Agilent Technologies

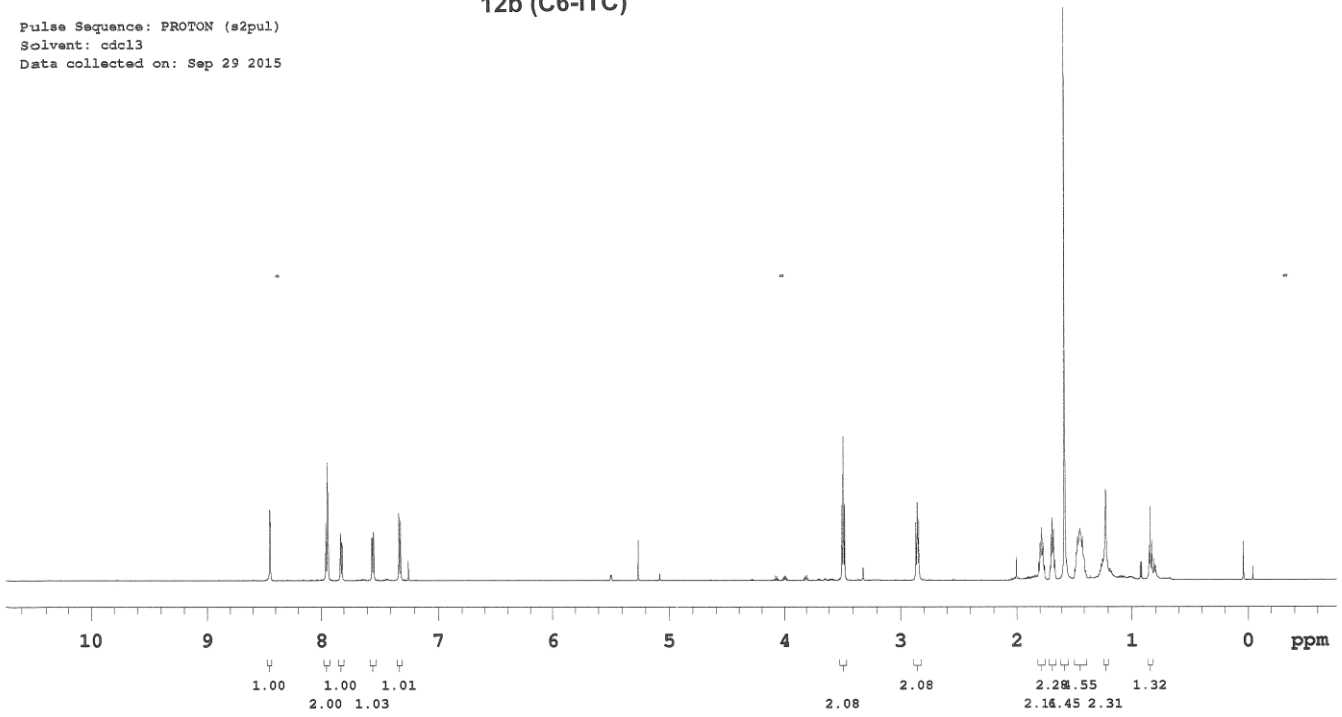

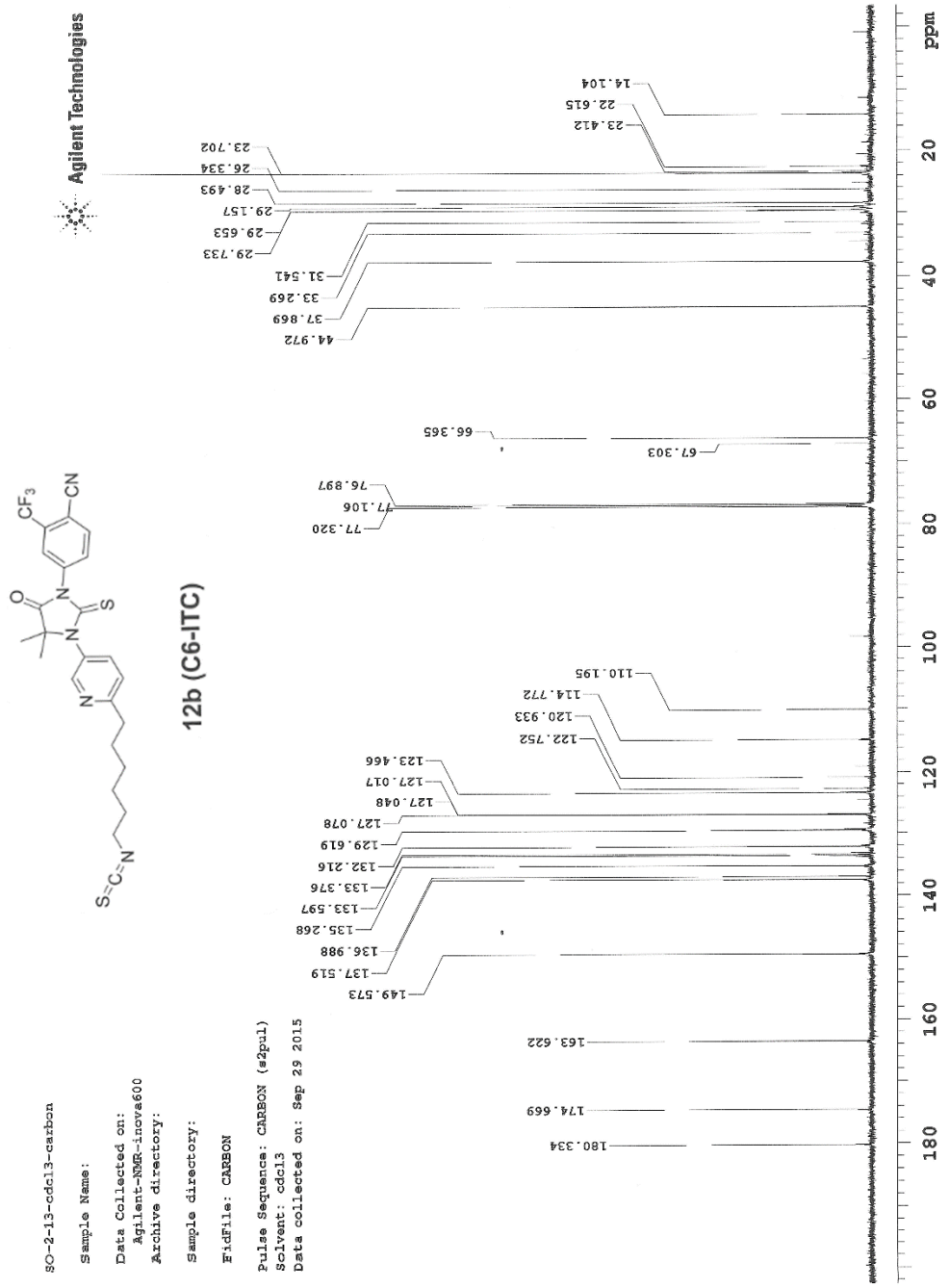
SO-2-13-cdcl3-carbon
Sample Name:
Data Collected on:
Agilent-NMR-inova600
Archive directory:
Sample directory:
FidFile: CARBON
Pulse Sequence: CARBON (s2pul)
Solvent: cdcl3
Data collected on: Sep 29 2015
Agilent Technologies
12b (C6-ITC)
CF3
CN
O
N
S
N
N
S=C=N
ppm
14.104
22.615
23.412
23.702
26.334
28.493
29.157
29.653
29.733
31.541
33.269
37.869
44.972
66.365
67.303
76.897
77.106
77.320
110.195
114.772
120.933
122.752
123.466
127.017
127.048
127.078
129.619
132.216
133.376
133.597
135.268
136.988
137.519
149.573
163.622
174.669
180.334

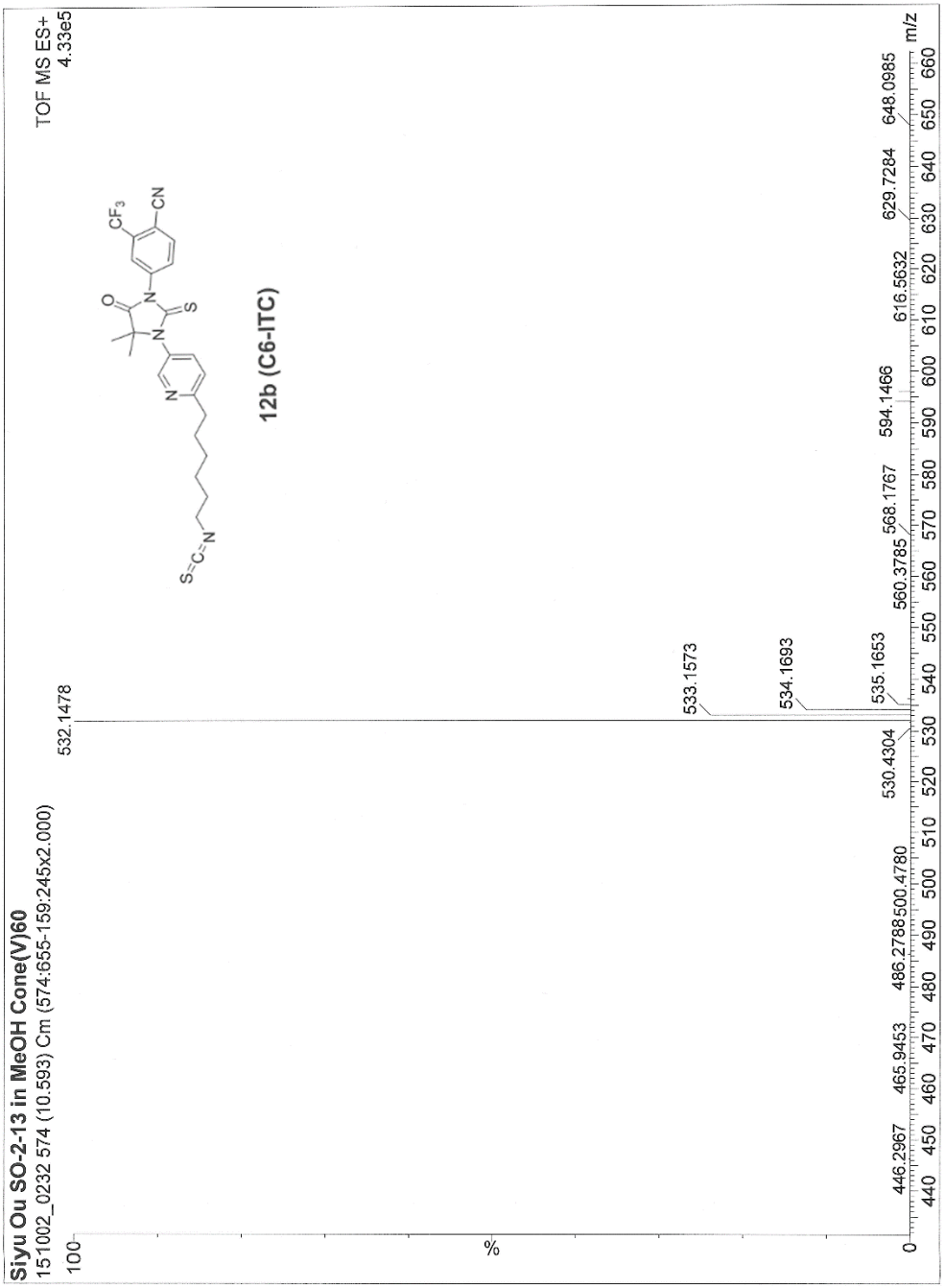
Siyu Ou SO-2-13 in MeOH Cone(V)60
151002_0232 574 (10.593) Cm (574:655-159:245x2.000)
TOF MS ES+
4.33e5
100
%
0
12b (C6-ITC)
532.1478
533.1573
534.1693
535.1653
530.4304
560.3785
568.1767
594.1466
616.5632
629.7284
648.0985
446.2967
465.9453
486.2788
500.4780
m/z

SO-2-63-1-cdcl3

Sample Name:

Data Collected on:
Agilent-NMR-inova600
Archive directory:

Sample directory:

FidFile: PROTON

Pulse Sequence: PROTON (s2pul)
Solvent: cdcl3
Data collected on: Mar 23 2016

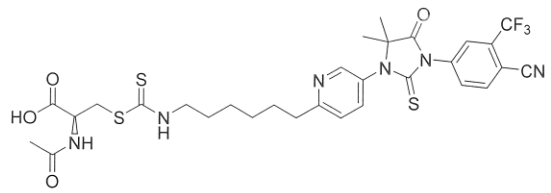

13 (C6-NAC)

Agilent Technologies

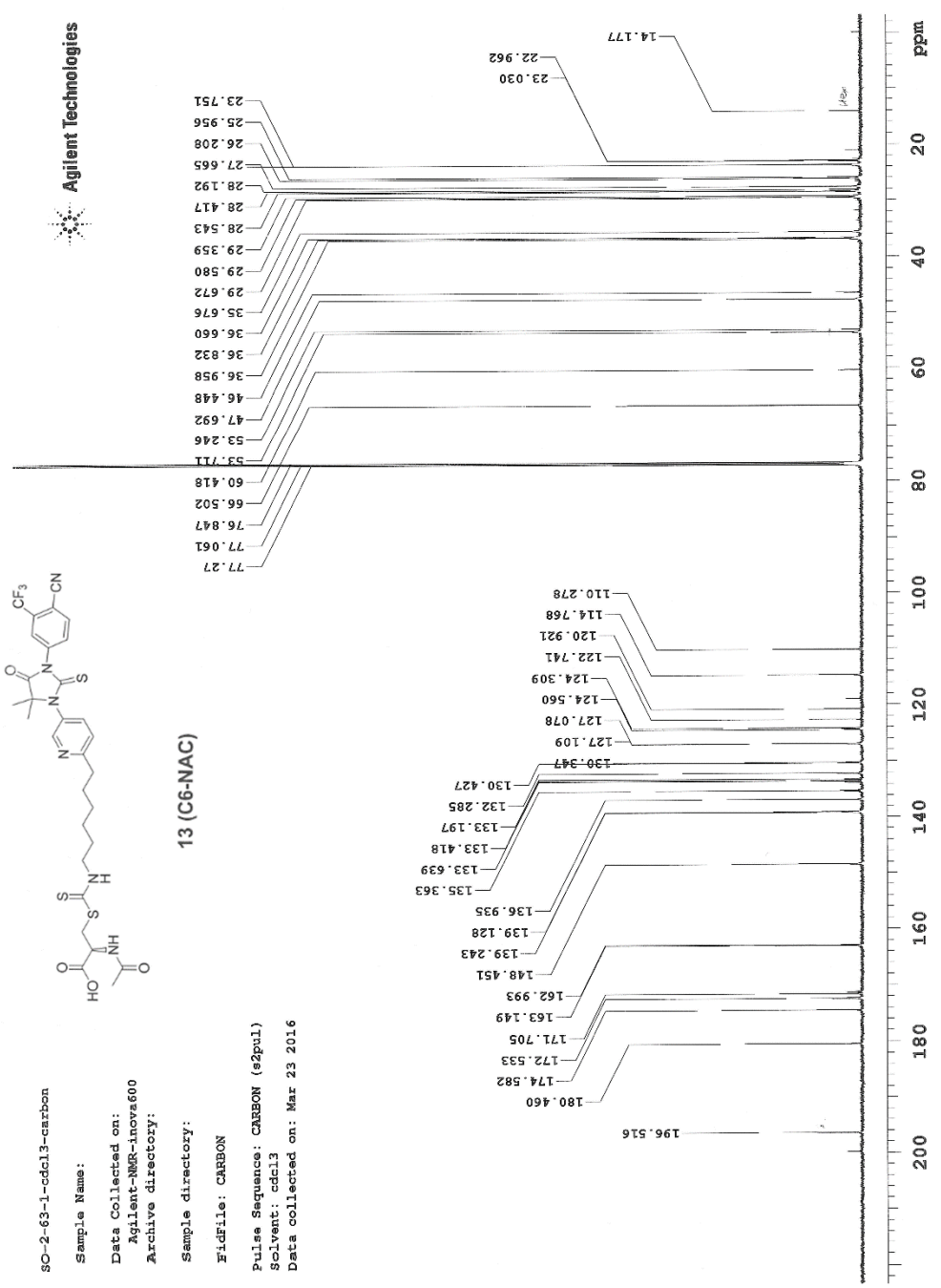
Agilent Technologies
SO-2-63-1-cdcl3-carbon
Sample Name:
Data Collected on:
Agilent-NMR-inova600
Archive directory:
Sample directory:
FidFile: CARBON
Pulse Sequence: CARBON (s2pul)
Solvent: cdcl3
Data collected on: Mar 23 2016
13 (C6-NAC)
ppm

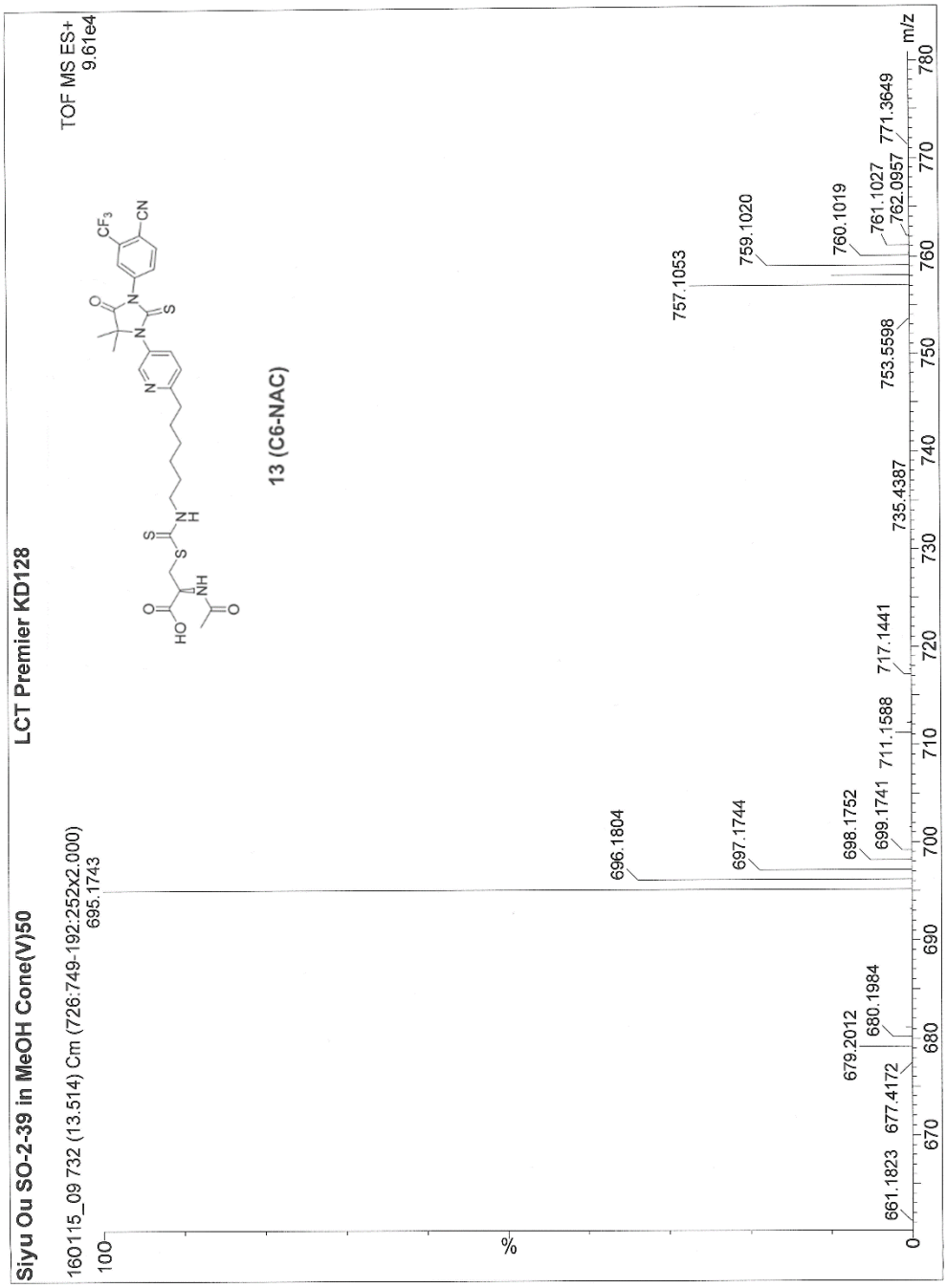
Siyu Ou SO-2-39 in MeOH Cone(V)50
LCT Premier KD128
160115_09 732 (13.514) Cm (726:749-192:252x2.000)
TOF MS ES+
9.61e4
100
%
0
13 (C6-NAC)
661.1823
677.4172
679.2012
680.1984
695.1743
696.1804
697.1744
698.1752
699.1741
711.1588
717.1441
735.4387
753.5598
757.1053
759.1020
760.1019
761.1027
762.0957
771.3649
670
680
690
700
710
720
730
740
750
760
770
780
m/z

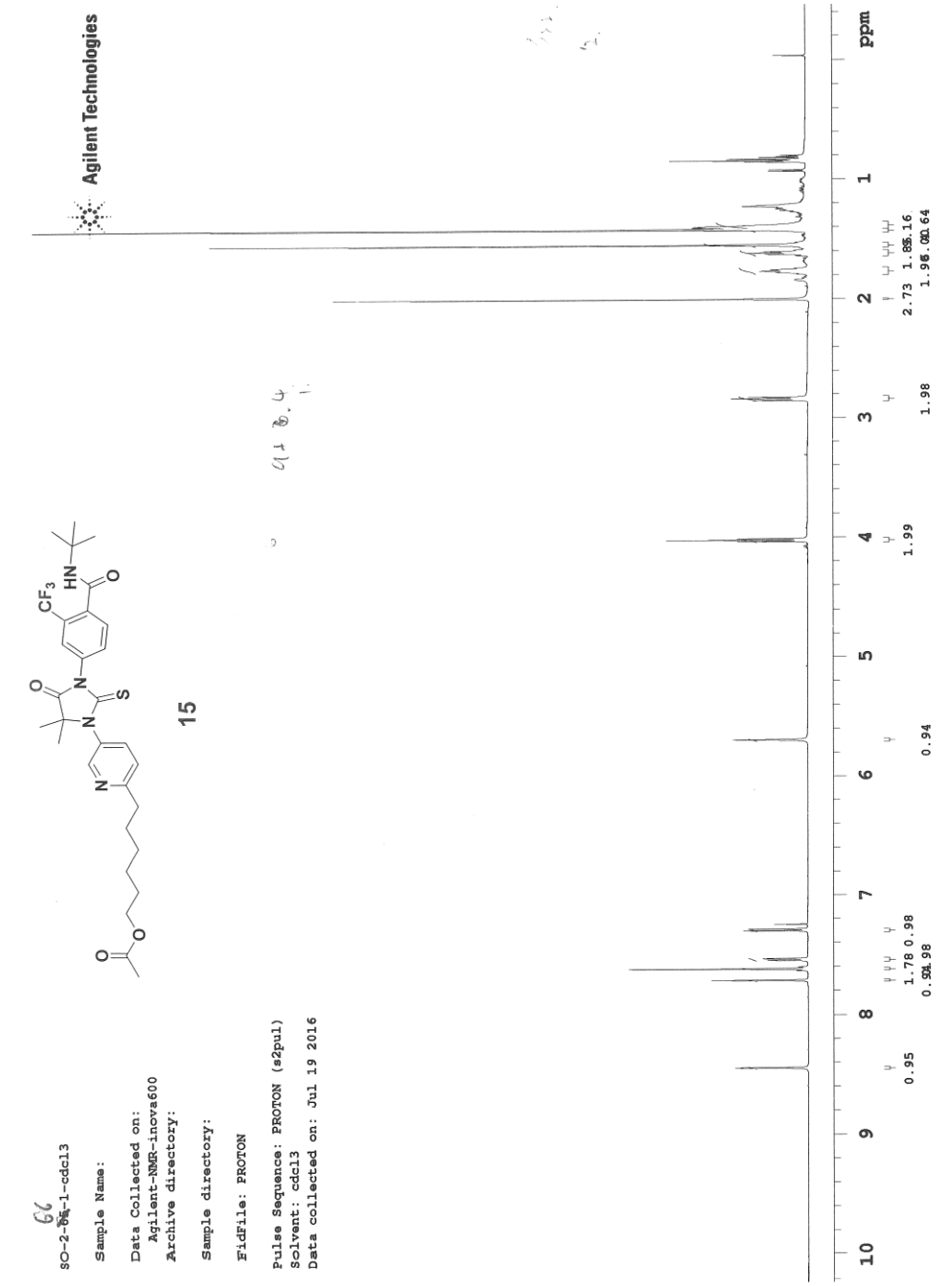
SO-2-66-1-cdcl3
Sample Name:
Data Collected on:
Agilent-NMR-inova600
Archive directory:
Sample directory:
FidFile: PROTON
Pulse Sequence: PROTON (s2pul)
Solvent: cdcl3
Data collected on: Jul 19 2016
15
Agilent Technologies
ppm

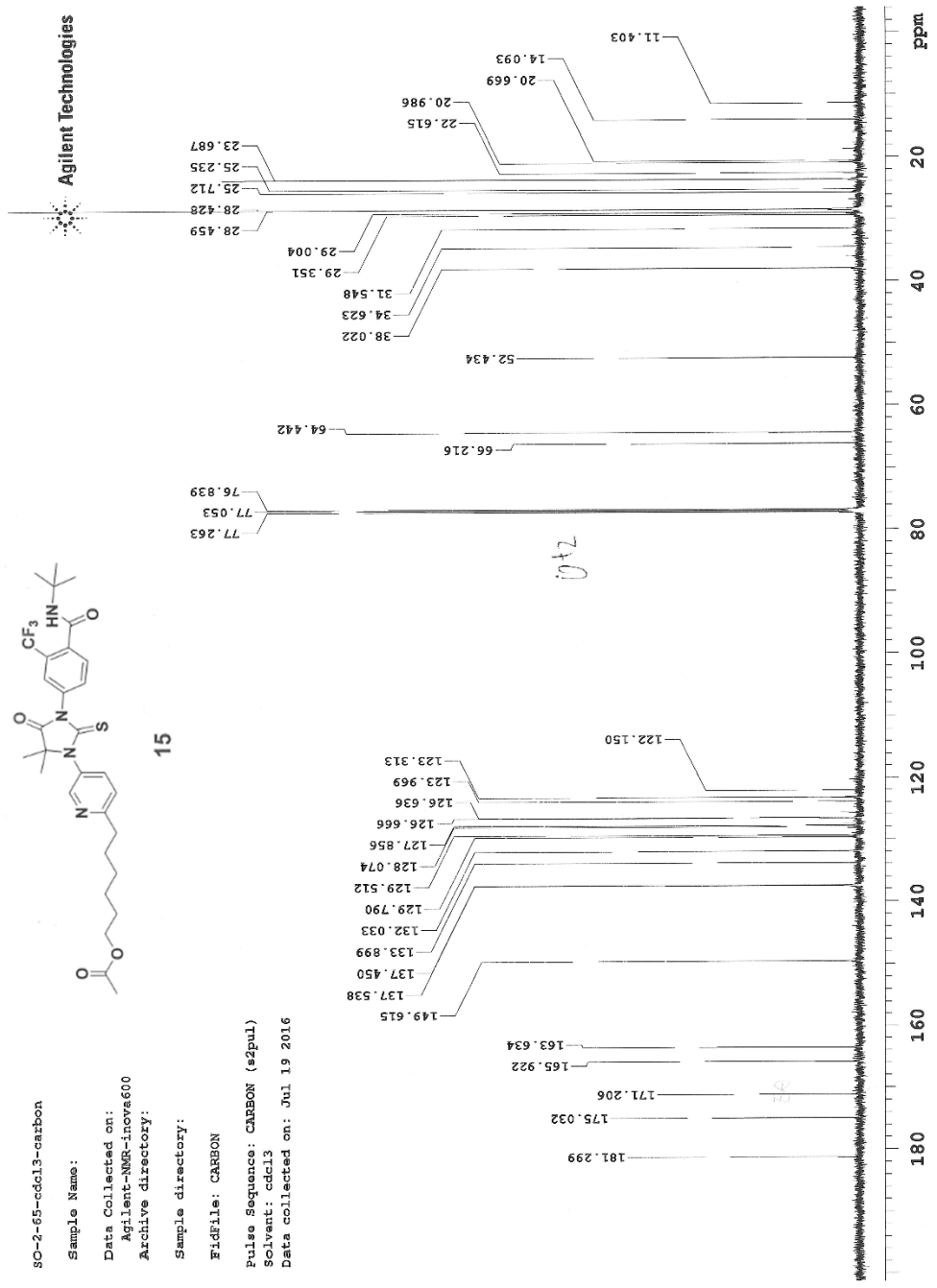
SO-2-65-cdcl3-carbon
Sample Name:
Data Collected on:
Agilent-NMR-inova600
Archive directory:
Sample directory:
FidFile: CARBON
Pulse Sequence: CARBON (s2pul)
Solvent: cdcl3
Data collected on: Jul 19 2016
15
Agilent Technologies
ppm
11.403
14.093
20.669
20.986
22.615
23.687
25.235
25.712
28.428
28.459
29.004
29.351
31.548
34.623
38.022
52.434
64.442
66.216
76.839
77.053
77.263
122.150
123.313
123.969
126.636
126.666
127.856
128.074
129.512
129.790
132.033
133.899
137.450
137.538
149.615
163.634
165.922
171.206
175.032
181.299

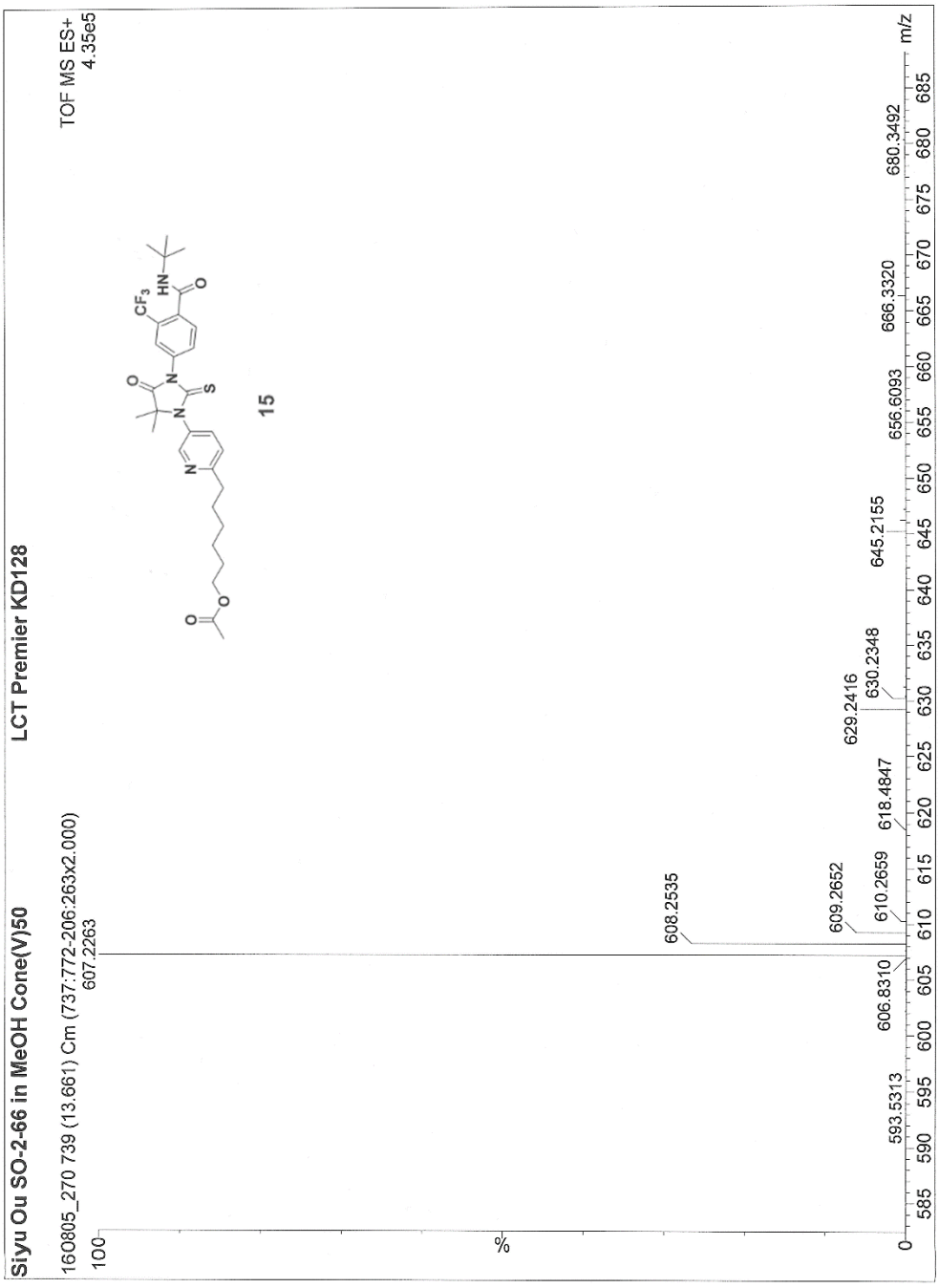
Siyu Ou SO-2-66 in MeOH Cone(V)50
LCT Premier KD128
160805_270 739 (13.661) Cm (737:772-206:263x2.000)
TOF MS ES+
4.35e5
100
%
0
15
607.2263
608.2535
609.2652
610.2659
606.8310
593.5313
618.4847
629.2416
630.2348
645.2155
656.6093
666.3320
680.3492
585 590 595 600 605 610 615 620 625 630 635 640 645 650 655 660 665 670 675 680 685
m/z

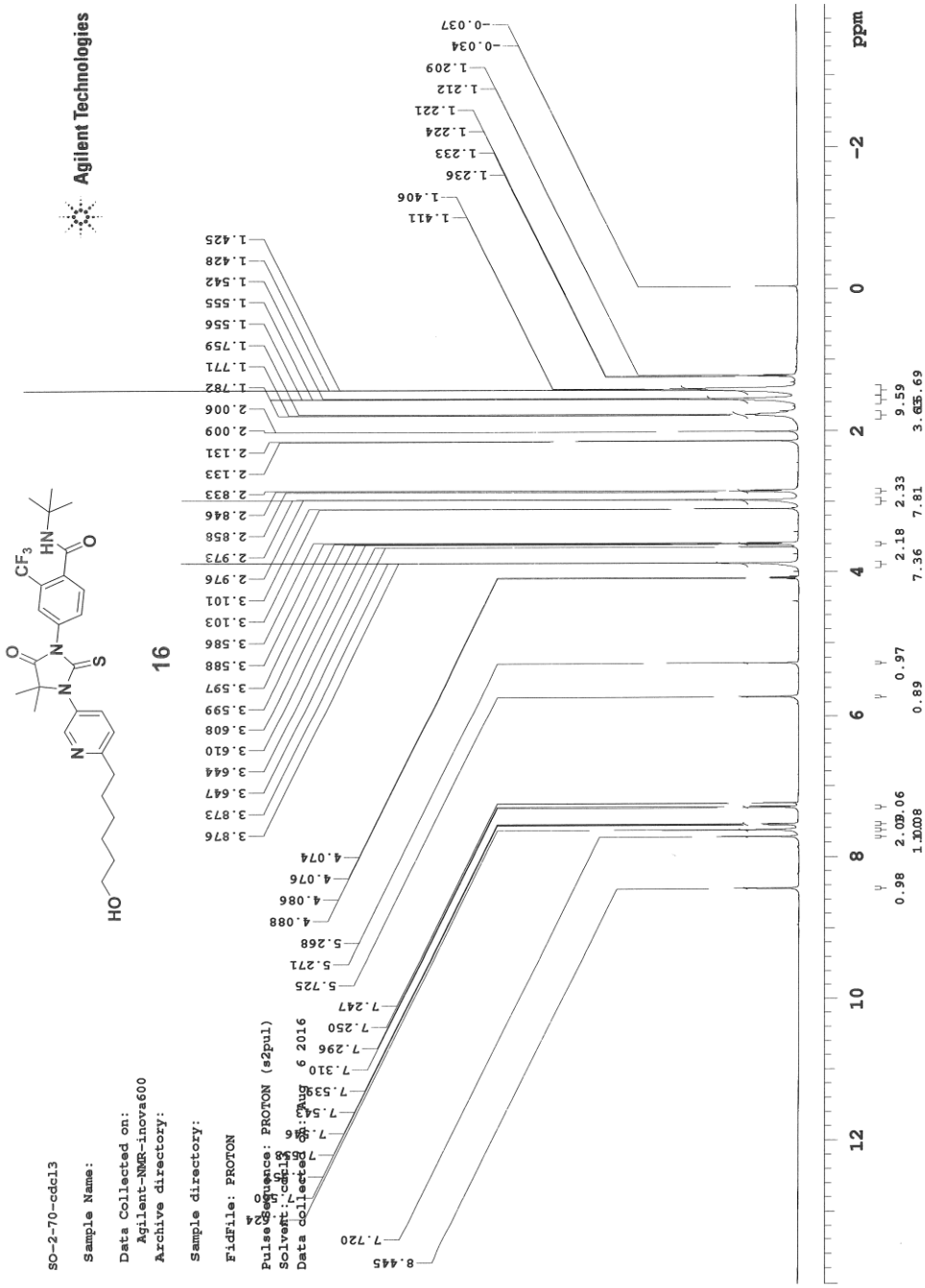
Agilent Technologies
SO-2-70-cdcl3
Sample Name:
Data Collected on:
Agilent-NMR-inova600
Archive directory:
Sample directory:
FidFile: PROTON
Pulse Sequence: PROTON (s2pul)
Solvent: cdcl3
Data collected: Aug 6 2016
16
CF3
HN
O
N
S
HO
ppm

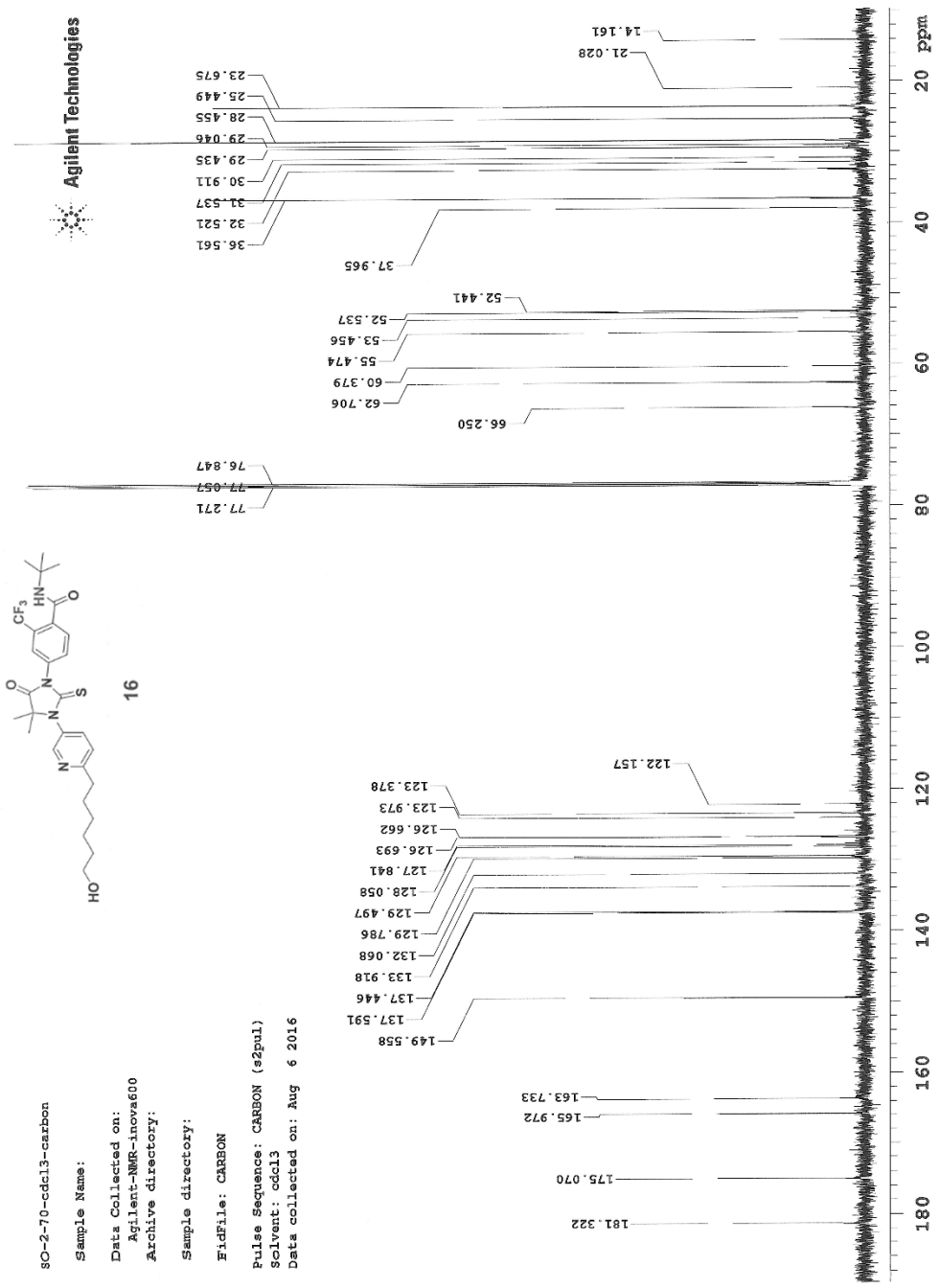
Agilent Technologies
14.161
21.028
23.675
25.449
28.455
29.046
29.435
30.911
31.537
32.521
36.561
37.965
52.441
52.537
53.456
55.474
60.379
62.706
66.250
76.847
77.057
77.271
122.157
123.378
123.973
126.662
126.693
127.841
128.058
129.497
129.786
132.068
133.918
137.446
137.591
149.558
163.733
165.972
175.070
181.322
ppm
20
40
60
80
100
120
140
160
180
16
HO
CF3
HN
O
N
S
sO-2-70-cdcl3-carbon
Sample Name:
Data Collected on:
Agilent-NMR-inova600
Archive directory:
Sample directory:
FidFile: CARBON
Pulse Sequence: CARBON (s2pul)
Solvent: cdcl3
Data collected on: Aug 6 2016

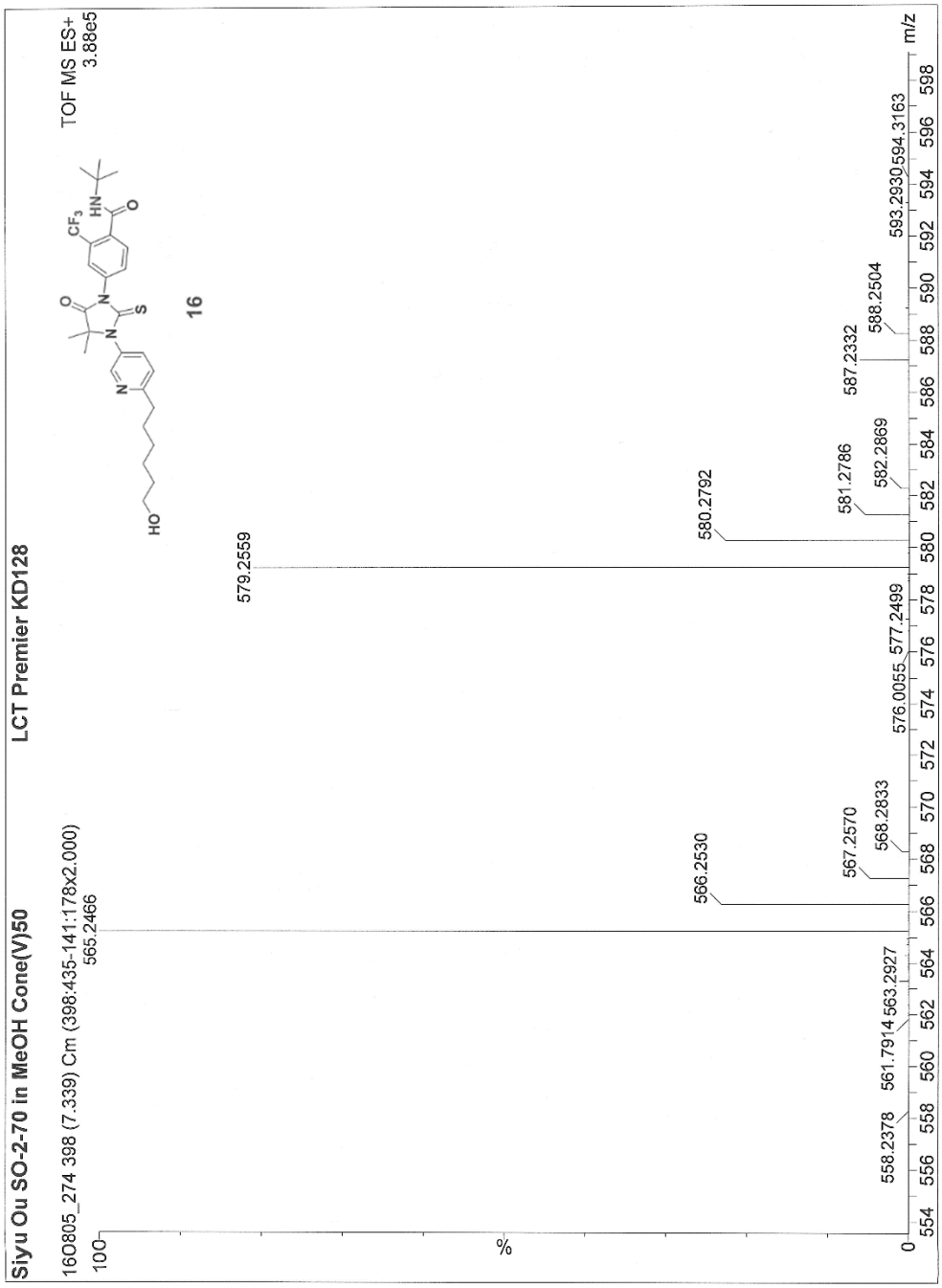
Siyu Ou SO-2-70 in MeOH Cone(V)50
LCT Premier KD128
160805_274 398 (7.339) Cm (398:435-141:178x2.000)
TOF MS ES+
3.88e5
100
%
0
16
565.2466
579.2559
580.2792
566.2530
567.2570
568.2833
576.0055
577.2499
581.2786
582.2869
587.2332
588.2504
593.2930
594.3163
558.2378
561.7914
563.2927
m/z

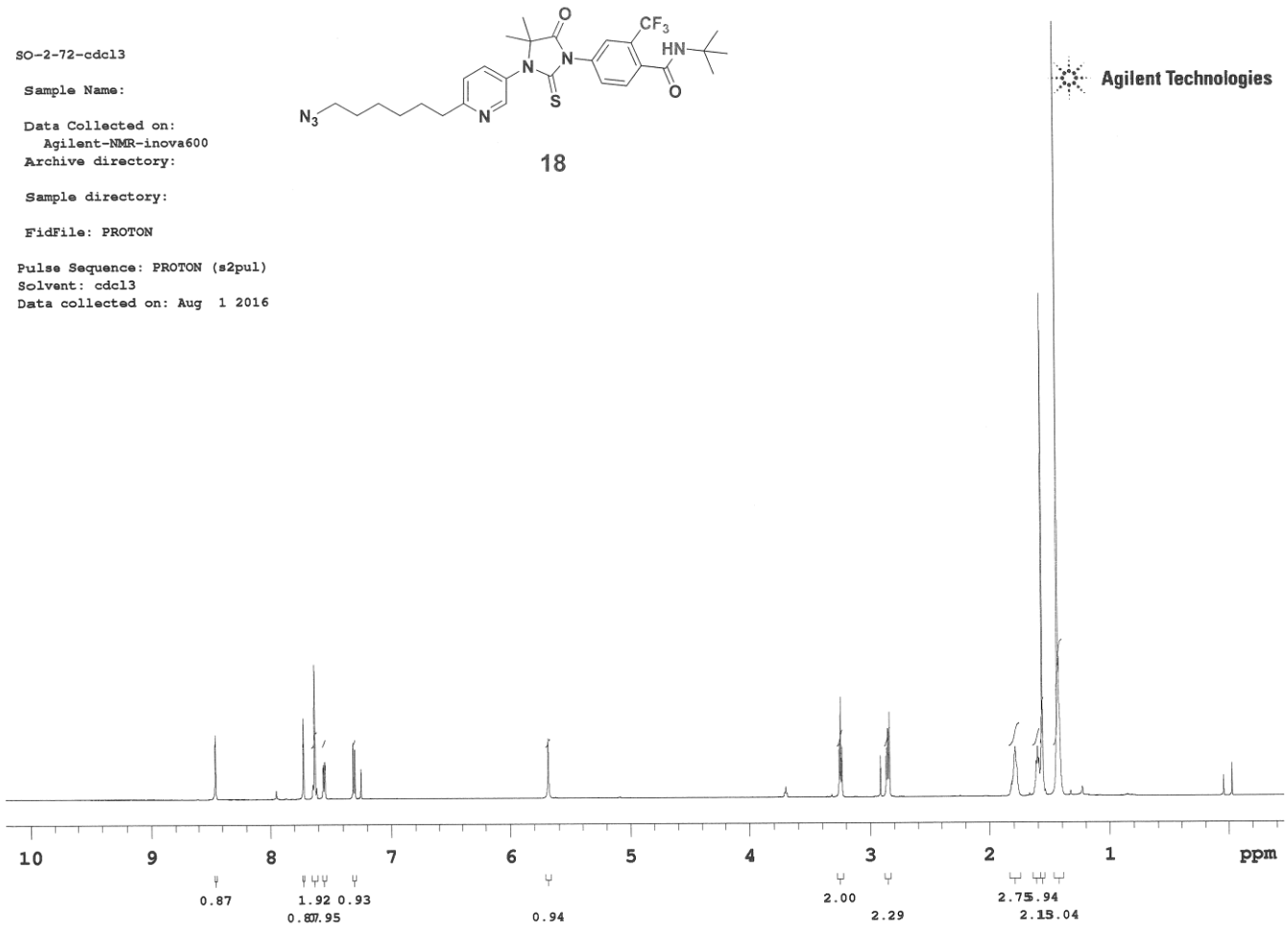
SO-2-72-cdcl3
Sample Name:
Data Collected on:
Agilent-NMR-inova600
Archive directory:
Sample directory:
FidFile: PROTON
Pulse Sequence: PROTON (s2pul)
Solvent: cdcl3
Data collected on: Aug 1 2016
18
Agilent Technologies
10
9
8
7
6
5
4
3
2
1
ppm
0.87
1.92
0.93
0.94
2.00
2.29
2.75
5.94
2.15
5.04

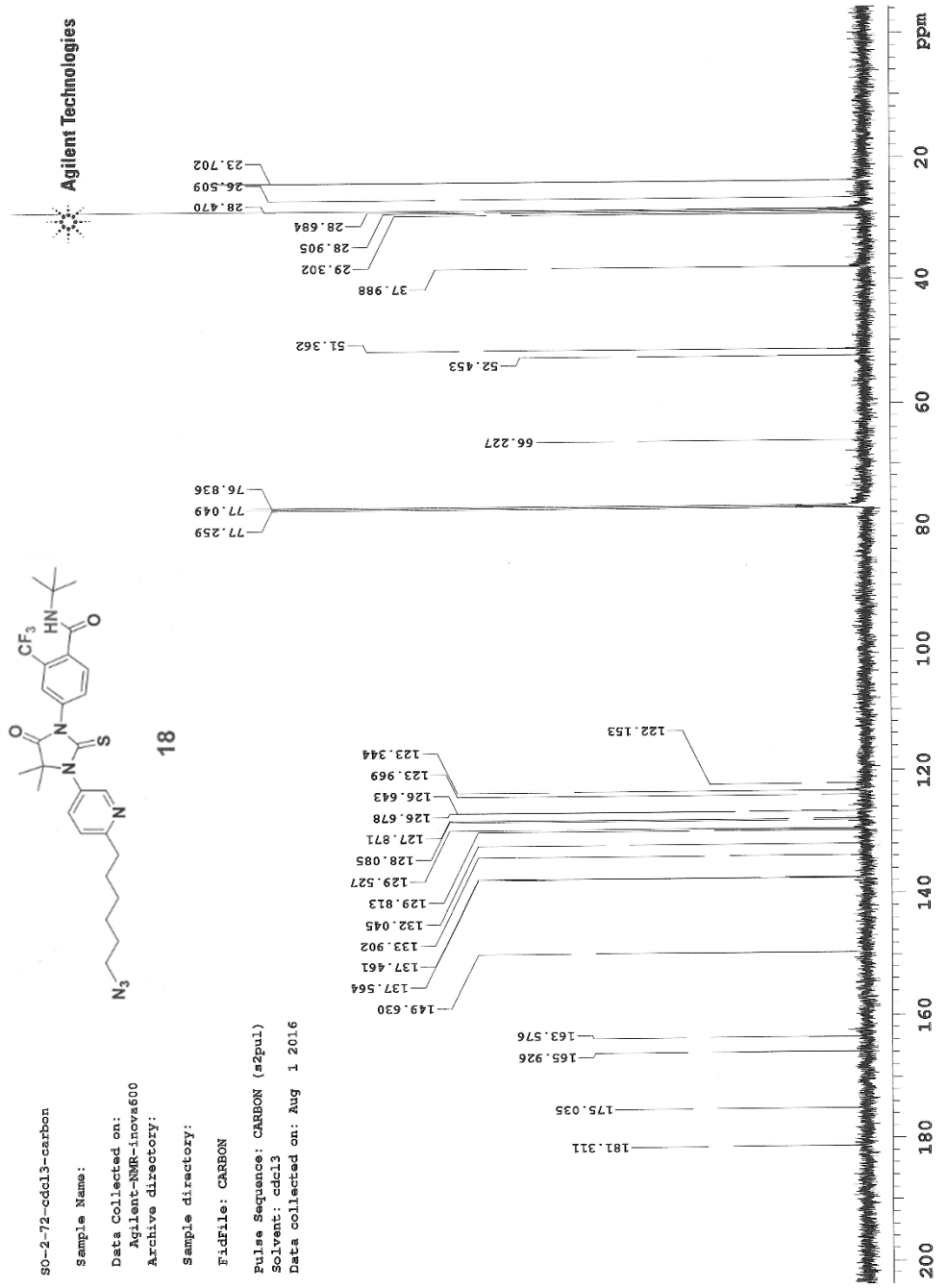
Agilent Technologies
SO-2-72-cdcl3-carbon
Sample Name:
Data Collected on:
Agilent-NMR-inova600
Archive directory:
Sample directory:
FidFile: CARBON
Pulse Sequence: CARBON (s2pul)
Solvent: cdcl3
Data collected on: Aug 1 2016
18
ppm

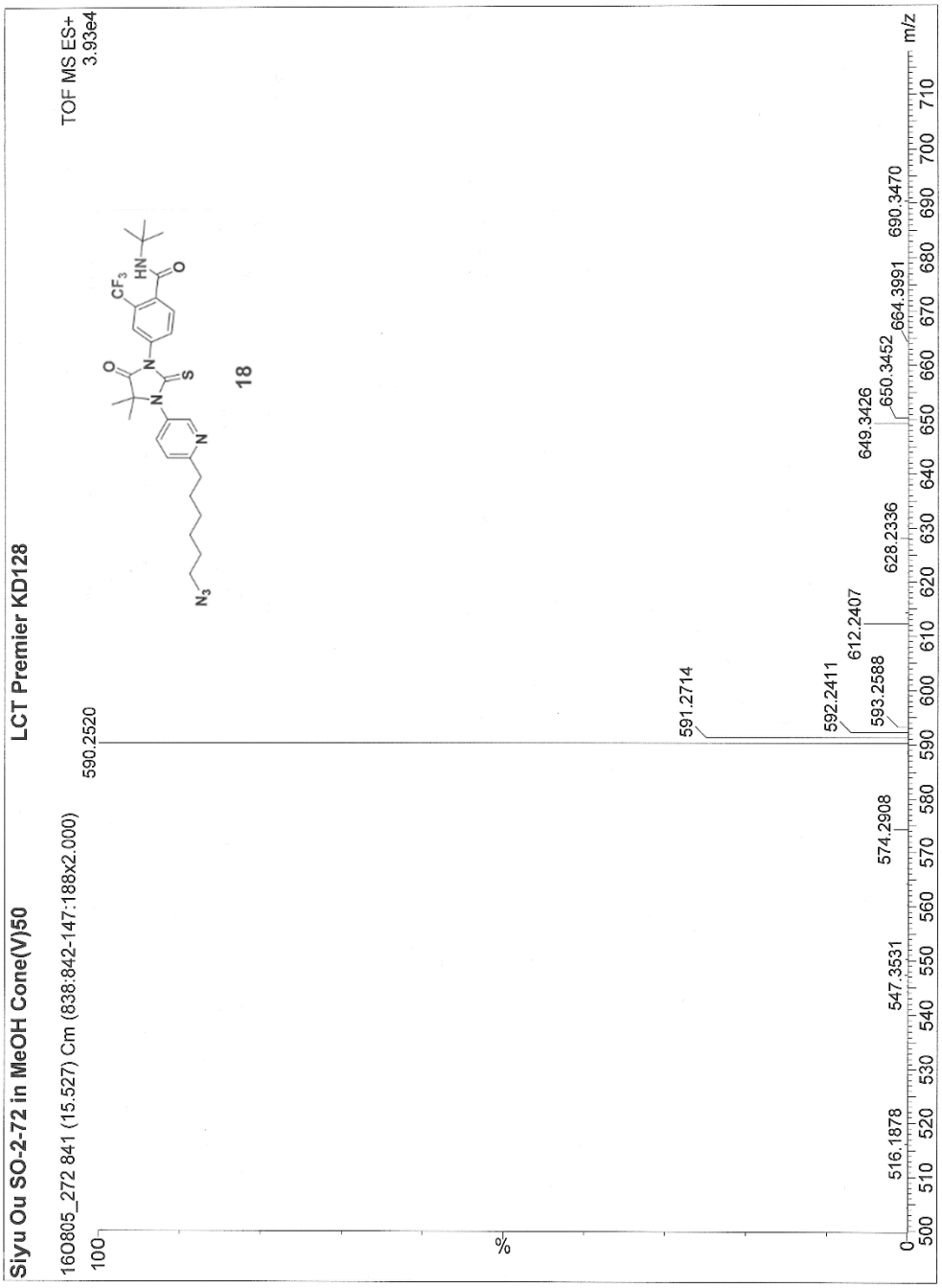
Siyu Ou SO-2-72 in MeOH Cone(V)50
LCT Premier KD128
160805_272 841 (15.527) Cm (838:842-147:188x2.000)
TOF MS ES+
3.93e4
100
%
0
m/z
18
590.2520
591.2714
592.2411
612.2407
593.2588
628.2336
649.3426
650.3452
664.3991
690.3470
574.2908
547.3531
516.1878

SO-2-73-cdcl3

Sample Name:

Data Collected on:
Agilent-NMR-inova600
Archive directory:

Sample directory:

FidFile: PROTON

Pulse Sequence: PROTON (s2pul)
Solvent: cdcl3
Data collected on: Jul 22 2016

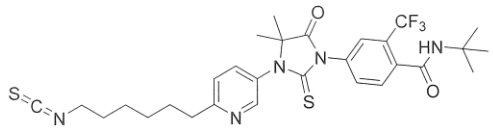

19 (C6-amide-ITC)

Agilent Technologies

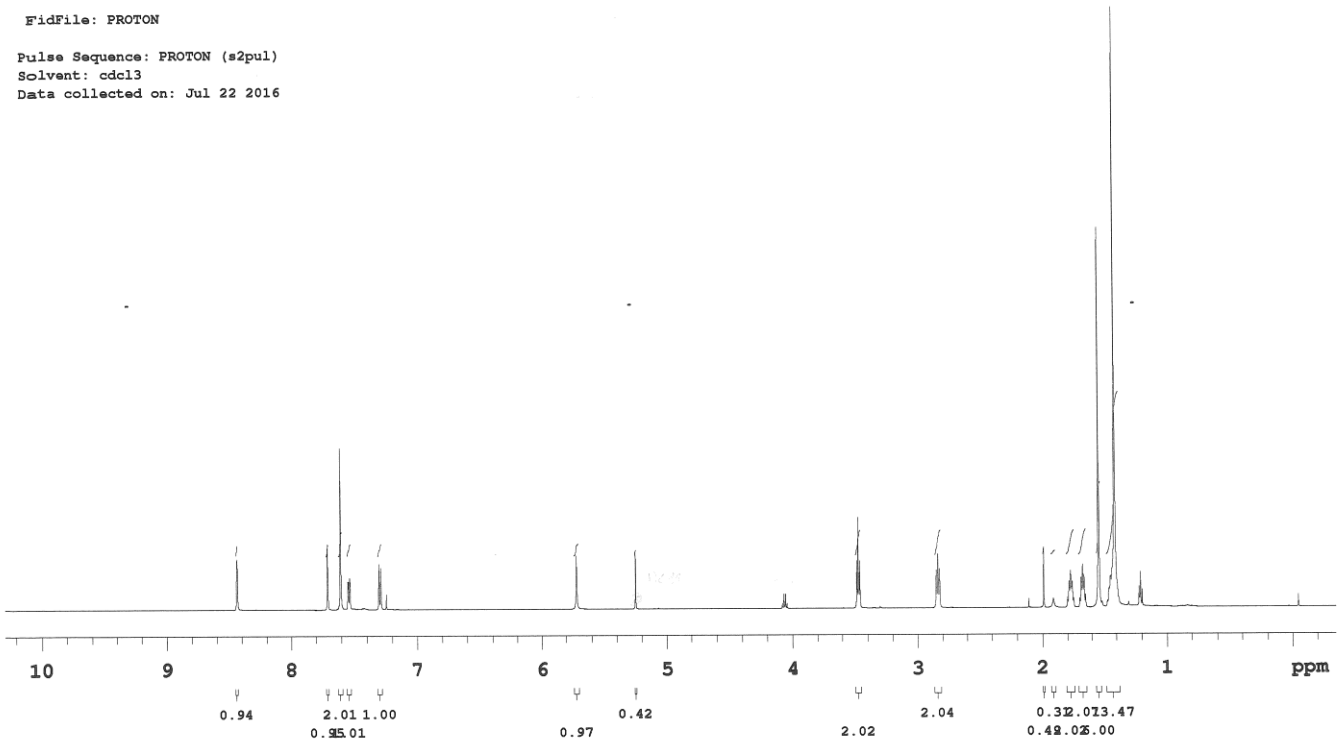

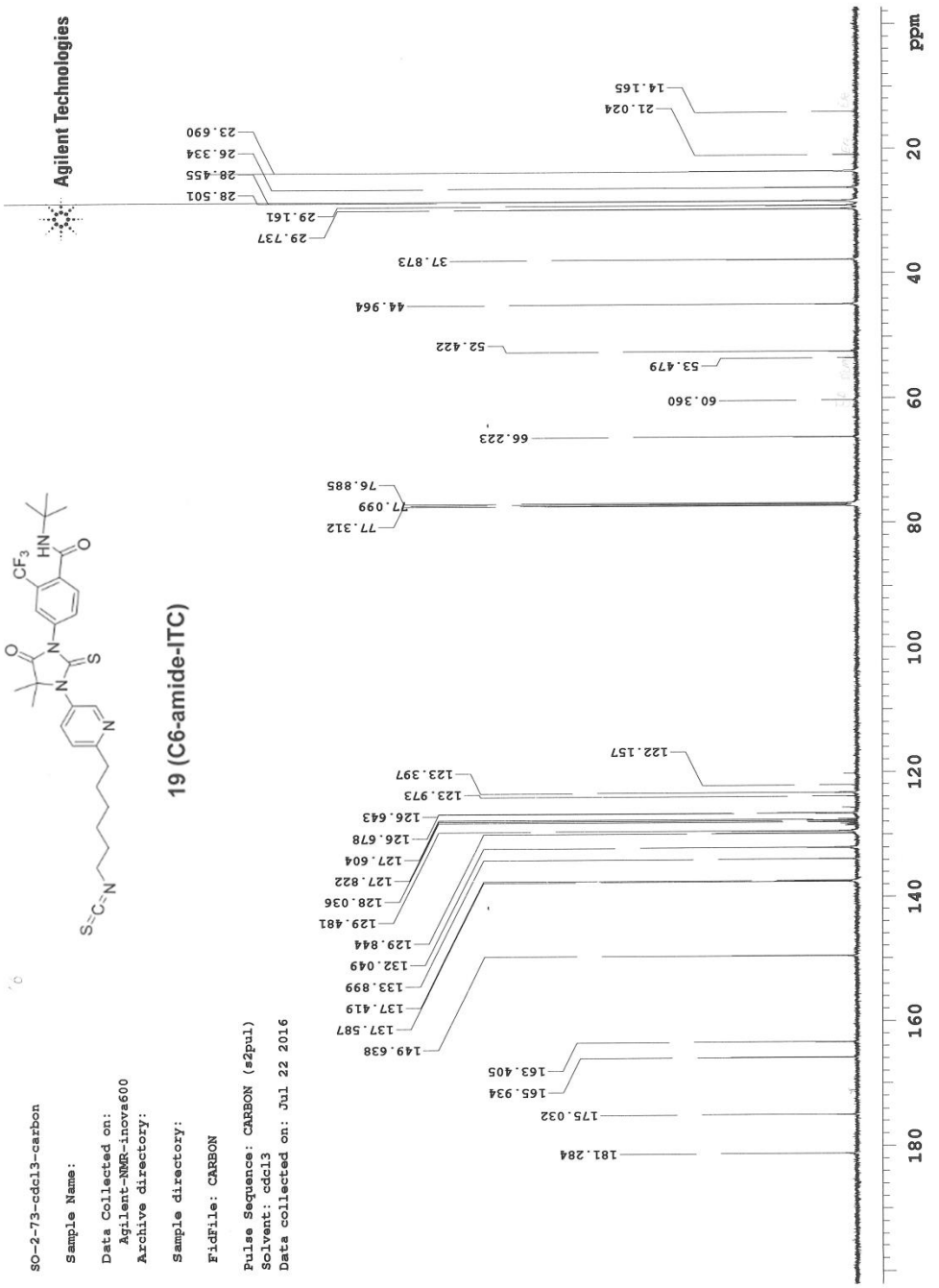
Agilent Technologies
SO-2-73-cdcl3-carbon
Sample Name:
Data Collected on:
Agilent-NMR-inova600
Archive directory:
Sample directory:
FidFile: CARBON
Pulse Sequence: CARBON (s2pul)
Solvent: cdcl3
Data collected on: Jul 22 2016
19 (C6-amide-ITC)
ppm

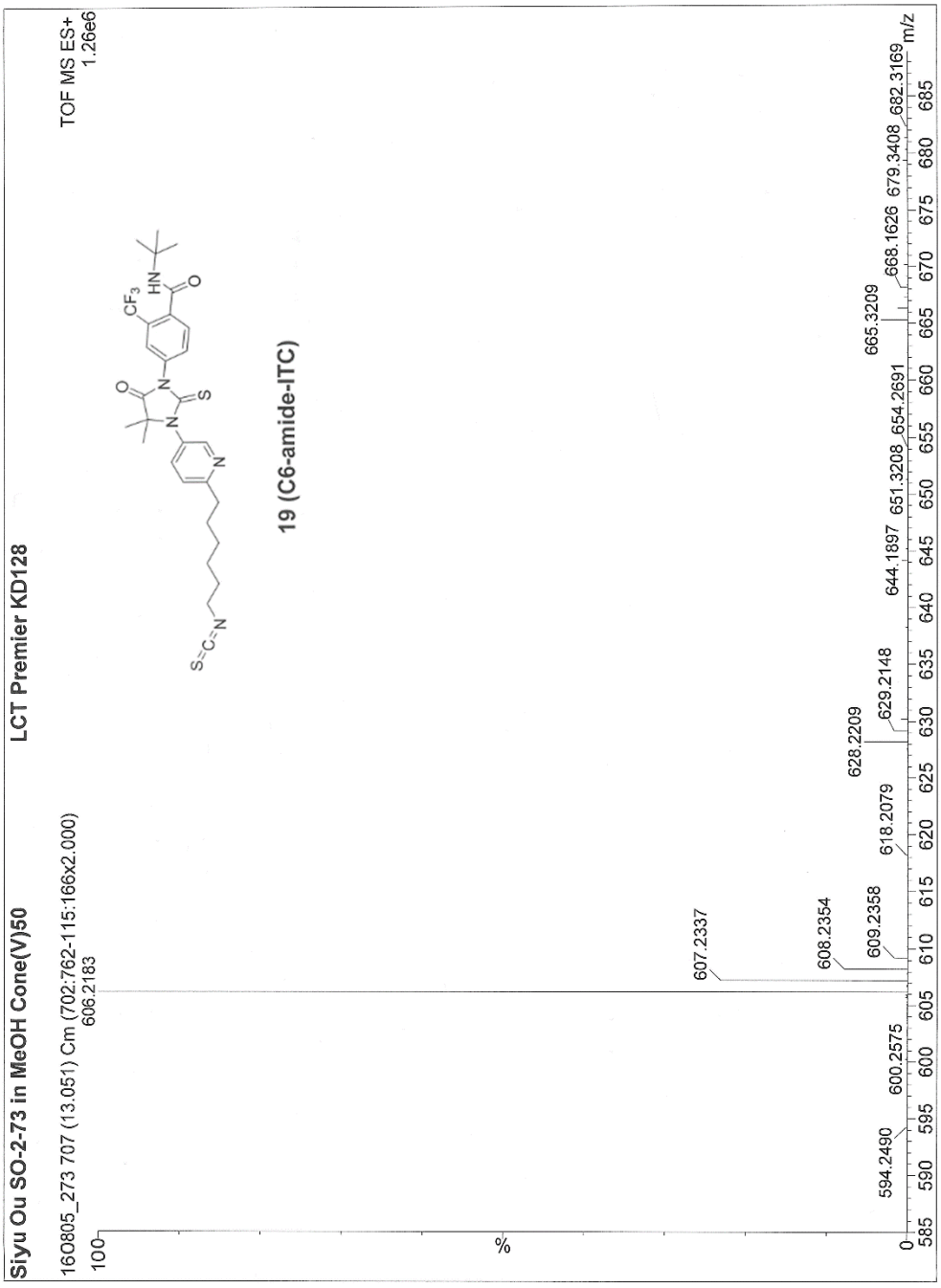
Siyu Ou SO-2-73 in MeOH Cone(V)50
LCT Premier KD128
160805_273 707 (13.051) Cm (702:762-115:166x2.000)
TOF MS ES+
1.26e6
100
%
0
19 (C6-amide-ITC)
606.2183
607.2337
608.2354
609.2358
618.2079
628.2209
629.2148
644.1897
651.3208
654.2691
665.3209
668.1626
679.3408
682.3169
594.2490
600.2575
m/z

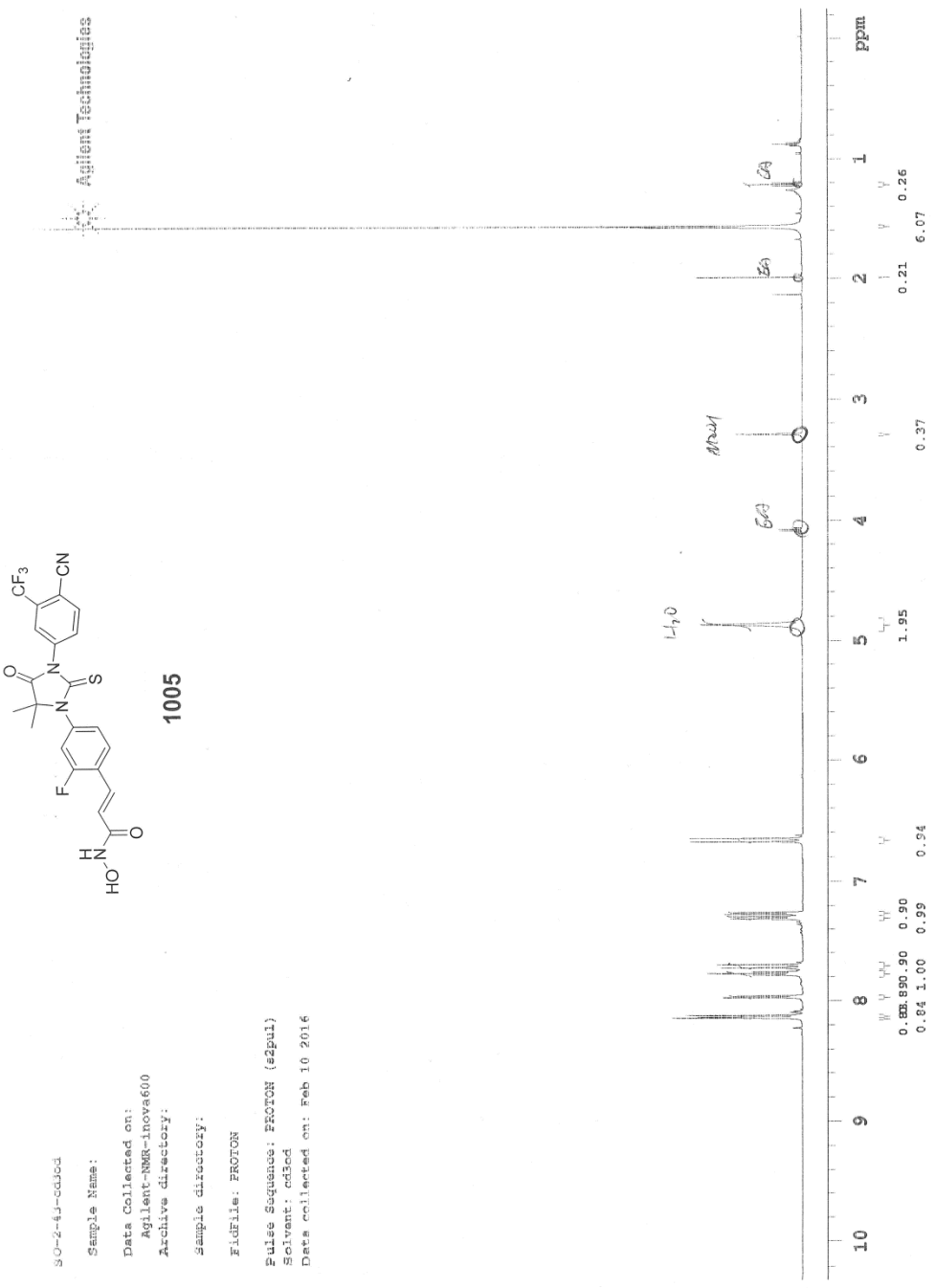
SO-2-4d-cdjcd
Sample Name:
Data Collected on:
Agilent-NMR-inova600
Archive directory:
Sample directory:
FidFile: PROTON
Pulse Sequence: PROTON (s2pul)
Solvent: cd3cd
Data collected on: Feb 10 2016
1005
Agilent Technologies
ppm

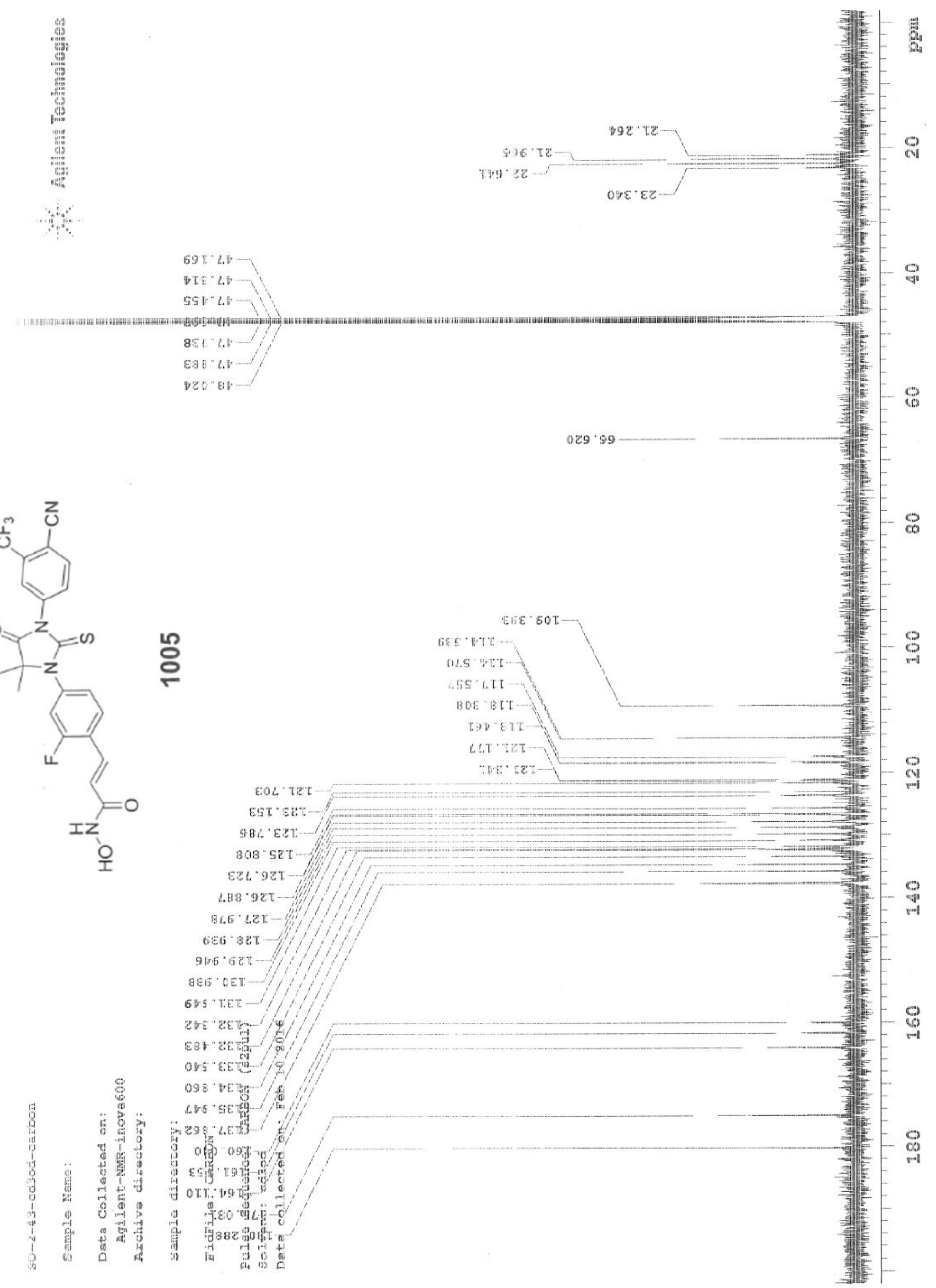
SO-2-43-cd3od-carbon
Sample Name:
Data Collected on:
Agilent-NMR-inova600
Archive directory:
Sample directory:
Agilent Technologies
1005
ppm

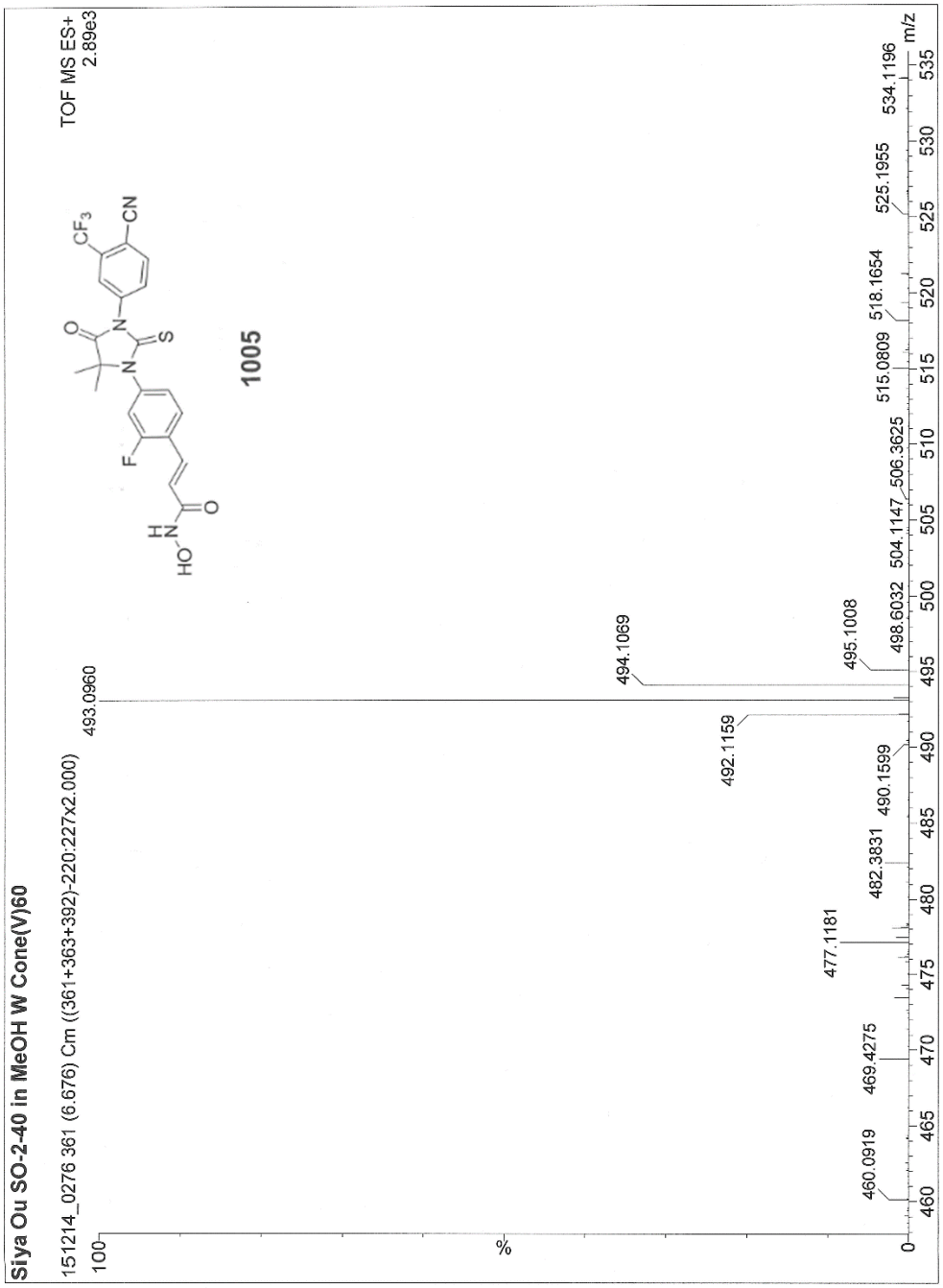
Siya Ou SO-2-40 in MeOH W Cone(V)60
151214_0276 361 (6.676) Cm ((361+363+392)-220:227x2.000)
TOF MS ES+
2.89e3
1005
100
%
0
493.0960
494.1069
492.1159
495.1008
498.6032
504.1147
506.3625
515.0809
518.1654
525.1955
534.1196
477.1181
482.3831
490.1599
460.0919
469.4275
460
465
470
475
480
485
490
495
500
505
510
515
520
525
530
535
m/z

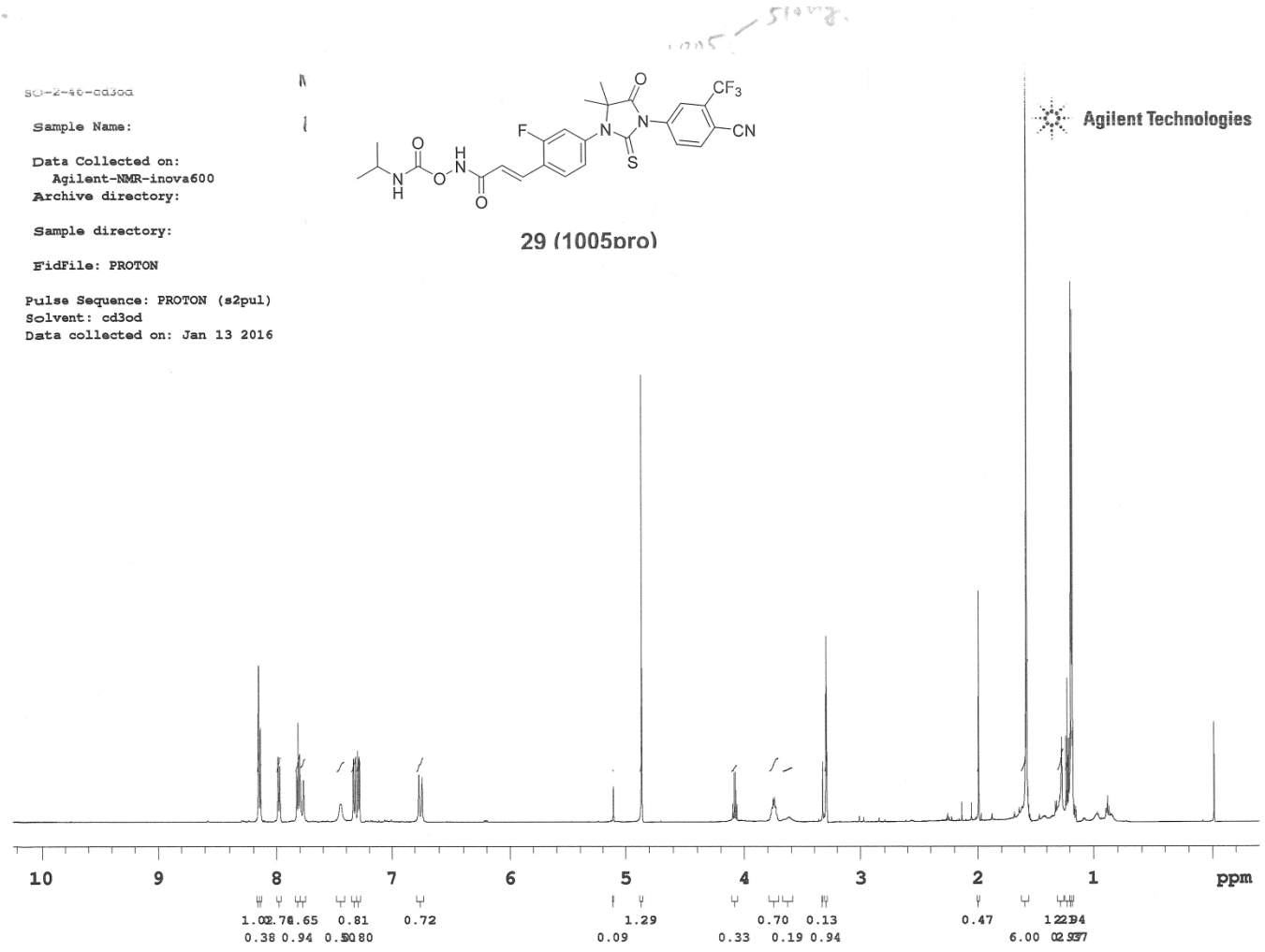
SO-2-46-cd3od
Sample Name:
Data Collected on:
Agilent-NMR-inova600
Archive directory:
Sample directory:
FidFile: PROTON
Pulse Sequence: PROTON (s2pul)
Solvent: cd3od
Data collected on: Jan 13 2016
29 (1005pro)
Agilent Technologies
10
9
8
7
6
5
4
3
2
1
ppm

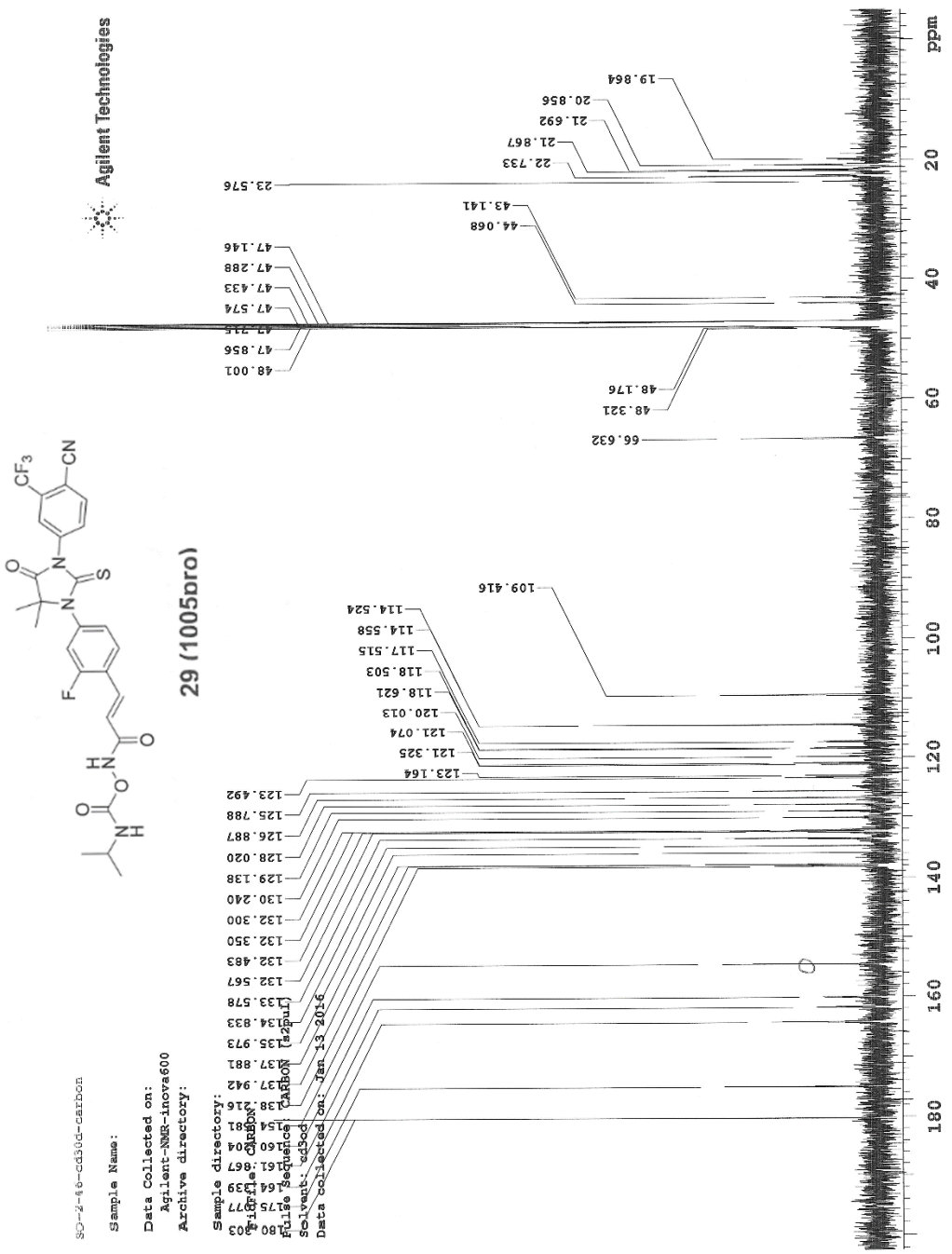
Agilent Technologies
29 (1005pro)
SG-2-48-cd30d-carbon
Sample Name:
Data Collected on:
Agilent-NMR-inova600
Archive directory:
Sample directory:
Pulse Sequence: CARBON
Solvent: cd3od
Data collected on: Jan 13 2016
ppm

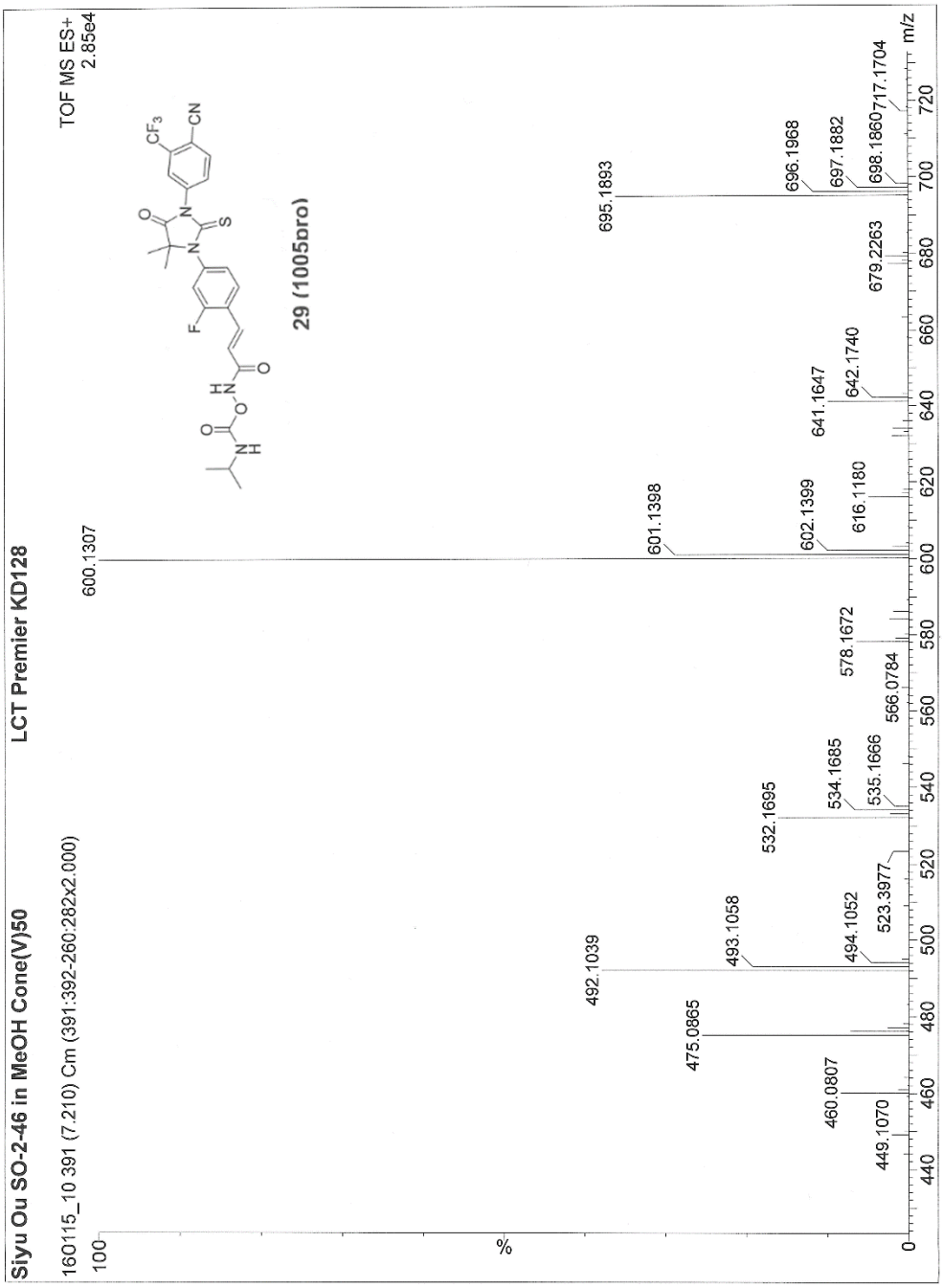
Siyu Ou SO-2-46 in MeOH Cone(V)50
LCT Premier KD128
160115_10 391 (7.210) Cm (391:392-260:282x2.000)
TOF MS ES+
2.85e4
29 (1005bro)
100
%
0
m/z
600.1307
601.1398
602.1399
616.1180
641.1647
642.1740
679.2263
695.1893
696.1968
697.1882
698.1860
717.1704
578.1672
566.0784
534.1685
535.1666
532.1695
492.1039
493.1058
494.1052
523.3977
475.0865
460.0807
449.1070

REFERENCES

1. Marugame, T. and K. Katanoda, *International comparisons of cumulative risk of breast and prostate cancer, from cancer incidence in five continents Vol. VIII.* Jpn J Clin Oncol, 2006. **36**(6): p. 399-400.
2. Attard, G., et al., *Prostate cancer.* The Lancet, 2016. **387**(10013): p. 70-82.
3. MJ, B., *Clinical practice. Prostate-specific-antigen testing for early diagnosis of prostate cancer.* N Engl J Med, 2001. **344**(18): p. 1373-7.
4. Force, M.V.U.S.P.S.T., *Screening for prostate cancer: U.S. Preventive Services Task Force recommendation statement.* Ann Intern Med, 2012. **157**(2): p. 120-34.
5. Gerald L. Andriole, M.D., E. David Crawford, M.D., Robert L. Grubb III, M.D.,, et al., *Mortality Results from a Randomized Prostate-Cancer Screening Trial.* N Engl J Med, 2009. **360**(13): p. 1310-9.
6. Fritz H. Schröder, M.D., Jonas Hugosson, M.D., Monique J. Roobol, Ph.D.,, et al., *Screening and Prostate-Cancer Mortality in a Randomized European Study.* N Engl J Med, 2009. **360**(13): p. 1320-8.
7. CHARLES HUGGINS, M.D.R.E.S.J., M.D.; CLARENCE V. HODGES, M.D., *Studies on prostate cancer II. The effects of castration on advanced carcinoma of the prostate gland.* Arch Surg, 1941. **43**(2): p. 209-23.
8. Chandrasekar, T., et al., *Mechanisms of resistance in castration-resistant prostate cancer (CRPC).* Transl Androl Urol, 2015. **4**(3): p. 365-80.
9. Harris, W.P., et al., *Androgen deprivation therapy: progress in understanding mechanisms of resistance and optimizing androgen depletion.* Nat Clin Pract Urol, 2009. **6**(2): p. 76-85.

10. Visakorpi T1, H.E., Koivisto P, Tanner M, Keinänen R, Palmberg C, Palotie A, Tammela T, Isola J, Kallioniemi OP, *In vivo amplification of the androgen receptor gene and progression of human prostate cancer.* Nat Genet, 1995. **9**(4): p. 401-6.

11. Bubendorf L, K.J., Koivisto P, Schraml P, Moch H, Gasser TC, Willi N, Mihatsch MJ, Sauter G, Kallioniemi OP, *Survey of gene amplifications during prostate cancer progression by high-throughout fluorescence in situ hybridization on tissue microarrays.* Cancer Res, 1999. **59**(4): p. 803-6.

12. Haapala, K., et al., *Androgen receptor amplification is associated with increased cell proliferation in prostate cancer*. Hum Pathol, 2007. **38**(3): p. 474-8.

13. Gregory CW, J.R.J., Mohler JL, French FS, Wilson EM, *Androgen receptor stabilization in recurrent prostate cancer is associated with hypersensitivity to low androgen.* Cancer Res, 2001. **61**(7): p. 2892-8.

14. Feldman BJ, F.D., *The development of androgen-independent prostate cancer.* Nat Rev Cancer, 2001. **1**(1): p. 34-45.

15. Zhao XY, M.P., Krishnan AV, Swami S, Navone NM, Peehl DM, Feldman D, *Glucocorticoids can promote androgen-independent growth of prostate cancer cells through a mutated androgen receptor.* Nat Med, 2000. **6**(6): p. 703-6.

16. Hara T, M.J., Araki H, Yamaoka M, Kanzaki N, Kusaka M, Miyamoto M, *Novel mutations of androgen receptor: a possible mechanism of bicalutamide withdrawal syndrome.* Cancer Res, 2003. **63**(1): p. 149-53.

17. Locke, J.A., et al., *Androgen levels increase by intratumoral de novo steroidogenesis during progression of castration-resistant prostate cancer.* Cancer Res, 2008. **68**(15): p. 6407-15.

18. Chang KH, L.R., Papari-Zareei M, Watumull L, Zhao YD, Auchus RJ, Sharifi N, *Dihydrotestosterone synthesis bypasses testosterone to drive castration-resistant prostate cancer.* Proc Natl Acad Sci U S A, 2011. **108**(33): p. 13728-33.

19. de Bono JS, L.C., Molina A, Fizazi K, North S, Chu L, Chi KN, Jones RJ, Goodman OB Jr, Saad F, Staffurth JN, Mainwaring P, Harland S, Flaig TW, Hutson TE, Cheng T, Patterson H, Hainsworth JD, Ryan CJ, Sternberg CN, Ellard SL, Fléchon A, Saleh M, Scholz M, Efstathiou E, Zivi A, Bianchini D, Loriot Y, Chieffo N, Kheoh T, Haqq CM, Scher HI; COU-AA-301 Investigators, *Abiraterone and Increased Survival in Metastatic Prostate Cancer.* N Engl J Med, 2011. **364**(21): p. 1995-2005.

20. Hornberg, E., et al., *Expression of androgen receptor splice variants in prostate cancer bone metastases is associated with castration-resistance and short survival.* PLoS One, 2011. **6**(4): p. e19059.

21. Sun, S., et al., *Castration resistance in human prostate cancer is conferred by a frequently occurring androgen receptor splice variant.* J Clin Invest, 2010. **120**(8): p. 2715-30.

22. Culig Z, H.A., Cronauer MV, Radmayr C, Trapman J, Hittmair A, Bartsch G, Klocker H, *Androgen receptor activation in prostatic tumor cell lines by insulin-like growth factor-I, keratinocyte growth factor, and epidermal growth factor.* Cancer Res, 1994. **54**(20): p. 5474-8.

23. Craft N, S.Y., Carey M, Sawyers CL, *A mechanism for hormone-independent prostate cancer through modulation of androgen receptor signaling by the HER-2/neu tyrosine kinase.* Nat Med, 1999. **5**(3): p. 280-5.

24. Yeh S, L.H., Kang HY, Thin TH, Lin MF, Chang C, *From HER2/Neu signal cascade to androgen receptor and its coactivators: a novel pathway by induction of androgen target genes through MAP kinase in prostate cancer cells.* proc Natl Acad Sci U S A, 1999. **96**(10): p. 5458-63.

25. Xin, L., et al., *Progression of prostate cancer by synergy of AKT with genotropic and nongenotropic actions of the androgen receptor.* Proc Natl Acad Sci U S A, 2006. **103**(20): p. 7789-94.

26. Carver, B.S., et al., *Reciprocal feedback regulation of PI3K and androgen receptor signaling in PTEN-deficient prostate cancer.* Cancer Cell, 2011. **19**(5): p. 575-86.

27. Thomas, C., et al., *Synergistic targeting of PI3K/AKT pathway and androgen receptor axis significantly delays castration-resistant prostate cancer progression in vivo.* Mol Cancer Ther, 2013. **12**(11): p. 2342-55.

28. Toren, P., et al., *Combination AZD5363 with Enzalutamide Significantly Delays Enzalutamide-resistant Prostate Cancer in Preclinical Models.* Eur Urol, 2015. **67**(6): p. 986-90.

29. Jung, M.E., et al., *Structure-activity relationship for thiohydantoin androgen receptor antagonists for castration-resistant prostate cancer (CRPC).* J Med Chem, 2010. **53**(7): p. 2779-96.

30. Clegg, N.J., et al., *ARN-509: a novel antiandrogen for prostate cancer treatment.* Cancer Res, 2012. **72**(6): p. 1494-503.

31. Yu, Z., et al., *Galeterone prevents androgen receptor binding to chromatin and enhances degradation of mutant androgen receptor.* Clin Cancer Res, 2014. **20**(15): p. 4075-85.

32. Chris Tran, S.O., Nicola J. Clegg,Yu Chen, Philip A. Watson, Vivek Arora,, et al., *Development of a Second-Generation Antiandrogen for Treatment of Advanced Prostate Cancer.* Science, 2009. **324**(5928): p. 787-90.

33. Scher, H.I., et al., *Increased survival with enzalutamide in prostate cancer after chemotherapy.* N Engl J Med, 2012. **367**(13): p. 1187-97.

34. Beer, T.M., et al., *Enzalutamide in metastatic prostate cancer before chemotherapy.* N Engl J Med, 2014. **371**(5): p. 424-33.

35. Ning, Y.M., et al., *U.S. Food and Drug Administration Approval Summary: Enzalutamide for the Treatment of Patients With Chemotherapy-Naive Metastatic Castration-Resistant Prostate Cancer.* Oncologist, 2015. **20**(8): p. 960-6.

36. Balbas, M.D., et al., *Overcoming mutation-based resistance to antiandrogens with rational drug design.* Elife, 2013. **2**: p. e00499.

37. Buttigliero, C., et al., *Understanding and overcoming the mechanisms of primary and acquired resistance to abiraterone and enzalutamide in castration resistant prostate cancer.* Cancer Treat Rev, 2015. **41**(10): p. 884-92.

38. Laurence N. Kolonel, J.H.H., Alice S. Whittemore, Anna H. Wu, Richard P. Gallagher, Lynne R. Wilkens, Esther M. John, Geoffrey R. Howe, Darlene M. Dreon, Dee W. West, and Ralph S. Paffenbarger, Jr., *Vegetables, Fruits, Legumes*

and Prostate Cancer: A Multiethnic Case-Control Study. Cancer Epidemiol Biomarkers Prev, 2000. **9**(8): p. 795-804.

39. Higdon, J.V., et al., *Cruciferous vegetables and human cancer risk: epidemiologic evidence and mechanistic basis.* Pharmacol Res, 2007. **55**(3): p. 224-36.

40. Traka, M.H., A. Melchini, and R.F. Mithen, *Sulforaphane and prostate cancer interception.* Drug Discov Today, 2014. **19**(9): p. 1488-92.

41. Thangstad OP, W.P., Husebye H, Bones A., *The myrosinase (thioglucoside glucohydrolase) gene family in Brassicaceae.* Plant Mol Biol, 1993. **23**(3): p. 511-24.

42. Matusheski NV, S.R., Juvik JA, Mithen R, Bennett M, Jeffery EH., *Epithiospecifier Protein from Broccoli (Brassica oleracea L. ssp. italica) Inhibits Formation of the Anticancer Agent Sulforaphane.* J Agric Food Chem, 2006. **54**(6): p. 2069-76.

43. Matusheski, N.V., J.A. Juvik, and E.H. Jeffery, *Heating decreases epithiospecifier protein activity and increases sulforaphane formation in broccoli.* Phytochemistry, 2004. **65**(9): p. 1273-81.

44. Ganai, S.A., *Histone deacetylase inhibitor sulforaphane: The phytochemical with vibrant activity against prostate cancer.* Biomed Pharmacother, 2016. **81**: p. 250-7.

45. Alumkal, J.J., et al., *A phase II study of sulforaphane-rich broccoli sprout extracts in men with recurrent prostate cancer.* Invest New Drugs, 2015. **33**(2): p. 480-9.

46. Herman-Antosiewicz, A., et al., *Induction of p21 protein protects against sulforaphane-induced mitotic arrest in LNCaP human prostate cancer cell line.* Mol Cancer Ther, 2007. **6**(5): p. 1673-81.

47. Singh, S.V., et al., *Sulforaphane-induced G2/M phase cell cycle arrest involves checkpoint kinase 2-mediated phosphorylation of cell division cycle 25C.* J Biol Chem, 2004. **279**(24): p. 25813-22.

48. Cho, S.D., et al., *Involvement of c-Jun N-terminal kinase in G2/M arrest and caspase-mediated apoptosis induced by sulforaphane in DU145 prostate cancer cells.* Nutr Cancer, 2005. **52**(2): p. 213-24.

49. Singh AV, X.D., Lew KL, Dhir R, Singh SV., *Sulforaphane induces caspase-mediated apoptosis in cultured PC-3 human prostate cancer cells and retards growth of PC-3 xenografts in vivo.* Carcinogenesis, 2004. **25**(1).

50. Choi, S., et al., *D,L-Sulforaphane-induced cell death in human prostate cancer cells is regulated by inhibitor of apoptosis family proteins and Apaf-1*. Carcinogenesis, 2007. **28**(1): p. 151-62.

51. Wiczk, A., et al., *Sulforaphane, a cruciferous vegetable-derived isothiocyanate, inhibits protein synthesis in human prostate cancer cells.* Biochim Biophys Acta, 2012. **1823**(8): p. 1295-305.

52. Kalluri, R. and R.A. Weinberg, *The basics of epithelial-mesenchymal transition.* J Clin Invest, 2009. **119**(6): p. 1420-8.

53. Zhu, M.L. and N. Kyprianou, *Role of androgens and the androgen receptor in epithelial-mesenchymal transition and invasion of prostate cancer cells.* FASEB J, 2010. **24**(3): p. 769-77.

54. Pećina-Šlaus, N., *Tumor suppressor gene E-cadherin and its role in normal and malignant cells.* Cancer Cell Int, 2003. **3**(17).

55. Gopalan, A., et al., *TMPRSS2-ERG gene fusion is not associated with outcome in patients treated by prostatectomy.* Cancer Res, 2009. **69**(4): p. 1400-6.

56. Sakao, K., et al., *CXCR4 is a novel target of cancer chemopreventative isothiocyanates in prostate cancer cells.* Cancer Prev Res (Phila), 2015. **8**(5): p. 365-74.

57. Labsch, S., et al., *Sulforaphane and TRAIL induce a synergistic elimination of advanced prostate cancer stem-like cells.* Int J Oncol, 2014. **44**(5): p. 1470-80.

58. Peng X, Z.Y., Tian H, Yang G, Li C, Geng Y, Wu S, Wu W, *Sulforaphane inhibits invasion by phosphorylating ERK1/2 to regulate E-cadherin and CD44v6 in human prostate cancer DU145 cells.* Oncol Rep, 2015. **34**(3): p. 1567-72.

59. Kallifatidis, G., et al., *Sulforaphane increases drug-mediated cytotoxicity toward cancer stem-like cells of pancreas and prostate.* Mol Ther, 2011. **19**(1): p. 188-95.

60. Li, Y., et al., *Sulforaphane, a dietary component of broccoli/broccoli sprouts, inhibits breast cancer stem cells.* Clin Cancer Res, 2010. **16**(9): p. 2580-90.

61. Novio, S., et al., *Effects of Brassicaceae Isothiocyanates on Prostate Cancer.* Molecules, 2016. **21**(5).

62. Zhang, Y., *The molecular basis that unifies the metabolism, cellular uptake and chemopreventive activities of dietary isothiocyanates.* Carcinogenesis, 2012. **33**(1): p. 2-9.

63. Wang, Y., et al., *Identification of histone deacetylase inhibitors with benzoylhydrazide scaffold that selectively inhibit class I histone deacetylases.* Chem Biol, 2015. **22**(2): p. 273-84.

64. Weichert, W., et al., *Histone deacetylases 1, 2 and 3 are highly expressed in prostate cancer and HDAC2 expression is associated with shorter PSA relapse time after radical prostatectomy.* Br J Cancer, 2008. **98**(3): p. 604-10.

65. Dharam Kaushik, V.V., Sudhir Isharwal, Soud A. Sediqe and Ming-Fong Lin, *Histone deacetylase inhibitors in castrationresistant prostate cancer: molecular mechanism of action and recent clinical trials.* Ther Adv Urol, 2015. **7**(6): p. 388-95.

66. Halkidou, K., et al., *Nuclear accumulation of histone deacetylase 4 (HDAC4) coincides with the loss of androgen sensitivity in hormone refractory cancer of the prostate.* Eur Urol, 2004. **45**(3): p. 382-9; author reply 389.

67. Nakagawa M, O.Y., Eguchi T, Aishima S, Yao T, Hosoi F, Basaki Y, Ono M, Kuwano M, Tanaka M, Tsuneyoshi M, *Expression profile of class I histone deacetylases in human cancer tissues.* Oncol Rep, 2007. **18**(4): p. 769-74.

68. Kojima, K., et al., *A role for SIRT1 in cell growth and chemoresistance in prostate cancer PC3 and DU145 cells.* Biochem Biophys Res Commun, 2008. **373**(3): p. 423-8.

69. Chen, L., et al., *Chemical ablation of androgen receptor in prostate cancer cells by the histone deacetylase inhibitor LAQ824.* Mol Cancer Ther, 2005. **4**(9): p. 1311-9.

70. David B. Solit, F.F.Z., et al., *17-Allylamino-17-demethoxygeldanamycin Induces the Degradation of Androgen Receptor and HER-2/neu and Inhibits the Growth of Prostate Cancer Xenografts.* Clin. Cancer Res., 2002. **8**(5): p. 986-93.

71. Welsbie, D.S., et al., *Histone deacetylases are required for androgen receptor function in hormone-sensitive and castrate-resistant prostate cancer.* Cancer Res, 2009. **69**(3): p. 958-66.

72. Melinda C. Myzak, P.A.K., 2 Fung-Lung Chung,4 and Roderick H. Dashwood1,3, *A Novel Mechanism of Chemoprotection by Sulforaphane: Inhibition of Histone Deacetylase.* Cancer Res, 2004. **64**(16): p. 5767-74.

73. Myzak, M.C., et al., *Sulforaphane inhibits histone deacetylase activity in BPH-1, LnCaP and PC-3 prostate epithelial cells.* Carcinogenesis, 2006. **27**(4): p. 811-9.

74. Myzak MC, D.W., Orner GA, Ho E, Dashwood RH, *Sulforaphane inhibits histone deacetylase in vivo and suppresses tumorigenesis in Apc-minus mice.* FASEB J, 2006. **20**(3): p. 506-8.

75. Myzak MC, T.P., Dashwood WM, Dashwood RH, Ho E, *Sulforaphane retards the growth of human PC-3 xenografts and inhibits HDAC activity in human subjects.* Exp Biol Med (Maywood), 2007. **232**(2): p. 227-34.

76. Kramer, O.H., S. Mahboobi, and A. Sellmer, *Drugging the HDAC6-HSP90 interplay in malignant cells.* Trends Pharmacol Sci, 2014. **35**(10): p. 501-9.

77. Kovacs, J.J., et al., *HDAC6 regulates Hsp90 acetylation and chaperone-dependent activation of glucocorticoid receptor.* Mol Cell, 2005. **18**(5): p. 601-7.

78. Bali, P., et al., *Inhibition of histone deacetylase 6 acetylates and disrupts the chaperone function of heat shock protein 90: a novel basis for antileukemia*

activity of histone deacetylase inhibitors. J Biol Chem, 2005. **280**(29): p. 26729-34.

79. Gibbs, A., et al., *Sulforaphane destabilizes the androgen receptor in prostate cancer cells by inactivating histone deacetylase 6.* Proc Natl Acad Sci U S A, 2009. **106**(39): p. 16663-8.

80. Li, Y., et al., *Sulforaphane inhibits pancreatic cancer through disrupting Hsp90-p50(Cdc37) complex and direct interactions with amino acids residues of Hsp90.* J Nutr Biochem, 2012. **23**(12): p. 1617-26.

81. Shibata, T., et al., *Transthiocarbamoylation of proteins by thiolated isothiocyanates.* J Biol Chem, 2011. **286**(49): p. 42150-61.

82. Zhang, Y., et al., *Sulphoxythiocarbamates modify cysteine residues in HSP90 causing degradation of client proteins and inhibition of cancer cell proliferation.* Br J Cancer, 2014. **110**(1): p. 71-82.

83. Ferraldeschi, R., et al., *Second-Generation HSP90 Inhibitor Onalespib Blocks mRNA Splicing of Androgen Receptor Variant 7 in Prostate Cancer Cells.* Cancer Res, 2016. **76**(9): p. 2731-42.

84. Guo, C., et al., *Discovery of aryloxy tetramethylcyclobutanes as novel androgen receptor antagonists.* J Med Chem, 2011. **54**(21): p. 7693-704.

85. Sharma AK, S.A., Desai D, Madhunapantula SV, Huh SJ, Robertson GP, Amin S, *Synthesis and anticancer activity comparison of phenylalkyl isoselenocyanates with corresponding naturally occurring and synthetic isothiocyanates.* J Med Chem, 2009. **51**(24): p. 7820-6.

86. Jiao D, S.T., Yang CS, Pittman B, Desai D, Amin S, Chung FL, *Chemopreventive activity of thiol conjugates of isothiocyanates for lung tumorigenesis.* carcinogenesis, 1997. **18**(11): p. 2143-7.

87. Bhattacharya, A., et al., *The principal urinary metabolite of allyl isothiocyanate, N-acetyl-S-(N-allylthiocarbamoyl)cysteine, inhibits the growth and muscle invasion of bladder cancer.* Carcinogenesis, 2012. **33**(2): p. 394-8.

88. Conaway CC, K.J., Amin S, Chung FL, *Decomposition rates of isothiocyanate conjugates determine their activity as inhibitors of cytochrome p450 enzymes.* Chem Res Toxicol, 2001. **14**(9): p. 1170-6.

89. Daniel, K.B., et al., *Dual-Mode HDAC Prodrug for Covalent Modification and Subsequent Inhibitor Release.* J Med Chem, 2015. **58**(11): p. 4812-21.

90. Schlimme S, H.A., Carafa V, Heinke R, Kannan S, Stolfa DA, Cellamare S, Carotti A, Altucci L, Jung M, Sippl W, *Carbamate prodrug concept for hydroxamate HDAC inhibitors.* ChemMedChem, 2011. **6**(7): p. 1193-8.

91. Wilson VS, B.K., Lambright CR, Gray LE Jr., *A novel cell line, MDA-kb2, that stably expresses an androgen- and glucocorticoid-responsive reporter for the detection of hormone receptor agonists and antagonists.* Toxicol Sci, 2002. **66**(1).

92. Sobel, R.E. and M.D. Sadar, *Cell lines used in prostate cancer research: a compendium of old and new lines--part 1.* J Urol, 2005. **173**(2): p. 342-59.

93. Barton, V.N., et al., *Multiple molecular subtypes of triple-negative breast cancer critically rely on androgen receptor and respond to enzalutamide in vivo.* Mol Cancer Ther, 2015. **14**(3): p. 769-78.

94. Kumar R, T.E., *The structure of the nuclear hormone receptors.* Steroids, 1999. **64**(5): p. 310-9.

95. Georget V, T.B., Nicolas JC, Sultan C, *Mechanism of antiandrogen action: key role of hsp90 in conformational change and transcriptional activity of the androgen receptor.* Biochemistry, 2002. **41**(39): p. 11824-31.

96. Pepe, A., et al., *Synthesis and structure-activity relationship studies of novel dihydropyridones as androgen receptor modulators.* J Med Chem, 2013. **56**(21): p. 8280-97.

97. Wilkinson, J.M., et al., *Compound profiling using a panel of steroid hormone receptor cell-based assays.* J Biomol Screen, 2008. **13**(8): p. 755-65.

98. Kauppi, B., et al., *The three-dimensional structures of antagonistic and agonistic forms of the glucocorticoid receptor ligand-binding domain: RU-486 induces a transconformation that leads to active antagonism.* J Biol Chem, 2003. **278**(25): p. 22748-54.

99. Yoshino, H., et al., *Design and synthesis of an androgen receptor pure antagonist (CH5137291) for the treatment of castration-resistant prostate cancer.* Bioorg Med Chem, 2010. **18**(23): p. 8150-7.

100. Graubaum, H. and R. Ozegowski, *Inter- und intramolekulare Acylwanderungen an 1(9)H-2,3-Dihydro-imidazo[1,2-a]benzimidazolen.* J prakt Chem, 1998. **340**: p. 11-9.

101. Elokdah H, S.T., Abou-Gharbia M, Butera JA, Chai SY, McFarlane GR, McKean ML, Babiak JL, Adelman SJ, Quinet EM, *Design, synthesis, and biological*

evaluation of thio-containing compounds with serum HDL-cholesterol-elevating properties. J Med Chem, 2004. **47**(3): p. 681-95.

102. García-Moreno MI, D.-P.P., Benito JM, Ortiz Mellet C, Defaye J, García Fernández JM, *One-step synthesis of non-anomeric sugar isothiocyanates from sugar azides.* Carbohydr Res, 2002. **337**(21-23): p. 2329-34.

103. Sun, C., et al., *Androgen receptor mutation (T877A) promotes prostate cancer cell growth and cell survival.* Oncogene, 2006. **25**(28): p. 3905-13.

104. Pereira de Jesus-Tran, K., et al., *Comparison of crystal structures of human androgen receptor ligand-binding domain complexed with various agonists reveals molecular determinants responsible for binding affinity.* Protein Sci, 2006. **15**(5): p. 987-99.

105. Martins, A.S., et al., *A pivotal role for heat shock protein 90 in Ewing sarcoma resistance to anti-insulin-like growth factor 1 receptor treatment: in vitro and in vivo study.* Cancer Res, 2008. **68**(15): p. 6260-70.

106. Whitaker HC, H.S., Totty N, Gamble SC, Waxman J, Cato AC, Hurst HC, Bevan CL, *Androgen receptor is targeted to distinct subcellular compartments in response to different therapeutic antiandrogens.* Clin Cancer Res, 2004. **10**(21): p. 7392-401.

107. Vyas, A.R., et al., *Sulforaphane Inhibits c-Myc-Mediated Prostate Cancer Stem-Like Traits.* J Cell Biochem, 2016.

108. Lin, X., et al., *Design and synthesis of orally bioavailable aminopyrrolidinone histone deacetylase 6 inhibitors.* J Med Chem, 2015. **58**(6): p. 2809-20.

ABSTRACT

DESIGN AND SYNTHESIS OF ENZALUTAMIDE-ISOTHIOCYANATE HYBRID DRUG AS ANTI-PROSTATE CANCER AGENT

by

SIYU OU

August 2016

Advisor: Dr. Zhihui Qin

Major: Pharmaceutical Sciences

Degree: Master of Science

Isothiocyanate (ITC), such as sulforaphane (SFN), is an active metabolite of dietary glucosinolate from cruciferous vegetables. SFN-rich extracts have been recently tested in recurrent prostate cancer (PCa) patients and notably prolonged PSA doubling time without Grade 3 adverse events. One of the anti-PCa mechanisms of SFN is to inhibit HDAC6, which further triggering androgen receptor (AR) degradation. We have incorporated ITC to the chemical scaffold of enzalutamide (Enz) to create Enz-ITC hybrid molecules with an intention to intracellularly deliver ITC to AR-Hsp90-HDAC6 complex and therefore improving anti-PCa efficacy of both parental drugs. Two Enz-ITCs and one Enz-ITC *N*-acetyl cysteine (NAC) conjugate, i.e. compound **12b** (C6-ITC), **12a** (C4-ITC) and **13** (C6-NAC) were successfully synthesized. Our results support that Enz-ITCs inhibit AR transcriptional activity, induce AR protein down-regulation (more effective than SFN) and suppress proliferation of both androgen-sensitive and insensitive prostate cancer cells. The AR antagonist activity of Enz-ITC was confirmed by the results of MTT and ARE-luciferase assays. We've also synthesized amide analogue of Enz-ITC **19** with

reduced AR affinity while keeps the activity of ITC for future mechanistic studies. As a relevant strategy to study AR-directed HDAC inhibition, a representative Enz-HDAC inhibitor (HDACi) hybrid, compound **1005** was synthesized. **1005** and its prodrug **29** suppressed proliferation of both androgen-sensitive and insensitive prostate cancer cells.

AUTOBIOGRAPHICAL STATEMENT

Name: Siyu Ou

Education: 2016 M.S. Pharmaceutical Sciences, Wayne State University, Detroit, Michigan, U.S.A.

2013 B.S. Pharmacy, China Pharmaceutical University, Nanjing, Jiangsu, China.